CHARACTERISTICS OF BISPHOSPHONATE ELUTION FROM ORTHOPAEDIC IMPLANTS

Courtney Ellen White

Department of Biomedical Engineering

McGILL UNIVERSITY, MONTREAL

May, 2006

A thesis submitted to McGill University
in partial fulfillment of the requirements
of the degree of Master's of Engineering

Your file Votre référence
ISBN: 978-0-494-25017-4
Our file Notre référence
ISBN: 978-0-494-25017-4

Abstract

Bisphosphonates, drugs typically used to prevent bone loss for patients with osteoporosis, could also be used to enhance bone growth into porous implants. Since systemic administration of bisphosphonates is not appropriate for all patients, there is a need to develop a localized drug delivery system and characterize the drug release. The chemical affinity of bisphosphonates for hydroxyapatite was used to temporarily bind them to hydroxyapatite coatings on porous implants. Implants were immersed in aqueous solution and the drug elution was measured using UV spectrophotometry. With hydroxyapatite coating there was an initial burst of elution followed by more gradual drug release over several weeks. Without hydroxyapatite coating, all of the drug eluted in a maximum of three hours. This study served to demonstrate the feasibility of binding bisphosphonate compounds to hydroxyapatite coatings and characterized the elution characteristics as a function of time.

Resumé

Les Bisphosphonates, drogues typiquement employées pour empêcher la perte d'os dans les patients souffrant d'ostéoporose, peuvent également être employés pour augmenter la croissance d'os dans les implants poreux. Puisque l'administration systémique des bisphosphonates n'est pas appropriée pour tous les patients, il y a un besoin de développer un système de livraison localisé de drogue et de caractériser le dégagement de cette drogue. L'affinité chimique des bisphosphonates pour le hydroxyapatite a été employée pour les lier temporairement aux enduits de hydroxyapatite sur les implants poreux. Les implants ont été immergés dans le soluté et l'élution de drogue a été mesurée en utilisant la spectrophotométrie UV. Avec l'enduit de hydroxyapatite, il y a eu un premier éclat d'élution suivi d'un dégagement plus progressif de drogue sur plusieurs semaines. Sans enduit de hydroxyapatite, toute la drogue a été éluée dans un maximum de trois heures. Cette étude a servi à démontrer la faisabilité de lier des composés de bisphosphonate aux enduits de hydroxyapatite et à caractériser les caractéristiques d'élution en fonction du temps.

Acknowledgements

I would like to extend my sincerest thanks to my supervisor, Dr. Bobyn (Department of Biomedical Engineering, McGill University). He has lent his vast knowledge of orthopaedic engineering both to this project and the author. His problem solving, guidance, understanding and patience has been a strong force behind the completion of this thesis. I am honoured that I had the opportunity to work with such a respected orthopaedic researcher.

I would also like to thank Jan Krygier (Jo Miller Orthopaedic Research Laboratory, Montreal General Hospital) for his technical support. Jan built the jig used to dose the implants for this thesis, helped with photos, and provided a friendly face in the lab.

Dr. Tabrizian (Department of Biomedical Engineering, McGill University) and her students and Dr. Rosenberg and his students were very generous to this project in allowing the use of their spectrophotometers. I would like to especially thank Kim Douglas for teaching me how to use the spectrophotometer and software and helping when needed.

This thesis could not have been completed without the assistance of Implex Corp (Allendale, NJ) who provided all of the implants used for this project.

Thank you to Sonia Krajicek for providing the French translation of the abstract and for being a friend.

Finally, I would like to thank my parents for their love and encouragement. They have steadily supported my education from kindergarten through my master's and I would not have been able to do any of if without them.

Table of Contents

ABSTRACT I

RESUME II

ACKNOWLEDGEMENTS III

TABLE OF CONTENTS IV

LIST OF FIGURES VIII

LIST OF TABLES XI

CHAPTER 1. INTRODUCTION 1

CHAPTER 2. LITERATURE REVIEW 4

2.1 Non-cemented prosthesis history 4

2.2 Factors affecting bone ingrowth 7
2.2.1 Motion 7
2.2.2 Gaps 8
2.2.3 Pore Size 9
2.2.4 Other factors 10

2.3 Human and canine bone ingrowth 11

2.4 Methods of enhancing bone ingrowth 13
2.4.1 Bone graft materials 13
2.4.2 Growth Factors 15
2.4.3 Hydroxyapatite 17

2.5 Bisphosphonates 20
2.5.1 Clinical Applications of Bisphosphonates 22
2.5.2 Bisphosphonate Chemical Affinity for Hydroxyapatite 23
2.5.3 Bisphosphonates – Bone Ingrowth Applications 23
2.5.4 Local Delivery of Bisphosphonates for Bone Ingrowth Enhancement 27

CHAPTER 3. PURPOSE 31

CHAPTER 4. MATERIALS AND METHODS 32

4.1 Implants 32
4.1.1 Introduction to porous tantalum 32
4.1.2 Rationale for using porous tantalum 33
4.1.3 Hydroxyapatite coating 35
4.1.4 Porous tantalum implants 36
4.1.5 Titanium Implants 36

4.2 Pamidronate 37

4.3 Zoledronate 38

4.4 Application of Bisphosphonate Coating to Implants 41

4.5 Sterilization 43

4.6 Elution Studies 44

4.7 Spectrophotometry 45

4.8 Bisphosphonates and spectrophotometry 46

4.9 Bisphosphonate analysis with copper (II) ions 47

4.10 Zoledronate analysis with iron (III) ions 48

4.11 Ultraviolet Spectrophotometry 49

4.12 Reliability of Polymethacrylate Cuvettes 49

4.13 Ultraviolet spectrophotometry analysis of bisphosphonates 50

CHAPTER 5. RESULTS 55

5.1 Bisphosphonate Deposition 55

5.2 Pamidronate Calibration in Water 58

5.3 Pamidronate Calibration in saline 60

5.4 Zoledronate Calibration in Water with Copper (II) Sulfate 61

5.5 Zoledronate Calibration in Saline with Iron (III) Chloride 67

5.6 Pamidronate elution from Hydroxyapatite coated implants 75
5.6.1 Elution Results for Implant P1 75
5.6.2 Elution Results for Implant P2 78
5.6.3 Elution Results for Implant P3 80

5.6.4 Elution Results for Implant P4 82
5.6.5 Elution Results for Implant P5 83
5.6.6 Average Pamidronate Elution in Water from HA-coated Implants 85

5.7 Pamidronate Elution from non-HA Coated Porous Tantalum Implants 86
5.7.1 Elution Results for Implant Ta1 86
5.7.2 Elution Results for Implant Ta2 87
5.7.3 Average Pamidronate Elution from non-HA coated implants 88

5.8 Pamidronate Elution in Saline 89

5.9 Zoledronate Elution in Saline 90
5.9.1 Zoledronate Elution from Implant Z1 and Z2 91
5.9.2 Elution Results for Implant Z3 92
5.9.3 Elution results for implant Z4 93
5.9.4 Elution results for implant Z5 94
5.9.5 Elution results for implant Z6 95
5.9.6 Average Zoledronate elution from HA-coated implants 96

5.10 Zoledronate Elution from Ethylene Oxide Sterilized HA-Coated Implants 97
5.10.1 Elution Results for Implant Z7 98
5.10.2 Elution Results for Implant Z8 99
5.10.3 Elution Results for Implant Z9 100
5.10.4 Average Zoledronate Elution from HA-coated, EtO-sterilized implants 102

5.11 Zoledronate Elution from Autoclave Sterilized, HA-coated implant 102

5.12 Zoledronate Elution from non-HA Coated Implants 104
5.12.1 Elution Results from Implant Ta3 105
5.12.2 Elution Results for Implant Ta4 106
5.12.3 Elution Results from Implant Ta5 107
5.12.4 Elution Results for Implant Ta6 108
5.12.5 Average Zoledronate Elution from non-HA Coated Implants 109

5.13 Zoledronate Elution from HA-coated Solid Titanium Implants 110
5.13.1 Zoledronate Elution from Implant Ti1 110
5.13.2 Zoledronate Elution from Implant Ti2 111
5.13.3 Zoledronate Elution from Implant Ti3 112
5.13.4 Average Zoledronate Elution from HA-coated Titanium Implants 114

5.14 Average Zoledronate Elution 114

5.15 Spectrophotometric Results for Non-Bisphosphonate Dosed Implants 116

5.16 Reliability of Methacrylate Cuvettes 116

CHAPTER 6. DISCUSSION 118

6.1 Deposition of bisphosphonate onto implants 118

6.2 Assay Method 119

6.3 Release Profiles 120

6.4 Future Directions 125

CHAPTER 7. CONCLUSIONS 127

REFERENCES 128

List of Figures

2.1 - Scanning electron micrograph (SEM) of a fibre metal porous surface 5
2.2 - SEM of a sintered bead porous surface 6
2.3 - SEM of a plasma spray porous surface 7
2.4 - Bisphosphonate structure 21
2.5 - SEM of bone growth into porous tantalum implants. 26
4.1 - Scanning electron micrograph (SEM) of porous tantalum 33
4.2 - SEM of hydroxyapatite-coated porous tantalum 35
4.3 - Tantalum ulnar implant 36
4.4 - Hydroxyapatite-coated tantalum implant 36
4.5 - Hydroxyapatite-coated titanium implant 37
4.6 - Chemical structure of pamidronate 38
4.7 - Chemical structure of zoledronate 39
4.8 - Zometa packaging 40
4.9 - Tantalum implant in jig for coating 41
4.10 - A 96-well UV transparent well plate 51
5.1 - Bisphosphonate solution on HA-coated porous tantalum implant 55
5.2 – Bisphosphonate solution beaded on a non-HA coated porous tantalum implant 56
5.3 - Calibration of pamidronate in water 59
5.4 - Calibration of pamidronate in saline 61
5.5 - Calibration of zoledronate in water with copper (II) ions, at 240 nm 62
5.6 - Calibration of sodium citrate in water with copper (II) sulfate solution, at 240 nm 63
5.7 - Spectral scan of sodium citrate in water 63
5.8 - Spectral scan of sodium citrate in water with copper (II) sulfate 64
5.9 - Calibration of mannitol in water with copper (II) sulfate solution 64
5.10 - Spectral scan of mannitol in water 65
5.11 - Spectral scan of mannitol in water with copper (II) sulfate 65
5.12 - Spectral scans of Zometa, sodium citrate, and mannitol, each in water with copper (II) sulfate. 66
5.13 – Calibration of Zometa in saline with iron (III) chloride solution 68
5.14 - Calibration of sodium citrate in saline with iron (III) chloride solution at 290 nm 69
5.15 – Calibration of mannitol in saline with iron (III) chloride solution at 290 nm 70
5.16 - Spectral scans of standard solutions of Zometa in saline with iron (III) chloride, from 200 nm to 999 nm 71

5.17 - Spectral scans of Zometa in saline with iron (III) chloride, from 280 nm to 310 nm 72
5.18 - Spectral scans of sodium (Na) citrate in saline with iron (III) chloride, from 200nm to 350nm. The concentrations represent the concentration Zometa that corresponds to the concentration of sodium citrate 72
5.19 - Spectral scans of mannitol in saline with iron (III) chloride, from 200nm to 350 nm. The concentrations represent the concentration of Zometa that corresponds to the concentration of mannitol 73
5.20 - Spectral scans of Zometa, saline, mannitol, and sodium citrate in saline with iron (III) chloride. All concentrations are equivalent 73
5.21 - Spectral scans of Zometa, saline, mannitol, and sodium citrate in saline with iron (III) chloride. All concentrations are equivalent 74
5.22 - Percent of pamidronate eluted from implant P1 against time 78
5.23 - Percent elution of pamidronate over time from implant P2, time scaled 79
5.24 - Percent elution from implant P2, not time scaled 80
5.25 - Percent elution of pamidronate against time from implant P3, with time-scaled x-axis 81
5.26 - Percent elution of pamidronate against time from implant P3, not time-scaled 82
5.27 - Percent elution of pamidronate against time for implant P4 83
5.28 - Percent elution of pamidronate against time for implant P5 84
5.29 - Average percent of pamidronate elution from HA-coated implants against time 85
5.30 - Percent of pamidronate eluted against time for implant Ta1 87
5.31 - Percent elution of pamidronate against time for implant Ta2 88
5.32 - Average percent of pamidronate elution from non-HA coated implants against time 89
5.33 - Average percent of pamidronate elution from HA-coated and non-HA coated implants against time 89
5.34 - Percent elution of zoledronate against time for implant Z3 93
5.35 - Percent elution of zoledronate against time from implant Z4 94
5.36 – Percent elution of zoledronate against time from implant Z5 95
5.37 - Percent elution of zoledronate against time from implant Z6 96
5.38 - Average percent of zoledronate elution from HA-coated implants 97
5.39 - Percent elution of zoledronate against time from implant Z7 99
5.40 - Percent elution of zoledronate against time from implant Z8 100
5.41 - Percent elution of zoledronate against time for implant Z9 101
5.42 - Average percent of zoledronate eluted from HA-coated, ethylene oxide sterilized implants over time 102
5.43 – Percent of zoledronate eluted from implant Z10 103
5.44 - Zoledronate elution from autoclave sterilized implant and non-sterilized implants 104

5.45 - Zoledronate elution from implant Ta3 against time 105
5.46 - Zoledronate elution from implant Ta4 against time 106
5.47 - Zoledronate elution from implant against time 107
5.48 - Zoledronate elution from implant Ta6 against time 108
5.49 - Average zoledronate elution from non-HA coated implants 109
5.50 - Zoledronate elution from implant Ti1 against time 111
5.51 - Zoledronate elution from implant Ti2 against time 112
5.52 - Zoledronate elution from implant Ti3 against time 113
5.53 - Average zoledronate elution from HA-coated titanium implants 114
5.54 - Average zoledronate elution 115

List of Tables

4.1 - Mechanical characteristics of porous tantalum 34
4.2 - Characteristics of pamidronate disodium 38
4.3 - Characteristics of zoledronic acid 40
4.4 - Volumes of solutions used for pamidronate in water calibration curve and final concentration of pamidronate 50
4.5 - Volumes of solutions used for zoledronate in saline calibration curve and final concentration of zoledronate 52
4.6 - Volumes of solutions used for zoledronate in saline or water calibration curve with iron (III) chloride and final concentration of zoledronate 53
5.1 - Hydroxyapatite coated porous tantalum implants for pamidronate elution studies 57
5.2 - Porous tantalum implants for pamidronate elution studies 57
5.3 - Hydroxyapatite coated porous tantalum implants for zoledronate elution studies 57
5.4 - Porous tantalum implants for zoledronate elution studies 58
5.5 - HA-coated solid titanium implants for zoledronate elution studies 58
5.6 - Absorbance of known concentrations of pamidronate in water, at 240 nm 59
5.7 - Blanked absorbance of known concentrations of pamidronate in water, at 240 nm 59
5.8 - Absorbance of known concentrations of pamidronate in saline, at 240 nm 60
5.9 - Blank absorbance of known concentrations of pamidronate in saline, at 240 nm 60
5.10 - Absorbance of known concentrations of zoledronate in water, at 240 nm 61
5.11 - Blanked absorbance of known concentrations of zoledronate in water, at 240 nm 62
5.12 - Absorbance of standard solutions of Zometa in saline with Fe(III), at 290 nm 68
5.13 - Blanked absorbance of standard solutions of Zometa in saline with Fe(III), at 290 nm 68
5.14 - Absorbance of standard solutions of sodium citrate in saline with Fe(III), at 290 nm 69
5.15 - Blanked absorbance of standard solutions of sodium citrate in saline with Fe(III), at 290 nm 69
5.16 - Absorbance of standard solutions of mannitol in saline with Fe(III), at 290 nm 69
5.17 - Blanked absorbance of standard solutions of mannitol in saline with Fe(III), at 290 nm 70
5.18 - Elution data and calculated values of pamidronate elution from implant P1 76
5.19 - Elution results for implant P2 79
5.20 - Elution results for implant P3 81
5.21 - Elution results for implant P4 83
5.22 - Elution results for implant P5 84
5.23 - Elution results for Implant Ta1 86
5.24 - Elution results for implant Ta2 87
5.25 - Elution results for implant P6 90

5.26 - Elution results for implant Z1 91
5.27 - Elution results for implant Z3 92
5.28 - Elution results for implant Z4 94
5.29 - Elution results for implant Z5 95
5.30 - Elution results for implant Z6 96
5.31 - Elution results for implant Z7 98
5.32 - Elution results for implant Z8 100
5.33 - Elution results for implant Z9 101
5.34 - Elution results for implant Z10 103
5.35 - Elution results for implant Ta3 105
5.36 - Elution results for implant Ta3 106
5.37 - Elution results for implant Ta5 107
5.38 - Elution results for implant Ta6 108
5.39 - Elution results for implant Ti1 110
5.40 - Zoledronate elution from implant Ti2 against time 112
5.41 - Elution results from implant Ti3 113
5.42 – Absorbance at 290 nm for cuvettes with distilled water 117

Chapter 1. Introduction

Total joint arthroplasty is a surgical procedure whereby the articulating surfaces of a diarthrodial joint are replaced by artificial implants; commonly made of metal and polymer. The goal of joint replacement is to eliminate pain while providing the patient with a durable, functional joint. Approximately half a million hip arthroplasties are performed annually worldwide. With an aging population and increasing age expectancies the number of total hip arthroplasty procedures is increasing. Osteoarthritis, rheumatoid arthritis, avascular necrosis, congenital dislocation and trauma are all orthopaedic problems that can lead to the deterioration of joint cartilage and necessitate joint replacement. Osteoarthritis is the most common of these pathologies.

Osteoarthritis is caused by degenerative changes in joints. This is generally seen more in the lower extremities because of the relatively severe mechanical loading that occurs in the hip and knee joint. There is progressive degradation of the articular cartilage until the surface of the underlying bone is exposed. This causes pain and eventually a reduction in the range of movement. The pain can be so great that patients have to stop most, if not all, physical activity. Arthroplasty offers substantial relief from the pain since the affected joint surfaces are replaced with prosthetic materials that have smooth articulating surfaces.

Periprosthetic bone loss is a main factor limiting the life span of current orthopaedic implants, and is responsible for approximately 70% of all implant failures. There are two mechanisms by which bone loss occurs. Both hip and knee implants disrupt the natural stress patterns that promote the maintenance of bone mass, which leads to disuse atrophy of the bone surrounding the prosthesis. This mechanism, which occurs acutely during the first six months

following surgery, is termed stress shielding. Over 30% of the periprosthetic bone mass may be lost due to stress shielding [1].

Wear particle induced osteolysis results from a host response to the particulate wear debris that is inevitably generated during joint function. The small particles stimulate a foreign-body granulomatous response, leading to osteoclastic bone resorption. The activity of the osteoclasts is stimulated by the release of bone resorbing cytokines from macrophages that have phagocytosed wear debris particles [2]. This type of bone loss can cause an eventual loosening of the implant, through progressive loss of mechanical support.

The effects of these two mechanisms of bone loss are additive, though it is not known what effect bone loss due to stress shielding during the early postoperative phase may have on osteolysis from a reaction to accumulated wear particles. The predictable, defined period of bone loss caused by stress shielding may provide a window for prophylactic antiresorptive drug therapy during the early postoperative period to minimize bone resorption and later complications [1].

When prostheses are implanted there are two types of fixation modalities that can be used to secure the implants to bone. One involves using polymethyl methacrylate (PMMA) as bone cement, which is a type of grouting agent that fills the space between the implant and the host bone. This provides a tight fit and immediate stability for the implant.

The other involves using implants with porous coatings that allow for host bone to heal and grow into the pores, thus establishing a more natural or biological fixation. Biological fixation is more dependable over time than bone cement because the bone that is integrated into the implant undergoes remodeling like host bone. This is especially true in younger, more active

individuals who place greater mechanical demands on the bone-implant interface.

A method of enhancing the rate and extent of bone growth into and surrounding porous coated prostheses would be beneficial to the clinical outcome in a wide spectrum of reconstructive procedures. More rapid biological fixation could reduce recovery time for patients by creating increased stability earlier after surgery. Enhanced local bone formation could also make cementless joint replacement prostheses a more reliable treatment in cases of metabolic bone disease, joint replacement, tumor resection, or revision for failed primary arthroplasty. This thesis investigates a method for local delivery of bisphosphonates from a porous implant to bone, as an approach to alter local bone metabolism in favour of enhancing bone formation around and within an implant.

Chapter 2. Literature Review

2.1 Non-cemented prosthesis history

It is believed that the first patent for the concept of biological fixation by bone ingrowth was obtained by Greenfield, in 1909, when he developed a metallic cage-like framework for an artificial tooth root [3]. The first orthopaedic implant to use bone ingrowth as its fixation method was the self-locking, cobalt-based alloy Moore endoprosthesis [4]. The implant had bone grafts inserted into large fenestrations in the implant surface. The ensuing fusion between the graft and the native bone augmented the implant fixation.

The development of porous materials for use as implant coatings began in the 1960s. In 1968, Hirschhorn and Reynolds [5] used powder metallurgy techniques to manufacture a porous cobalt-chromium alloy with an average pore size of 10 to 20 μm. By coating small cylinders with this porous material and surgically implanting them into the muscles of dogs, they found that tissue ingrowth occurred in the pores and thus the porous cobalt-chromium alloy could provide a means of bonding an implant to surrounding tissue. Later, Hirschhorn et al [6] also used powder metallurgy techniques to fabricate porous coated titanium implants with either large or small pores and compared the effect of the two different pore sizes on bone ingrowth. When implants with a pore size of 200 μm were surgically implanted, bone ingrowth was observed. When the pore size was less than 15 μm, only fibrous tissue ingrowth was observed, thus leading to the idea that there is a minimum pore size required for bone ingrowth.

However, materials made with powder metallurgy techniques exhibit poor mechanical characteristics when the degree of porosity is sufficient to allow bone ingrowth. Therefore, Lueck et al [7] began to investigate another type of porous metal material. In 1969, they produced and implanted a porous, commercially

pure titanium fibre composite metal (figure 2.1). Subsequently, Galante et al [8-10] further developed this type of porous titanium coating by molding and sintering titanium fibres to the surface of implants. Titanium fibres were produced by cutting 0.19 mm diameter wire into 6.35 mm lengths. The fibres were kinked and pressed into an aggregate by compression in a die-punch. Pressed samples were then place in an annealing furnace. The implants were made with 50% porosity and pores between 170 and 350 μm in diameter. Following animal implantation, bone ingrowth was seen by histological analysis at two weeks and there was deep penetration of bone ingrowth at three weeks.

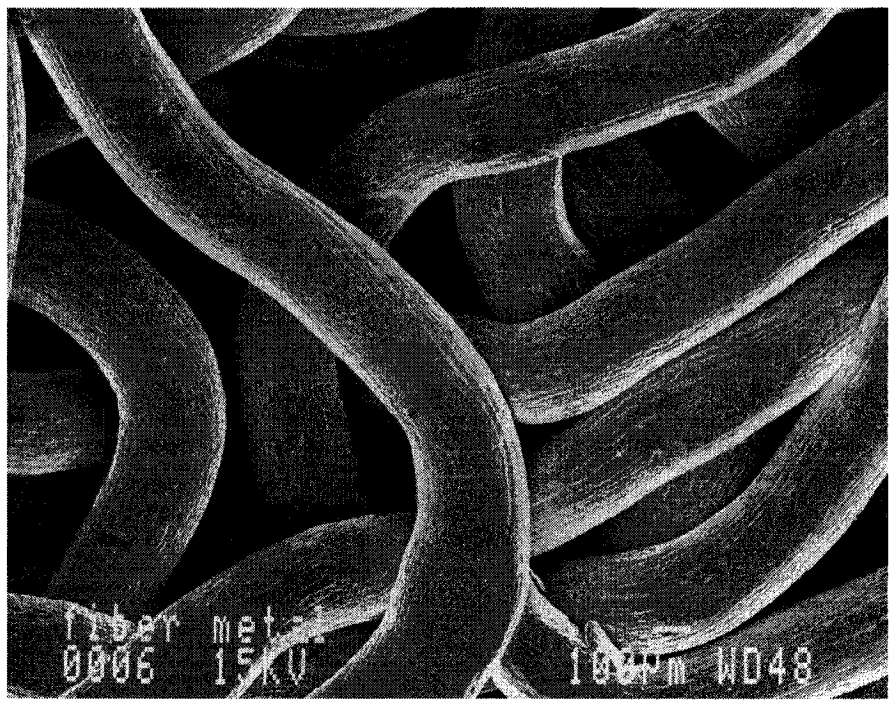

Figure 2.1 - Scanning electron micrograph (SEM) of a fibre metal porous surface

In the early 1970s, several studies [11-13] examined the use of powder-made porous coated cobalt-chromium implants. The porous coating was formed by high-temperature sintering of metal alloy powder onto the substrate surface, creating a beaded surface (figure 2.2). The cobalt-base powder was formed by atomization. The particles were then bound to the substrate using an inorganic binder to allow for a controlled and uniform coating. Sintering was then

conducted in a high-temperature annealing furnace. Welsh et al [14] prepared two implants with different pore sizes; one with pore size 20 to 30 μm and the other with 50 to 100 μm pores. Mechanical push out tests and histological analysis indicated that both materials were effective for biological fixation by bone ingrowth.

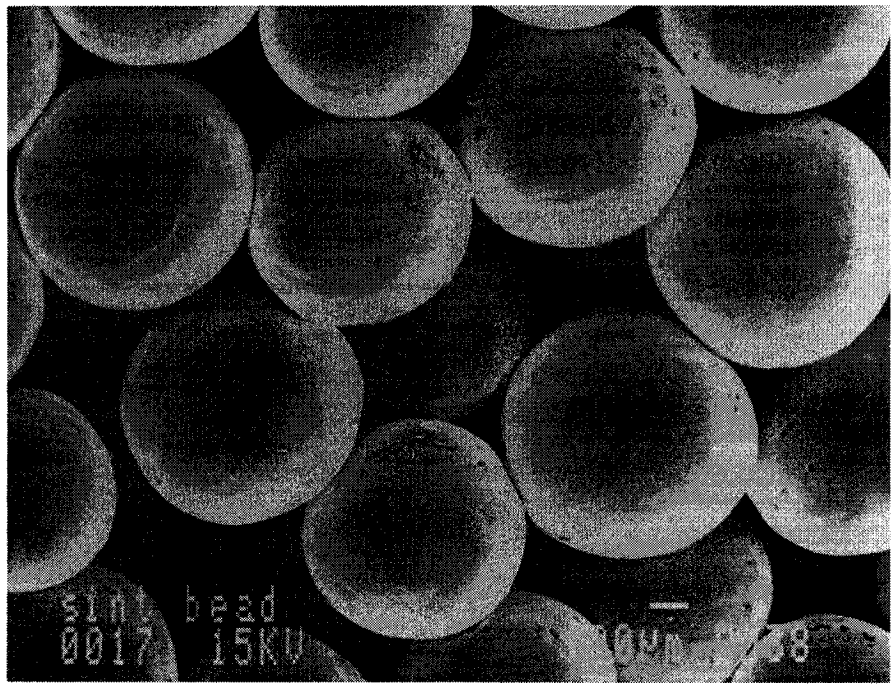

Figure 2.2 - SEM of a sintered bead porous surface

Plasma-sprayed titanium porous coatings (figure 2.3) were developed by Hahn et al in 1970 [15]. Plasma-sprayed porous titanium is advantageous because the plasma spray process allows titanium to retain 90% of its fatigue strength, compared to less than 50% for sintered or diffusion bonded porous implants [16]. They fabricated titanium implants that were coated with a plasma spray of titanium hydride powder, with pores ranging from 50 to 75 μm. The implants were surgically implanted into sheep femora. Torque testing at 26 weeks showed that the bone ingrowth lead to very high attachment strength into the implants [15].

Figure 2.3 - SEM of a plasma spray porous surface

2.2 Factors affecting bone ingrowth

While the type of material is important for bone growth, bone will grow into a variety of biocompatible surfaces. There are other factors which also influence bone ingrowth, some of which are surgically based and others of which are design based. The presence of motion and gaps in the implant environment affect the ability of bone to integrate with an implant surface. The pore size and surface roughness also affect bone ingrowth.

2.2.1 Motion

Cameron et al [17] devised a series of experiments to determine the effect of micromotion on bone ingrowth. They implanted a porous coated cobalt chromium staple into rabbit tibiae and attached the soleus tendon to the staple to

create micromotion. Bony ingrowth occurred in the porous coating without any adverse effect.

Cameron et al [18] later inserted porous coated staples across an osteotomy site, producing macromotion at the staple insertion. A fibrous tissue capsule formed around the staple and no bony ingrowth occurred. It was concluded that micromotion can lead to bone ingrowth but that bone ingrowth will not occur in the presence of macromotion. Pilliar et al [19] attempted to define the limits of micromotion and macromotion. They found that bone ingrowth will occur with motion up to 28 μm. When motion is 150 μm or more, fixation by fibrous tissue occurs.

2.2.2 Gaps

To determine the maximum amount of space between bone and the porous surface of an implant for which bone ingrowth will still occur, Cameron et al [20] evaluated the bone ingrowth over gaps of 0 mm, 0.5 mm, 1.0 mm, and 1.5 mm. The implants were examined between two and 12 weeks post-surgically. Histological analysis showed that bone ingrowth occurred in all implants except those with a surrounding gap of 1.5 mm.

Bobyn et al [21] evaluated bone ingrowth into non-loaded porous coated intermedullary implants. Using implants of varying diameters, they achieved gaps between the implant and the endosteal cortex of up to 4 mm. It was determined by histological analysis that little or no bone formation occurred when the gaps were 2 mm or greater. Bone ingrowth increased as the gap size decreased.

Sandborn et al [22] also investigated the effect of initial bone apposition on bone ingrowth. Implants were surgically inserted into the medullary canal of dogs, leaving gaps ranging from 0 mm to 2 mm. Bone ingrowth was observed

over all gap distances, but the rate of mineralization and bone maturity increased when the gap was 0.5 mm or less.

2.2.3 Pore Size

In a study conducted by Bobyn et al [23] to determine the effect of pore size on bone ingrowth, cylindrical rods of cast cobalt-base alloy were coated with cobalt-base alloy powder. The powder was in four particle size ranges, 25-45 μm, 45-150 μm, 150-300 μm, and 300-840 μm, which resulted in four different pore sizes: 20-50 μm, 50-200 μm, 200-400 μm, and 400-800 μm. All of the implants had a packed network of beads at least 3 particles thick and all of the porous coatings had a porosity of 30-35%. The implants were surgically inserted into canine fermora. When the fixation strength was tested, the smallest pore size had significantly lower interfacial shear strength than all other pore sizes. The strength of fixation of the 50-200 μm pores and the 200-400 μm pores was not statistically different at both 8 and 12 weeks postoperatively. Fixation strength of 400-800 μm pores was also significantly lower than that of the two mid-sized pores. Bone ingrowth appeared to be complete for implants with both mid-sized pores by 8 weeks. The large-pored implants had some bone ingrowth, but also had some fibrous tissue ingrowth.

Cook et al [24] investigated bone growth into Co-Cr-Mo implants with sintered bead porous surfaces. They used three different pore sizes (155, 235, and 350 μm) and fabricated the implants with one, two, or three layers of porosity or entirely porous implants. Porosity of all the porous portions of the implants was 38-40%. Implants were inserted transcortically into canine femora, and were left for 12 weeks before retrieval. The interface shear strength was tested and it was found that it increased with an increasing number of layers, but decreased when the implant was completely porous. Pore size did not affect the attachment strength. Histological analysis showed extensive mineralized bone growth into the pores of the layered porous coated implants. Into the totally porous implant

there was extensive but incomplete bone ingrowth, with the remainder of the space containing connective tissue. Pore size did not affect the histological results.

In a separate study, Robinson et al inserted Co-Cr-Mo implants were inserted into the femora of dogs. The cylinders were polished, sandblasted, or coated in sintered beads. Three bead sizes were used, resulting in three different pore sizes: 30 X 85 μm, 40 X 106 μm, and 50 X 125 μm. Bone ingrowth was present in the porous surfaced implants by one week. When tested for interfacial shear strength, the implants with larger pores had increased fixation strength. [25]

Clemow et al [26] investigated the interfacial shear properties of bone ingrowth into porous coated titanium implants with respect to pore size. The three different pore sizes were 175, 225, and 325 μm, with porosity of 36-40%. Titanium rods coated with titanium particles were implanted into the femoral medullary canal of dogs. The implants were placed so that they were adjacent to either cortical bone or cancellous bone. Results indicated that the shear interface strength and the mean interface stiffness increased as the pore size decreased.

As observed by several studies, there appears to be an optimum pore size for the promotion of bone ingrowth. When the pore size is too small, the bone ingrowth is not extensive and when then pore size is too large, soft tissue ingrowth occurs to a greater extent. Commercial implants generally have porous coatings with an average pore size between 100 μm and 450 μm.

2.2.4 Other factors

The factors discussed above that affect bone growth are all factors that can be controlled by either the implant design or by surgical technique. There

are also a variety of patient-related factors that cannot be controlled but can affect the extent and rate of bone ingrowth. These include age [27, 28], sex, whether the patient is a cigarette smoker [29], or whether the patient has osteoporosis or other metabolic bone diseases.

2.3 Human and canine bone ingrowth

Since the development of porous coatings, many studies have been conducted both experimentally in animal studies and clinically. Jatsy et al [30] compared the bone ingrowth between a cobalt-chromium spherical beaded coating and a titanium fibre mesh coating. Dogs were implanted with acetabular cups with one or the other porous coating. Six weeks postsurgically, substantial bone ingrowth was observed in both porous coatings and there was no difference in the histological quality of the ingrown bone. However, quantitative analysis showed that there was 10.5% bone ingrowth into the fibre mesh porous coating and 5.5% bone ingrowth into the beaded coating, a statistically significant difference. The mean area density of the ingrown bone was also significantly higher with the fibre mesh and bone penetrated deeper into the implant.

In a canine study of fibre metal porous coatings conducted by Ronningen et al [31], 13 dogs received total surface hip arthroplasties with titanium metal fibre rings molded onto the acetabular prostheses and cobalt-chromium fibre inserts sintered onto the femoral components. Bone ingrowth occurred in 20 of the 26 components, 12 femoral and 8 acetabular components.

Hedley et al [32] implanted dogs with an acetabular cup with a sintered titanium fibre mesh backing. The porous coating was 2-3 mm deep and had an average pore size of 350 μm. Radiologic analysis did not show progressive radiolucencies. Radiolucencies observed after implantation remained stable or lessened, indicating progressive bone ingrowth. Microradiographic analysis

showed calcified tissue within the porous coating, and fluorochrome labeling indicated rapid bone ingrowth during the first three weeks.

Cook et al [33] examined the bone growth into 45 retrieved human femoral components: 35 primary implants and 10 revision implants. Twenty-seven of the primary implants and five of the revision implants exhibited bone ingrowth, though no stem had bone ingrowth into more than 10% of the available porosity. The mean ingrowth occupied 5% of the available porosity.

In 1987 a Co-Cr-Mo prosthesis with a powder-made porous coating was retrieved during a revision operation seven years after a primary total hip arthroplasty. The average pore size was 80 to 100 μm, since it was a very early porous coated stem. The femoral component was well fixed by bone ingrowth and the bone appeared to adhere directly to the porous coating without a layer of connective tissue on the proximal portion of the stem despite the relatively small pore size [34].

Engh et al [35] conducted a 1993 study of nine porous coated acetabular implants that were retrieved at autopsy. The mean implantation time was 50 months. Every component examined displayed bone ingrowth and had a mean bony ingrowth of 32%. A year later, Pidhorz et al [36] also evaluated bone ingrowth into porous coated acetabular components retrieved post mortem. The 11 implants had a mean implantation time of 41 months. The mean bone ingrowth at the bone implant interface within the outer surface of the porous coating and host bone was 29.7 ± 20.1%. Within the porous coating, the mean bone ingrowth was 20.9 ± 16.6%.

A 1995 study by Engh et al [37] of three proximally porous coated and five extensively porous coated femoral implants found that all components had some degree of bone ingrowth, with a mean of 35% of the surfaces exhibiting ingrowth.

To date, histological analysis has shown that bone ingrowth does occur in patients to varying degrees. The results, however, are unpredictable and variable and it is not always possible to predict the clinical outcome for patients. It is still not known what amount of bone ingrowth is required for sustained biological fixation over a long time period.

2.4 Methods of enhancing bone ingrowth

A procedure that accelerates the rate and extent of bone ingrowth would increase the reliability and success of total joint replacement fixation and decrease post-surgical recovery times. Osseointegration is the direct contact of a material to a surface of bone without an intervening layer of fibrous tissue. Osseoconduction is the property of a material to support tissue ingrowth, osteoprogenitor cell growth and development for bone formation to occur. Osseoinduction refers to the ability of chemicals to stimulate primitive stem cells or immature bone cells to grow and mature into healthy bone tissue when implanted into non-bony sites. One of the goals of implant materials is to support osseointegration, which, as previously discussed, is readily achieved by both titanium and cobalt alloy materials. The addition of osseoconductive or osseoinductive agents to implants could enhance and accelerate bone ingrowth. Many different studies have been conducted on a variety of techniques designed to stimulate bone ingrowth. These include autogenous bone graft, allograft, demineralized bone matrix, fibrin glue, calcium phosphate granules, collagen, periosteal activation agent, hydroxyapatite coating, transforming growth factor, bone morphogenic protein, electrical stimulation and bisphosphonate therapy.

2.4.1 Bone graft materials

Autogenous bone grafts have long been the gold standard bone grafting material for filling defects due to trauma or skeletal deficiency diseases.

Allografts and demineralized bone matrix are also used for this purpose. All three materials have been investigated for the purpose of filling defects surrounding joint prostheses. Kienapfel et al [38] investigated the use of cancellous bone autografts and freeze dried allografts for enhancing bone ingrowth into porous coatings. Forty-one dogs were implants with cylindrical titanium implants with titanium fibre metal coating. The implants were placed in an over-reamed cavity of the humerus, creating a 3 mm gap between the implant and the host bone. In one side of each dog, the gap was filled with either autogenic bone particles or freeze dried allogenic bone particles. At four and eight weeks the amount of bone ingrowth was significantly greater for the autograft treated implants than the controls. By eight weeks the controls had approximately 2% bone ingrowth while the autograft treated implants had approximately 13% ingrowth. The allografted implants did not have a significant difference in bone ingrowth compared to the controls.

Greis et al [39] investigated the effect of different defect filling materials on bone ingrowth into fibre metal coated titanium implants. Dogs received total hip arthroplaties and their bony defects were treated either by filling with autogenic bone graft, filling with a mixture of autograft and hydroxyapatite/tricalcium phosphate ceramic, filling with a collagen-hydroxyapatite/tricalcium phosphate-bone marrow mixture, or by leaving the defects unfilled. Animals were sacrificed at 6, 12, or 24 weeks. While the defect filling materials did enhance bone growth into the defects, none of the three grafting materials consistently enhanced bone growth into the porous coating.

Shen et al [40] compared the effects of autogenic bone grafts, allogenic demineralized bone matrix (DBM), and DBM augmented with fibrin glue on bone ingrowth into porous coated titanium alloy implants. The control group received press fit implants, while all others were over-reamed and the gap was filled with one of the graft materials. At 12 weeks, the mean bone ingrowth for the autograft group was 21%, for the DBM group it was 22%, and for the DBM with fibrin glue

group it was 16% showing that all three were approximately equal in promoting bone ingrowth. However, the bone ingrowth of the press fit group was 32%, significantly higher than any of the grafted groups. Cook et al [41] also found that the presence of demineralized bone matrix gel did not enhance or accelerate attachment strength or bone ingrowth and resulted in a significant decrease in implant attachment strength at 3 weeks.

2.4.2 Growth Factors

More recently, with the advancement of recombinant DNA technology and gene cloning, growth factors have been investigated experimentally as osseoinductive agents. Over 30 different molecules have been identified as therapeutic molecules for bone formation. Of these, bone morphogenic proteins (BMPs) are some of the most important. Eight classes of BMP, from BMP-2 to BMP-9, have been identified as osteogenic regulatory molecules. BMPs were first cloned in 1988 by Wozney et al [42], and have been commercially available for more than a decade. Transforming growth factor has also been noted for its ability to augment bone growth.

Sumner et al [43] implanted 10 dogs with titanium-fibre metal coated rods bilaterally in the proximal humerus. All implants had a plasma sprayed hydroxyapatite coating. A 3 mm gap was created between the outer surface of the implant and the surrounding cancellous bone to impede bone ingrowth. In each animal, one implant was treated with recombinant transforming growth factor-β1 (rTGF-β1). Five animals received 335 μg of rTGF-β1 and five animals received 120 μg of rTGF-β1. At four weeks, the amount of bone ingrowth on the side with rTGF-β1 was three times higher than the paired control for the 120 μg dose. The side that received the growth factor had 30% bone ingrowth, compared to 10% on the control side. The animals that received the higher dose

of rTGF-β1 did not have a significantly higher extent of bone ingrowth on the treated side compared to the control side.

Later, Sumner et al [44] implanted porous coated implants bilaterally in dogs for 4 weeks in the presence of a 3 mm gap between the implant and host bone. The test groups had hydroxyapatite coated implants treated with recombinant human bone morphogenic protein-2 (rhBMP-2) at doses of 100 µg, 400 µg, and 800 µg. These were compared to a previously reported control group. The two lower dose groups exhibited significantly more bone ingrowth compared to controls. The 100 µg group had a 3.5 fold increase over the controls. All three rhBMP-2 groups had significantly more bone formation in the gap that the controls, the greatest effect was seen in the 800 µg dose group, with a 2.9 fold increase over the control data.

Itoh et al [45] implanted rats with titanium mesh implants that were uncoated, coated in hyaluronic acid, coated in bone morphogenic protein-2 (BMP-2) or coated in BMP-2 and hyaluronic acid. Histological analysis at 6 weeks showed that the extent of bone growth was greatest in the implants coated with hyaluronic acid and BMP-2, followed by those coated with BMP-2. The control implants and the hyaluronic acid coated implants had less than 5% bone ingrowth. The BMP-2 coated implants had approximately 45% bone ingrowth, while the BMP-2 and hyaluronic acid coated implants had approximately 65% bone ingrowth.

Bragdon et al [46] studied 15 dogs with porous coated total hip replacements. A circular defect was created behind the acetabular component to mimic bone loss. The porous surfaces and the defect were filled with rhBMP and α-bone substitute material (α-BSM), only α-BSM, or nothing. At 12 weeks contact micrographs showed that the control group defects remained nearly empty, while the rhBMP group defects were completely filled with trabecular bone. The α-BSM group had variable amounts of new bone formation in the

defect and some of the α-BSM was retained, the amount retained being relative to the amount of new bone formation. Scanning electron micrographs confirmed what was seen by contact micrograph and showed extensive bony ingrowth into the porous surface of the acetabular cups of the rhBMP group. The control group had a mean area fraction of bone ingrowth of 2.4%, the α-BSM group had mean ingrowth of 13.6% and the BMP group had a mean ingrowth of 22.6%. The control group had a mean appositional ingrowth of 31%, the α-BSM group had 63.9% and the rhBMP group had mean appositional ingrowth of 96.0%.

2.4.3 Hydroxyapatite

Calcium phosphate coatings, such as hydroxyapatite, have been used on orthopaedic implants since the mid 1980s. The most common application technique for calcium phosphate is by plasma spray, by which slightly molten calcium phosphate granules of micron size are applied to a metallic surface. While other calcium phosphates have been investigated, hydroxyapatite, the mineral component in bone, is by far the most used, in a calcium phosphate ratio as close as possible to that of natural hydroxyapatite (1.67). Generally hydroxyapatite coatings are 50-70 μm thick. Coatings that are too thick are brittle and those that are very thin resorb too quickly.

It has been shown that hydroxyapatite is an osseoconductive coating. The bioactivity of hydroxyapatite coatings comes from the chemical and compositional similarity of hydroxyapatite to bone mineral, the provision of supplementary calcium and phosphate for periprosthetic bone formation and the microtopographical environment provided for osteoblast colonization [47]. When a hydroxyapatite coated prosthesis is implanted, calcium and phosphate ions are released from the coating into the extracellular space. It is believed that the ion release creates an electromagnetic potential between the coating and the extracellular space, which leads to the precipitation of physiologic calcium carbonate onto the hydroxyapatite coating. When the surface becomes coated

with natural carbonated hydroxyapatite, the physiologic cascade of bone formation begins, leading to osseointegration [48-51].

In experimental canine studies, hydroxyapatite coated hip implants had improved bone ingrowth when compared to titanium press fit or porous coated implants after two to five years. With good initial implant stability, hydroxyapatite coated implants can bridge bone deficiencies as great as 2 mm [52], whereas porous metal coatings can only bridge up to 0.3 mm [53].

Stewart et al [47] investigated the effect of a hydroxyapatite/tricalcium phosphate coating on plasma-sprayed titanium implants in a rabbit model. One, three and six months post-surgically, they found that the hydroxyapatite/tricalcium phosphate coating increased bone apposition and increased both the rate and amount of bone formation on the surface of the implant when compared to controls.

Oonishi [54] prepared titanium implants with titanium sintered beads as the porous surface and coated half with hydroxyapatite. When implanted into rabbit femora, the rate of bone ingrowth was much faster with hydroxyapatite than without. At two, four, and six weeks the mean bonding strength was greater with hydroxyapatite than without hydroxyapatite, but by 12 weeks the mean bonding strength for both types of implants was the same.

Cook et al [55] implanted canine femora with titanium implants. The implants had a solid core and a porous coating of sintered titanium particulate. Mean pore size was 250 μm. Half of the implants received an additional hydroxyapatite coating, applied by plasma spray. Hydroxyapatite did not significantly increase the fixation strength of the implant. Histologically, both implants had bone ingrowth, the amount increasing with time. By 12 weeks, there was extensive bone ingrowth, organization and mineralization. At the bone-implant interface, the hydroxyapatite-coated implants had mineralization

directly on the surface, while the non-hydroxyapatite coated implants had a thin layer of connective tissue between the titanium and bone.

Jatsy et al [56] investigated the effect of a 50 μm thick plasma sprayed calcium phosphate coating on bone ingrowth into a titanium fibre mesh porous surfaced prosthesis in a canine model. At three weeks, there was significantly more bone ingrowth in the hydroxyapatite coated components that in the control components, provided that there was good initial contact between the bone and the implant. By six weeks, there was no difference in the degree of ingrowth between the two implant types. A closer contact of the ingrown bone and the implant occurred for the hydroxyapatite coated implants. However, when there were gaps between the implant and the bone, hydroxyapatite was not effective in bridging the gap.

A recent study by Tanzer et al [57] investigated whether the addition of hydroxyapatite and tricalcium phosphate to a porous coating would improve clinical and radiographic outcomes of cememtless femoral components of total hip arthroplasy. Patients received either an uncoated proximally porous-coated multilock femoral component or the same femoral component with a hydroxyapatite and tricalcium phosphate coating on the porous portion of the femoral stem. At two years, there were 159 non-coated hip stems and 159 coated stems. At a 2-5 year follow-up, no implants were revised due to aseptic loosening, there was no difference in clinical function and the frequency of bony ingrowth was almost the same in the two groups. However, the hydroxyapatite and tricalcium phosphate group had significantly fewer radiolucencies adjacent to the porous coating, which indicates improved osseointegration over non-hydroxyapatite coated implants.

However, Hacking et al [58] conducted a study to determine the relative contributions of chemistry and topography to the osseointegration of hydroxyapatite coatings. A canine femoral intermedullary implant model was

used, with titanium implants that were polished, grit-blasted, plasma-sprayed with hydroxyapatite, or plasma-sprayed with hydroxyapatite and masked with a thin layer of titanium applied by physical vapour deposition. The thin layer of vapour deposited titanium served to mask the chemistry of the hydroxyapatite, while conserving the surface topography. At 12 weeks, bone apposition averaged 3% for polished implants, 23% for grit-blasted implants, 74% for hydroxyapatite-coated implants, and 59% for titanium masked hydroxyapatite-coated implants. The extent of bone apposition was significantly greater for the hydroxyapatite-coated implants compared to the titanium masked implants, though it appeared that 80% of the bone forming response was due to the implant surface topography and not to the chemistry of the hydroxyapatite.

Hydroxyapatite coatings do have some disadvantages, including the fatigue of the coatings, delamination of the coating layer, premature coating dissolution, contribution to the wear particle load, and disguising the microtexture of the underlying surface. Some studies have shown that the dissolution of the coating leaves the implant without any bone contact. The initial increase in bone contact decreases over time, eventually leading to lower bone contact than found with non-hydroxyapatite coated implants. Decreased bone contact causes implant mobility and eventual loosening. Darimont et al [59], though, observed the behaviour of a hydroxyapatite coating on plasma-sprayed titanium implants and found that close bone contact protected the hydroxyapatite from resorption. After a year, hydroxyapatite coatings that were closely apposed to bone showed little dissolution.

2.5 Bisphosphonates

Bisphosphonates are pharmaceutical agents that are chemical analogues of pyrophosphate; a carbon atom replaces the oxygen atom that links the two phosphate groups of pyrophosphate. Pyrophosphate, which is produced by many anabolic processes, is a physiological regulator of calcification and bone

resorption. Bisphosphonates are completely resistant to hydrolysis. They bind to the hydroxyapatite crystals of bone via the P-C-P chemical structure and prevent the growth and dissolution of the bound crystals [60]. As carbon has a valence of 4, there are two other groups, R_1 and R_2, bonded to the central carbon in addition to the two bound phosphate groups. Most bisphosphonates that have been developed to date have a hydroxyl group at one site and a carbon chain at the other site. Many different bisphosphonates have been developed, and the differentiating characteristic between the various drugs are the side chains R_1 and R_2 (figure 2.4). A hydroxyl group side chain (-OH) enhances the binding of the bisphosphonate to bone mineral crystals. The structure and configuration of the other side chain (R_2) determines the bisphosphonate's cellular effects and its efficacy as a bone resorption inhibitor [61]. A primary nitrogen atom, which is a nitrogen atom that is only bound to one carbon atom, in the R_2 alkyl chain, such as in pamidronate and alendronate, increases the potency of the bisphosphonate about one hundred times over those without a primary nitrogen, such as etidronate. The effectiveness of bisphosphonates is further increased when R_2 contains a tertiary nitrogen atom, as in ibandronate. The most recent generation of bisphosphonates, including zoledronate, contain a nitrogen atom in a heterocyclic ring on the R_2 side chain and are up to 10 000 times more potent than the first generation bisphosphonates.

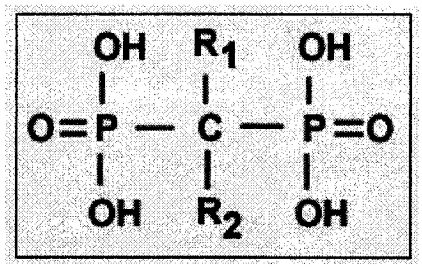

Figure 2.4 - Bisphosphonate structure

While the P-C-P structure of a bisphosphonate can bind to hydroxyapatite and prevent dissolution of bone mineral, the main mechanism of action of bisphosphonates involves the disruption of cellular processes of bone building

and bone absorbing cells. This is especially true in the newer generation bisphosphonates that are very potent. Due to the high level of potency of these bisphosphonates, the dosage received by patients is very small and therefore there is not enough of the drug present to effectively prevent bone mineral dissolution. Osteoclasts are bone cells that resorb bone mineral and osteoblasts are bone cells that deposit bone mineral. Bisphosphonates affect the osteoclasts by inhibiting their activity. The exact mechanism of osteoclastic inhibition is unknown, though there is evidence that bisphosphonates can trigger osteoclastic inhibition both directly or indirectly. The mechanism of inhibition is based on whether the osteoclast consumes the bisphosphonate-bound hydroxyapatite or the drug interacts with the osteoclast externally. There is also evidence that osteoblasts are affected by bisphosphonates by either increasing inhibitors or decreasing promoters of osteoclast formation and recruitment.

2.5.1 Clinical Applications of Bisphosphonates

Bisphosphonates have been shown to be clinically effective in reducing bone loss in many conditions associated with accelerated bone turnover, such as Paget's disease of bone [62] and metastatic [63], osteolytic [64], postmenopausal [65] or steroid induced [66] bone loss. A single-dose infusion of pamidronate has been shown to have a prolonged effect on bone turnover [1]. Alendronate is commonly used as an anti-resorptive pharmalogical agent, effective for reducing bone resorption, increasing bone density and decreasing the incidence of fracture in osteoporotic women [67]. Little et al [68] found that zoledronate improved femoral head sphericity in a rat model of perthes disease and increased the bone mass density. The ability to reduce bone loss makes bisphosphonates suitable to either prevent periprosthetic bone loss or enhance bone growth into implants with porous coatings.

2.5.2 Bisphosphonate Chemical Affinity for Hydroxyapatite

All bisphosphonates have a natural chemical affinity for hydroxyapatite. Bisphosphonates loosely bind to HA when exposed to the mineral. Studies have shown that the degree of affinity and the strength of the binding to the hydroxyapatite is not related to the type of bisphosphonate. All bisphosphonates, regardless of their R_2 groups, have roughly the same binding capacity to hydroxyapatite, though the presence of a hydroxyl group at the R_1 position does enhance binding to hydroxyapatite. Since both pamidronate and zoledronate have a hydroxyl group in the R_1 position, it can be expected that the release rates of pamidronate and zoledronate from hydroxyapatite would be similar.

2.5.3 Bisphosphonates – Bone Ingrowth Applications

Iwase et al [2] surgically inserted a Kirshner wire into the femur of rats and infused high density polyethylene particles continuously into the knee joint, to induce osteolysis. The rats were divided into two groups and one group received subcutaneous injections of saline while the other received injections of the bisphosphonate TRK-530. The rats that were given the TRK-530 had significantly thinner interfacial membranes and there were significantly fewer osteoclast-like cells surrounding the wire when compared to the control group. Also, there was a higher frequency of peri-implant osteolysis in the control group than in the bisphosphonate group.

Von Knoch et al [69] studied the effect of zoledronate on particle induced osteolysis with a murine calvana osteolysis model. Mice were implanted with polyethylene particles and received one of three treatments: no zoledronate, a subcutaneous injection of zoledronate directly following surgery, or a subcutaneous injection of zoledronate 4 days after surgery. All animals were sacrificed 14 days postoperatively. Bone resorption was lower in both groups

treated with zoledronate compared to the bone resorption in animals that did not receive bisphosphonate therapy.

J. Astrand et al [70] surgically implanted a titanium plate with a threaded hole fitted with a central plug on the proximal tibia of 26 male rats. After 28 days, the plug was removed, a topical treatment was administered and a pressure piston was inserted into the hole. Half of the rats received a treatment of 20 µl of 1 mg/ml alendronate solution, while the other half received the same volume of saline. Five days were given for fibrous tissue to form before applying cyclic pressure to the tissue. The group treated with bisphosphonate displayed less resorption of cortical bone under the plate and showed signs of increased remodeling. The rats treated with alendronate also had significantly smaller areas of soft tissue, which indicates less resorption.

Frenkel et al [67] used an implantable bone growth chamber to evaluate bone integration with surfaces commonly used in uncemented total hip arthroplasty when the patient is systemically treated with alendronate. Half of the canine subjects were given an ovariectomy, to simulate an estrogen deficiency, and fed at low calcium diet. The intact animals and the ovariectomy animals were then divided into an alendronate treatment group and a placebo group. Alendronate was injected subcutaneously three times a week from the seventh postoperative day until sacrifice. The intact dogs treated with the bisphosphonate had 84.0% bone penetration, while the untreated dogs had 75.9% penetration. Bone penetration in the OVX alendronate treated dogs was 92.0%, while the bone penetration was 69.5% in the group without the drug. The results showed that there was no detectable effect on bone growth or strength of attachment at the bone-implant interface.

Soininvaara et al [71] investigated the use of alendronate to inhibit early bone mineral density loss after total knee arthroplasty. Patients were divided into two groups. The first group received 500 mg of calcium carbonate per day, while

the other group received 500 mg of calcium carbonate and 10 mg of alendronate orally per day. At a one-year follow up, the bone mineral density was measured with fan-beam dual-energy X-ray absorptiometry. The group only receiving calcium showed a significant decrease in the bone mineral density, one year postoperative. The alendronate group did not have a significant reduction in bone mineral density.

Wilkinson et al [72] investigated the effect of a single systemic pamidronate dose on periprosthetic bone turnover and pelvic implant migration over two years following total hip arthroplasty. Five days after surgery, 22 patients received a 90 mg dose of pamidronate and 22 patients received a placebo. At various intervals over two years radiographs were taken, and bone mass density and biochemical markers of bone turnover were measured. Pamidronate therapy reduced both femoral bone loss and bone turnover compared to the placebo group, but was not shown to reduce acetabular cup migration.

In a recent study, Bobyn et al [73] placed porous tantalum ulnar implants bilaterally in seven dogs and administered a single post-operative intravenous dose of zoledronate to each animal. The ulnae were harvested for histological analysis after six weeks and the extent to bone ingrowth was compared to that observed in previous control animals. The control implants had a mean bone ingrowth of 6.6% and the zoledronate treated implants had a mean bone ingrowth of 12.2%, a relative difference of 85%, which was statistically significant (figure 2.5). The number of new bone islands found within the implants was similar for both groups, but the islands in the zoledronate treated implants were 69% larger than those in the controls. These results indicated that the administration of zoledronate caused a net gain in bone growth into porous tantalum implants.

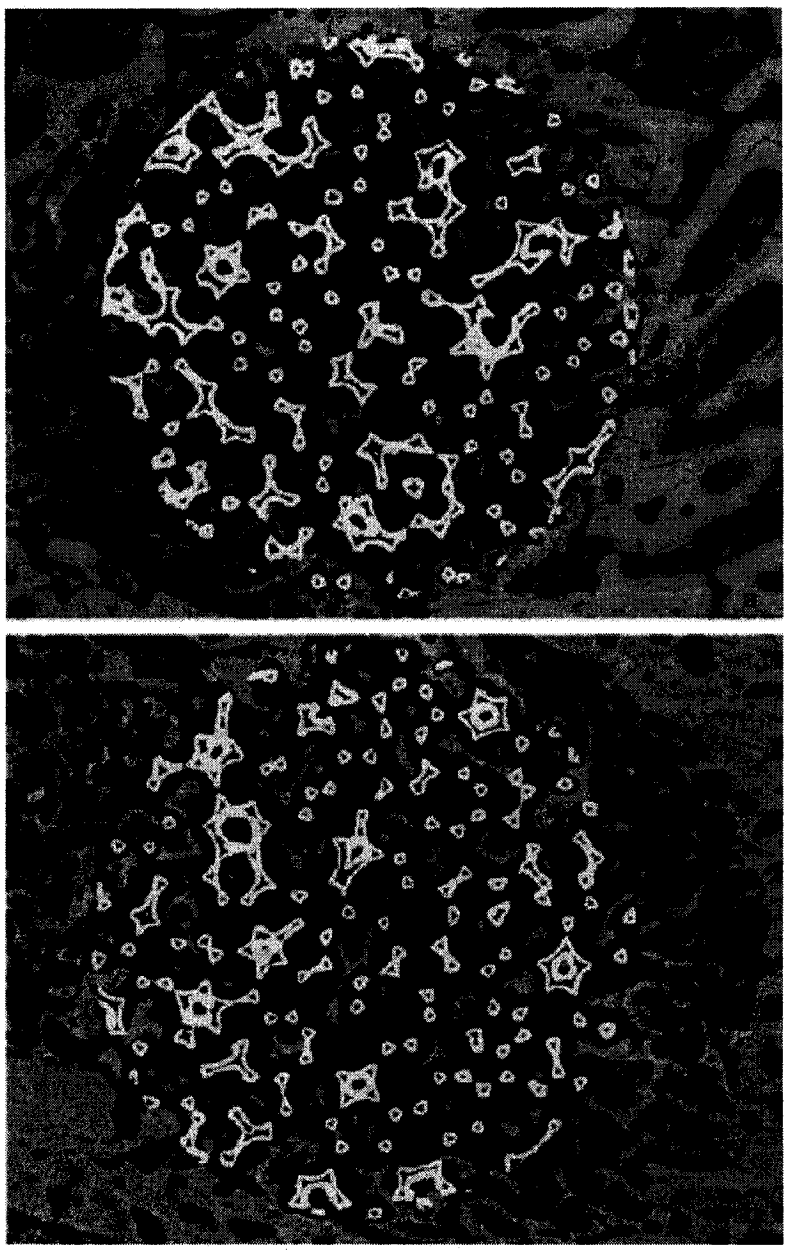

Figure 2.5 - SEM of bone growth into porous tantalum implants. The tantalum struts appear as white, bone as gray, and void space as black. (a) Control implant with 5.9% bone ingrowth and (b) zoledronate-treated implant with 12.9% bone ingrowth [73].

2.5.4 Local Delivery of Bisphosphonates for Bone Ingrowth Enhancement

In the past five years, various bisphosphonates have been used both in animal studies and clinical trials in an attempt to reduce periprosthetic bone loss and increase fixation of the implant to the bone. Methods of administration and doses have varied, but bisphosphonate treatment appears to minimize periprosthetic bone resorption. However, systemic administration is neither necessary nor ideal for joint replacement patients, given the need to affect the bone only immediately adjacent to the implant. In this regard it would seem that a local administration method is of interest. Local administration using both hydroxyapatite and fibrinogen for controlled release of bisphosphonates has also been investigated.

H. Denissen et al. [74] were the first to use hydroxyapatite as a bisphosphonate delivery system. Hydroxyapatite powder was precompressed into a metal mould and sintered into either macroporous (100-250 μm) or microporous (1-5μm). Cylindrical implants were machined from the bulk material. A ^{14}C-labelled bisphosphonate was applied to each of the implants by adsorption. The implants were each placed in solution and a vacuum was applied to remove air from the pores. The implants remained in the bisphosphonate solution under continuous stirring at 37°C for one week. The release rate of the bisphosphonate was measured by placing the implants in saline at 37°C and by measuring the amount of ^{14}C twice a week over three months. During the first three months, the microporous implants released 2.66% of the loaded bisphosphonate and the macroporous implants released 27.5% of bisphosphonate.

Yoshinari et al [75, 76] immobilized bisphosphonate onto calcium phosphonate-coated titanium implants. The titanium was grit blasted; some implants had no coating, some were CaP coated by plasma spray, and some were CaP coated and then soaked in a pamidronate solution. The implants were placed into beagle dog mandibles in bone cativites. The largest amount of bone

contact was found around the bisphosphonate-immobilized implants 12 weeks after implantation. However, the addition of the bisphosphonate to the implant did not result in a significant improvement, which could have been due to the release amounts, the release timing, the continuity of release or the direction of the histological samples.

Meraw et al [77, 78] used a similar approach in local administration of bisphosphonate from titanium implants and measured the periprosthetic bone per area and rate of bone growth. Forty-eight dental implants, divided evenly into four types: hydroxyapatite (HA)-coated implants with alendronate, titanium machine-polished (TMP) implants with alendronate, HA-coated implants without alendronate, and TMP implants without alendronate, were implanted into six adult male hound dogs. The periprosthetic bone per area increased significantly with alendronate treatment compared to the control group, with a mean increase of 5.8% [77]. Using intravenously administered fluorescent labels, the rate of bone formation was determined by measuring the distance between the labels [78]. The alendronate-coated implants had a mean inter-fluorescent label width of 0.02 mm from day 0 to day 6, and the control implants had a mean width of 0.01 mm. From day 6 to day 22, the bisphosphonate treated implants had a mean width of 0.036 mm, while the inter-fluorescent label width was 0.017 mm for the control implants.

Kajiwara et al [79] implanted 30 rats with one of three types of tibial implants: titanium, calcium-ion implanted titanium, or calcium-ion implanted titanium with immobilized pamidronate. Pamidronate was applied to the implants by immersing the calcium-ion implanted titanium implants in a 3 mg/ml pamidronate solution for 24 hours. The bone was labeled with fluorochromes at one week and three weeks, and after 4 weeks the extent of bone growth was determined by measuring the width of new bone around each implant. At one week, three weeks and four weeks the new bone growth was significantly wider around the pamidronate dosed implants than around either of the other groups.

Peter et al [80] divided rats into five groups and implants their femurs bilaterally with hydroxyapatite-coated titanium cylinders dosed with one of five amounts of zoledronate: 0 μg, 0.2 μg, 2.1 μg, 8.5 μg, or 16 μg. To apply the zoledronate to the implants, the implants were immersed for 48 hours in varying concentrations of aqueous zoledronate solution. The variability of zoledronate concentration in solution resulted in different doses of zoledronate loaded onto the implants. After three weeks, the implants were harvested for analysis of bone density and mechanical testing. In the 20 μm closest to the implant surface, the two lowest doses of zoledronate (0.2 μg and 2.1 μg) resulted in the highest bone density. Bone density decreased with increasing distance from the implant, though it remained greater than that observed in all other cases. The implants with 8.5 μg of zoledronate had lower but more constant bone density between the implant surface and 200 μm from the surface. The bone density was lowest in the first 20 μm surrounding the implants with no zoledronate and those with 16 μg of zoledronate. However, at increased distances from the implant surface the bone density increased for the 16 μg zoledronate-dosed implants, but decreased for the implants without zoledronate. Mechanical tests showed that the pull out force increased with increasing zoledronate dose up to 2.1 μg, but then decreased with increasing zoledronate dose for the two higher doses. The pull out force for the 8.5 μg and 16 μg doses was lower than that for the untreated implants. The results indicated that zoledronate can have a positive effect on bone density and mechanical fixation, though positive results are dose dependent and larger doses of zoledronate may have a negative effect on bone remodeling and biological fixation.

P. Tengvall et al [81] used surface modified stainless-steel screws to immobilize two bisphosphonates on the surface. The screws were further coated with ten layers of fibrinogen and pamidronate was immobilized onto fibrinogen using a coupling technique. A second bisphosphonate, ibandronate, was spontaneously adsorbed during overnight incubation. Bisphosphonate elution from the screw was determined by the incubation of the screws in distilled water

for up to 24 hours at room temperature, followed by surface drying and mass determination by null ellipsometry. The ibandronate layer decreased from 6 Å to 3 Å, but the pamidronate-fibrinogen layer remained constant. Screws prepared in the same way were also inserted into the tibia of male rats. The rats were sacrificed 14 days post-operatively and the screws were tested for pull-out strength. The bisphosphonate coated screws had a mean 28% increased pullout force at failure and 90% increased pullout energy compared to the controls.

Over the past several years there has been an evolution in orthopaedic implants. The addition of porous coatings to implant surfaces has created a means for biological fixation while reducing the amount of native bone that needs to be removed for prosthesis implantation. Optimization of physical variables has improved the extent of bone growth that occurs naturally. However, bone ingrowth remains unpredictable and is uncertain for patients such as those with osteoporosis or other bone diseases, or in revision cases where native bone stock is compromised. Various methods for enhancing bone ingrowth have been studied, with mixed results. The use of bisphosphonates is one of the more recent methods for bone ingrowth acceleration that has been investigated. Bisphosphonates have been shown to increase net peri-implant bone formation when delivered locally from dental implants. Systemic administration of bisphosphonates has been shown to prevent peri-prosthetic bone resorption, but has not necessarily augmented bone ingrowth. A method for local delivery of bisphosphonates from orthopaedic implants should be further investigated for its potential in enhancing the biological fixation of arthoplasty devices.

Chapter 3. Purpose

Bisphosphonates have been shown to both alter bone remodeling when administered systemically and enhance bone formation when delivered locally in dental applications. Therefore, it is logical to investigate orthopaedic applications of bisphosphonates and their ability to enhance bone formation when delivered locally from orthopaedic implants.

This thesis was designed to characterize an appropriate method of bisphosphonate delivery using porous tantalum orthopaedic implants as a carrier. The natural chemical affinity of bisphosphonates for hydroxyapatite and the current clinical use of hydroxyapatite as an osseoconductive coating on orthopaedic implants rendered hydroxyapatite a good candidate for a drug delivery system. The purpose of this study was to apply a bisphosphonate compound directly onto porous tantalum implants with and without hydroxyapatite coating and to measure the drug elution as a function of time. This required development of an appropriate chemical assay for measuring the bisphosphonate concentration in solution.

Chapter 4. Materials and Methods

4.1 Implants

4.1.1 Introduction to porous tantalum

Tantalum is a transition metal of atomic number 73 and an atomic mass of 180.9. Located in group VA in the periodic table, tantalum is highly biocompatible, corrosion resistant, strong and tough [82]. Tantalum was first used as an implant material by Burke in 1940 [83]. Porous tantalum is a structured form of tantalum that consists of regular, interconnecting pores that are formed by a continuous, three-dimensional lattice of struts. To manufacture porous tantalum, first a vitreous carbon skeleton with interconnecting dodecahedron shape is made by pyrolysis of a thermosetting polyurethane foam substrate. Tantalum is then deposited onto the carbon skeleton using chemical vapour infiltration technology. The tantalum is deposited to a depth of 40 to 50 μm, thereby retaining the porosity of the carbon skeleton (figure 4.1).

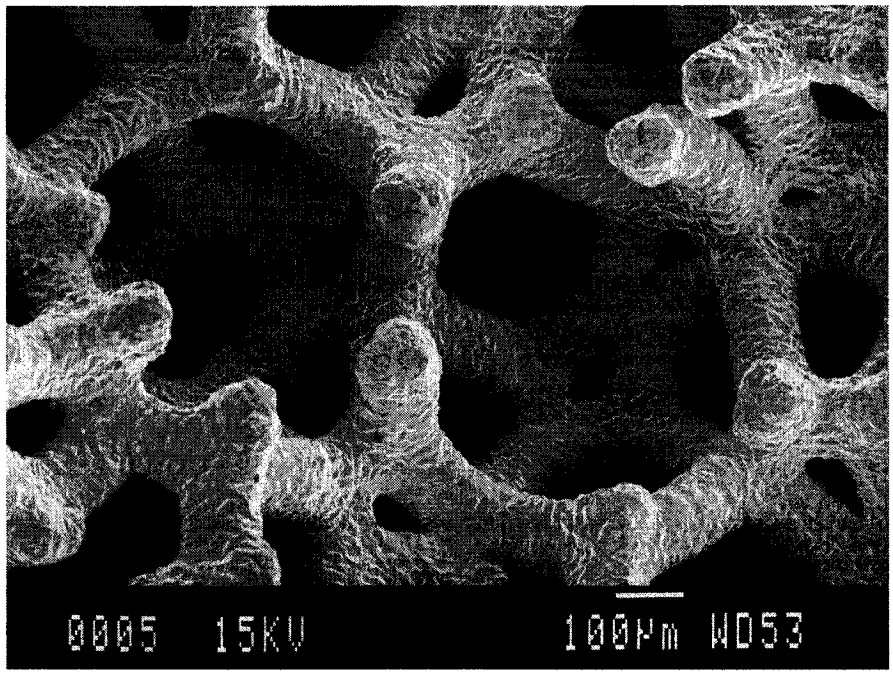

Figure 4.1 - Scanning electron micrograph (SEM) of porous tantalum

4.1.2 Rationale for using porous tantalum

There are several types of implants that could have been selected for this type of application, such as titanium or cobalt-chromium alloy, with a variety of porous coatings, such as sintered beads, fibre metal, or plasma sprayed. Porous tantalum was selected for a variety of reasons. Porous tantalum is more porous than other types of porous coatings, with a porosity of approximately 80%, compared to sintered beads (30%-35%) [24] and fibre metal (40%-50%) [84]. The greater degree of porosity of porous tantalum gives more available area within the implant for bone ingrowth, allowing for the development of a strong bone-implant interface. Porous tantalum also has desirable mechanical characteristics (table 4.1 [85]). It is less stiff than other implant metals, with an elastic modulus close to that of bone, therefore it causes less stress shielding of surrounding bone. Porous tantalum has an average pore size of approximately 450 µm [86], which is within the range of pore sizes conducive to bone ingrowth. Due to the interconnected, continuous structure of the struts it has a high strength to weight

ratio. It can be used as both a bulk material or as an implant coating. The material can easily be made into a variety of shapes. The chemical vapour deposition/infiltration of tantalum onto the carbon skeleton also results in a surface microtexture that may be conducive to stimulating osteogenesis.

Table 4.1 - Mechanical characteristics of porous tantalum

Compressive strength	60 ± 18 MPa
Tensile strength	63 ± 6 MPa
Bending strength	110 ± 14 MPa
Compressive strength fatigue endurance limit	23 MPa at 5 x 10^6 cycles
Cantilever bending fatigue endurance limit	35 MPa at 5 x 10^6 cycles

Clinically, porous tantalum has exhibited interesting bone ingrowth characteristics, showing increased bone ingrowth and interface strength over other porous technologies. Cortical implants of porous tantalum implanted into canine femora had 52.9% bone ingrowth after four weeks and 79.7% bone ingrowth by 52 weeks. Push out tests, designed to measure the shear strength of the bone-implant interface, indicated that the fixation strength at four weeks was greater than that observed with other types of porous coated implants. For example, the mean shear fixation strength of porous tantalum was 18.5 MPa, compared to 9.3 MPa for beaded cobalt-chrome implants [84]. Acetabular cups with a porous tantalum backing were studied in a canine total hip replacement model and all implants showed a stable bone-implant interface and regions of bone ingrowth after 6 months [87]. The extent of bone ingrowth was similar to that reported for canine acetabular cups with fibre metal and cobalt-chrome beads [31]. Porous tantalum has also been shown to allow rapid vascularized soft tissue ingrowth, with ingrowth across the entire depth of subcutaneous implants after 4 weeks. Higher fibrous tissue attachment strength was demonstrated to develop in comparison with porous coatings made of cobalt-chromium beads [88]. Clinical studies of various porous tantalum implants have

recently demonstrated consistent radiographic stability coupled with excellent clinical function [89].

4.1.3 Hydroxyapatite coating

Some of the porous tantalum implants in this study were coated with a thin layer of hydroxyapatite. Hydroxyapatite is the main mineral component of bone and has been widely used as a coating on orthopaedic implants to enhance bone ingrowth (as an osteoinductive agent). Commercially pure hydroxyapatite was applied to the porous tantalum by plasma spray techniques. The resulting coating of hydroxyapatite was 12- 15 μm thick. The line-of-sight plasma spray coated only the outermost 1-1.5 mm of the tantalum struts, leaving the interior struts uncoated by hydroxyapatite. The thin coating of hydroxyapatite did not significantly occlude the implant pores (figure 4.2).

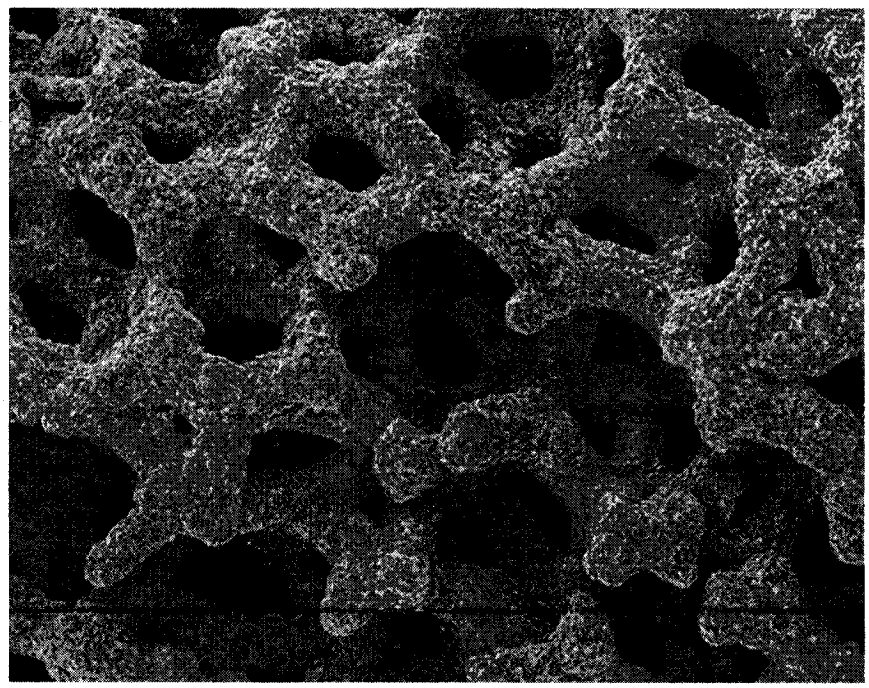

Figure 4.2 - SEM of hydroxyapatite-coated porous tantalum

4.1.4 Porous tantalum implants

The tantalum implants used in this study measured 50 millimetres in length and 5 millimetres in diameter (figure 4.3). This size of implant was for eventual use as an ulnar implant in a canine model to assess the effects of bisphosphonate release on bone ingrowth. All of the implants were manufactured by Implex Corp (Allendale, NJ). One group of implants was left as-manufactured while a second group was coated with hydroxyapatite, as described earlier (figure 4.4).

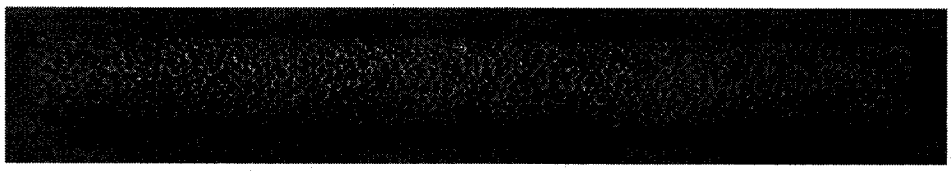

Figure 4.3 - Tantalum ulnar implant

Figure 4.4 - Hydroxyapatite-coated tantalum implant

4.1.5 Titanium Implants

In addition to the porous tantalum implants, hydroxyapatite-coated solid titanium rods were also manufactured (figure 4.5). The solid titanium rods were also 50 mm in length and 5 mm in diameter. All of the implants were manufactured by Implex Corp (Allendale, NJ) These solid titanium cylinders were coated with hydroxyapatite, as previously described. Solid rods were used to further ensure that the hydroxyapatite was responsible for any prolonged bisphosphonate elution that occurred, as opposed to the bisphosphonate remaining in the pores of the porous tantalum implants. Titanium, a metal commonly used in orthopaedic implants, was selected because it is less

expensive than tantalum and because the bulk material of the solid implants was relatively inconsequential given that the implant surface was covered by hydroxyapatite.

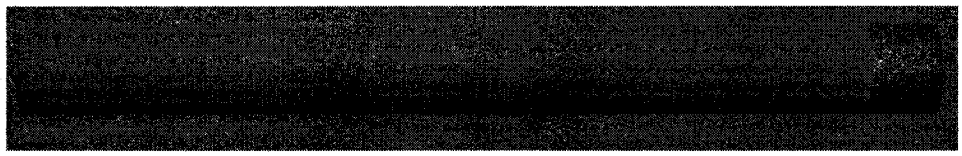

Figure 4.5 - Hydroxyapatite-coated titanium implant

4.2 Pamidronate

Pamidronate, disodium-3-amino-1-hydroxypropylidene-1,1-bisphosphonate, is a second generation bisphosphonate. It contains a primary nitrogen in the R_2 side chain (figure 4.6). The presence of the primary nitrogen enhances the potency of pamidronate compared to first generation bisphosphonates, such as clodronate and etidronate, so pamidronate is approximately 10 times stronger than those bisphosphonates. At therapeutic doses, pamidronate does not interfere with bone mineralization. The primary uses of pamidronate are for malignancy-related hypercalcemia, multiple myeloma, and osteolytic bone metastases. Pamidronate doses are given by intravenous infusion because oral absorption of pamidronate is less than 1%. The pharmaceutical composition of clinically used pamidronate (Aredia) is 30 mg, 60 mg or 90 mg of pamidronate disodium and 470 mg, 400 mg, or 375 mg of mannitol respectively. For infusion, the powder is reconstituted in 0.9% saline, though that solution is basic (pH ~ 8.3) so phosphoric acid is added to reduce the pH to 6.3 However, pure pamidronate was used for all experiments described in this study. All pamidronate samples were prepared by first weighing a sample of pamidronate in a clean and dry beaker. The pamidronate was then dissolved

in water with swirling to ensure the complete dissolution of the drug. The properties of pamidronate disodium can be found in table 4.2.

Table 4.2 - Characteristics of pamidronate disodium

Chemical name	disodium-3-amino-1-hydroxypropylidene-1,1-bisphosphonate
Empirical formula	$C_3H_9NO_7P_2Na_2$
Molecular weight	279.04 g/mol
Description	White crystalline powder
Solubility	Soluble in water and 2N NaOH solution Poorly soluble in 0.1 N HCl and 0.1N acetic acid Insoluble in organic solvents
pH	1% solution of pamidronate has a pH of ~ 8.2

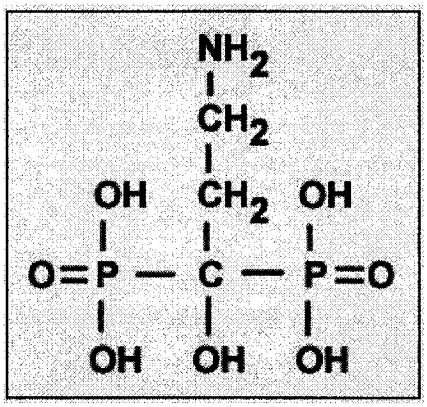

Figure 4.6 - Chemical structure of pamidronate

4.3 Zoledronate

Zoledronate, (1-hydroxy-2-imidazol-1-ylphophonoehthyl) phosphonic acid, is a third generation bisphosphonate. It contains a nitrogen atom in a heterocyclic ring in the R_2 side chain (figure 4.7). The presence of the nitrogen atom in a heterocyclic ring further enhances the potency of the drug and

zoledronate has been reported to be up to 10 000 times more potent than first generation bisphosphonates. The pharmaceutical formulation of zoledronate (Zometa®, Novartis) is 4.264 mg of zoledronic acid, 220 mg of mannitol, and 24 mg of sodium citrate. The mannitol is added as a bulking agent and sodium citrate is a buffering agent. The properties of zoledronate can be found in table 4.3.

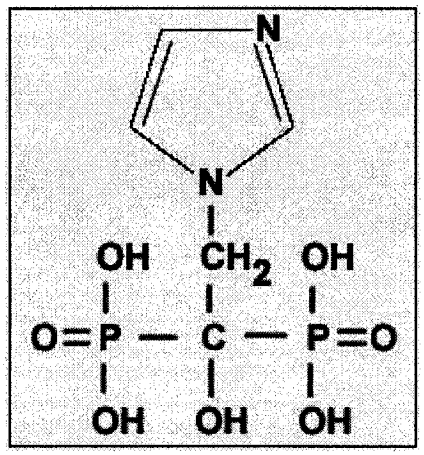

Figure 4.7 - Chemical structure of zoledronate

A vial of Zometa (figure 4.8) was reconstituted with distilled water, using a syringe to inject 4 ml of distilled water through the septum in the top of the Zometa vial. Zometa was then divided into 0.05 mg aliquots by placing 50 µl of the zoledronate solution into clean glass vials. Distilled water (450 µl) was then added to each vial, for a total volume of 500 µl. This resulted in 80 vials of Zometa, each containing 0.05 mg of zoledronic acid. The vials were then placed in the freezer and removed as required.

Table 4.3 - Characteristics of zoledronic acid

Chemical name	(1-hydroxy-2-imidazol-1-ylphophonoehthyl) phosphonic acid
Empirical formula	$C_5H_{10}N_2O_7P_2 \cdot H_2O$
Molecular weight	290.1 g/mol
Description	White crystalline powder
Solubility	Soluble in 0.1N NaOH solution Sparingly soluble in water and 0.1N HCl Insoluble in organic solvents
pH	0.7% solution of zoledronic acid has pH of ~2.0

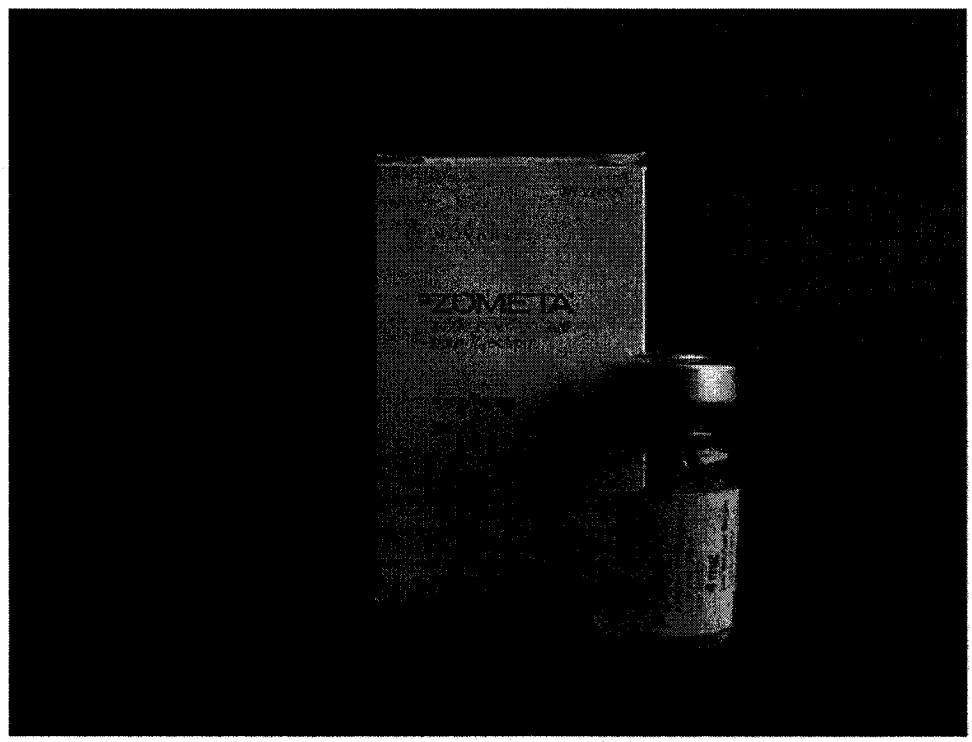

Figure 4.8 - Zometa packaging

4.4 Application of Bisphosphonate Coating to Implants

Porous tantalum ulnar devices were coated with aqueous solutions of either pamidronate or zoledronate. The implants were weighed prior to being coated. During the coating process, the implants were held by the ends in a jig so that all surfaces of the implant could be easily accessed (figure 4.9). One of the end pins was fixed, while the other could be turned, allowing the implant to be rotated.

Figure 4.9 - Tantalum implant in jig for coating

Pamidronate (2.1 ± 0.1 mg) was dissolved in 500 µl of distilled water. Using a micropipette, in increments of 50 µl, the entire volume of pamidronate was progressively applied to each implant. Small droplets were pipetted onto the implants along the top surface of the implant approximately ever 5 mm. The implant was then rotated on the jig by 45° and another row of drops of bisphosphonate solution was applied. The hydroxyapatite wicked the solution into the implant pores and onto the HA-coated tantalum struts. When covered

with the entire volume of the solution, the implant and jig were placed in an oven at 37°C to dry for 48 hours.

Implants were dosed with zoledronate in a similar method. A vial containing 0.05 mg of reconstituted zoledronate in 500 µl of solution, was removed from the freezer and thawed at room temperature. The entire contents of the vial were then applied evenly to each implant. The implant in the jig was then placed in the oven at 37°C to dry for 48 hours.

Porous tantalum implants that did not have hydroxyapatite coating were also dosed with bisphosphonate for use in elution studies in a similar manner. However, the absence of hydroxyapatite and the slightly hydrophobic nature of tantalum caused the aqueous solution to bead on the implant. To ensure uniform coating of the implant, the pipette tip was used to push the beads of solution together so that there was a layer of solution on the implant surface. Because the bisphosphonate solution stayed at the surface of the implant, all of the drug solution could not be added at one time. The non-hydroxyapatite coated implants were covered with a thin layer of solution and placed in an oven at 37°C for approximately half and hour to evaporate some of the solution before adding the remaining drug. Generally this was repeated a couple of times to apply the entire volume of solution. Once the entire volume of drug solution had been applied, the implant in the jig was placed in the oven at 37°C to dry for 48 hours.

Coating the hydroxyapatite-coated solid titanium implants was performed in a manner similar to that of the non-hydroxyapatite coated porous tantalum. While the implants had a hydroxyapatite coating, the implants were solid, leaving no pores for the solution to be wicked into. Therefore the applied solution sat on the implant surface and had to be applied in stages. However, instead of beading on the surface, the bisphosphonate solution tended to pool. A row of droplets was applied to the implant, which pooled together. The implant was

then placed in the oven until dry enough to rotate and apply another row of droplets.

4.5 Sterilization

Prior to surgery, all implants need to be sterilized. Therefore it was important to also investigate the elution profile of bisphosphonate from sterilized implants to ensure that the sterilization process did not negatively affect the release of bisphosphonate from hydroxyapatite coating. Three zoledronate-dosed HA-coated porous tantalum implants were sterilized with ethylene oxide. Ethylene oxide (EtO) is a gas well known for its biocide properties and is commonly used as a sterilizing agent in both industrial and hospital settings. EtO kills bacteria through alkylation, which prevents cells from reproducing. The item to be sterilized is wrapped inside a gas permeable protective layer and placed in a pressurized chamber with a temperature between 50°C and 80°C. EtO gas is then introduced to the chamber and the device is exposed to the gas for 4 to 5 hours. The EtO is then evacuated from the chamber and the chamber is purged to remove all of the EtO. EtO provides a very efficient means of sterilization with a high degree of penetration, though it is carcinogenic and it is therefore very important that the purging step is complete to ensure the safety of the sterilized device.

One additional implant was autoclaved. Autoclaving is another means of sterilization that uses steam to deactivate cells found on medical devices. The device to be sterilized is placed in an autoclave, which is a pressurized chamber, and steam is allowed to enter and the device is exposed to the steam for 15-45 minutes. The temperature in the autoclave is 121°C-132°C. This method of sterilization is efficient, simple and inexpensive, but cannot be used in all situations because the high temperatures can damage thermosensitive materials such as polymers.

4.6 Elution Studies

To measure the rate at which the drug was released from the implants, the implants were immersed in solution and the amount drug in solution was measured at various intervals. The drug elution was measured for several groups of implants. The pamidronate-dosed implants were divided into two groups: HA-coated porous tantalum and non-HA coated porous tantalum. The zoledronate-dosed implants were divided into five groups: HA-coated porous tantalum, non-HA coated porous tantalum, HA-coated ethylene oxide sterilized porous tantalum, HA-coated autoclave sterilized porous tantalum, and HA-coated solid titanium. Two control implants without bisphosphonate dosing, an HA-coated porous tantalum implant and a non-HA coated porous tantalum implant, were also immersed in solution to ensure that neither the porous tantalum nor the HA coating affected the measurements.

Two methods were used to measure the bisphosphonate elution from the implants. In the first method, the bisphosphonate-coated implants were placed into a small 10 ml test tube. Either 5 ml of distilled water or 5 ml of saline was added to the test tube with a micropipette until the implant was completely immersed in water. The test tube was then sealed with parafilm and placed in a water bath at 37°C. At selected intervals, the test tube was removed from the water bath. Using tweezers, the implant was removed from the test tube. The entire volume of liquid was removed from the test tube with a micropipette and placed in a vial, noting the volume of liquid removed. The implant was put back into the test tube and 4 ml of fresh distilled water or saline was added to re-immerse the implant in liquid. Only 4 ml of solution was needed to re-immerse the implant in solution because the pores of the implant were saturated with liquid and held approximately 1 ml of solution. The test tube was replaced in the water bath. Samples were taken at the following intervals: 5 minutes, 15 minutes, 30 minutes, 1 hour, 3 hours, 12 hours, 24 hours, 1 week, and weekly thereafter to 12 weeks. Samples were taken for the control implants only for the first 24 hours.

In the second method, the implants were placed in 15 ml test tubes with screw cap lids. The implants were immersed in 10 ml of saline and then vortexed for 3 seconds. At each interval, the test tubes were vortexed again to to mix the solution within the implant with the solution surrounding the implant and 2 ml of the solution was removed by pipette and placed in a separate test tube for analysis. The removed volume of solution was replaced by 2 ml of fresh saline, so that the volume of solution surrounding the implant remained 10 ml.

4.7 Spectrophotometry

Spectrophotometry is the measurement of the absorbance of a chemical compound at a particular wavelength of radiation, either in the ultraviolet or visible wavelength ranges. When radiation passes through a layer of solid, liquid or gas certain frequencies can be selectively removed by absorption. Absorption is the process by which electromagnetic radiation is transferred to the atoms, ions, or molecules in a sample, promoting the particles from ground state to an excited state. Atoms, molecules and ions have only a limited number of discrete energy levels and therefore, for absorption to occur, the energy of the exciting photon needs to exactly match the energy between the ground state and an excited state for the absorbing species to absorb the photon and promote an electron to the excited state. An absorbing species is called a chromaphore. Due to the uniqueness of the energy differences, a plot of the frequency against absorbance can be a means of characterizing a chemical species. Atomic absorption, the absorption by a monoatomic species, results in absorption of few, well defined frequencies because of the small number of energy states of an atom. Molecular absorption, the absorption by a molecular species, generally has absorption regions that include a range of wavelengths, resulting in broad bands.

There are two applications of ultraviolet/visible molecular absorption spectrophotometry. The first is the detection of functional groups. Certain functional groups act as chromaphores and thus absorb at certain wavelengths. Absorbance at particular wavelengths and characteristic band shapes can indicate the presence of functional groups, such as hydroxyl groups, carbonyl groups or aromatic rings. The second application of ultraviolet/visible molecular absorption spectrophotometry is quantitative analysis. The absorbance of a chemical species in solution is dependent on its concentration. By measuring the absorbance of known concentrations of a solution containing the molecule of interest and a blank solution, a calibration curve can be determined, which is a linear relation between the concentration and absorbance at the determined wavelength. From the calibration curve, the concentration of unknown solutions that contain all of the same solutes in the same solvent can be calculated [90].

4.8 Bisphosphonates and spectrophotometry

Bisphosphonates do not naturally contain an appreciable chromaphore, which means that bisphosphonates cannot normally by detected by ultraviolet/visible spectrophotometry. However, the known chelating properties of bisphosphonates to metal ions [91] can be applied to obtain a chromaphoric complex. Several methods have been developed to quantitatively analyze bisphosphonates in solution, such as ion-exchange chromatography [92, 93], capillary electrophoresis [94], complexometric titration [95] and liquid chromatography – mass spectrometry [96]. However, these methods are complicated, time consuming and require expensive equipment.

Ostovic et al [97] showed that copper (II) ions can complex with bisphosphonates for detection by ultraviolet spectrophotometry. Adding a constant concentration of copper (II) sulfate solution to a bisphosphonate solution creates a chromaphoric complex. They prepared a series of solutions with known concentrations of alendronate, pamidronate and etidronate, and with

constant concentrations of copper (II) ions (2.5×10^{-3} M) and nitric acid (1.5×10^{-3} M). When the concentrations were plotted against absorbance, a linear relation was seen for all three bisphosphonates. The absorbance was measured at 240 nm, which is within the ultraviolet range of light. This method of spectrophotometric analysis was successfully employed to measure the drug content and in vitro drug release of clodronate from polylactic-glycolic acid microspheres [98].

Kuljanin et al [99] used iron (III) ions for the spectrophotometric analysis of a bisphosphonate. The added a standard solution of ferric chloride hexahydrate and perchloric acid to known concentrations of alendronate in its pharmaceutical formulation. The solutions for analysis had 0.2 mM Fe(III) and 0.2 M perchloric acid. A highly acidic medium was necessary to prevent the hydrolysis of the iron (III) ions. The analysis was performed with measurements taken at 290, 300, and 310 nm, but it was concluded that the sensitivity increased with the lower wavelengths.

4.9 Bisphosphonate analysis with copper (II) ions

To assay the eluted bisphosphonate samples according to the method described by Ostovic et al [97], a concentrated copper (II) sulfate solution was added to each sample. Copper (II) sulfate (0.7832 g) was weighed and placed in a 50 ml volumetric flask. Nitric acid (0.1186 ml) was added to the volumetric flask using a micropipette. The flask was filled to the line with distilled water, with swirling to ensure complete dissolution of the copper sulfate. From the concentrated solution, it was necessary to add 0.1 ml of the solution to 5 ml of the elution solution to achieve the desired concentrations of copper (II) ions (2.5×10^{-3} M) and nitric acid (1.5×10^{-3} M). A relative amount of the standard solution was added to the sample solution, depending on the amount available so that the final concentration of copper (II) ions and nitric acid would always be the required

concentrations of 2.5 x 10^{-3} M for copper (II) ions and 1.5 x 10^{-3} M nitric acid. For example, if the sample solution was 4 ml, 0.08 ml of the standard solution would be added because it would result in the same concentration as adding 0.1 ml of the standard solution to 5 ml of sample solution.

A second standard solution was made with saline as a solvent. Copper (II) sulfate (2.5280 g) was weighed and placed in a 50 ml volumetric flask. Nitric acid (0.384 ml) was added to the volumetric flask using a micropipette. The flask was filled to the line with saline (0.9% NaCl) and was swirled to ensure that all of the copper (II) sulfate dissolved. It was necessary to add 0.05 ml of the standard solution to 4 ml of elution solution for 2.5 x 10^{-3} M copper (II) ions and 1.5 x 10^{-3} M nitric acid.

4.10 Zoledronate analysis with iron (III) ions

To assay the zoledronate samples using iron (III) ions as the complexing agent, a concentrated standard solution of iron (III) chloride was added to each sample. Iron (III) chloride hexahydrate (0.0351 g) was weighed and placed in a 25 ml volumetric flask. Some distilled water was added to dissolve the iron (III) chloride. Next, 11.2 ml of perchloric acid was added to the flask and the flask was filled to the line with distilled water. This solution had an iron (III) chloride concentration of 5.2 x 10^{-3}M, and a perchloric acid concentration of 5.2 M. An identical solution was made with the same amounts of iron (III) chloride hexahydrate and perchloric acid, with saline as the solvent instead of distilled water. It was necessary to add 0.160 ml of the standard solution to 4 ml of elution solution for 0.2 mM iron (III) ions and 0.2 M perchloric acid.

4.11 Ultraviolet Spectrophotometry

To conduct the spectrophotometric analysis of the eluted bisphosphonate samples, two different spectrophotometers were used. The first was a Bio-Tek® µ-Quant™ microplate spectrophotometer. This type of spectrophotometer read well plates and could measure the absorbance of up to 96 samples at a time. As well as measuring the absorbance of a sample at a given wavelength, this spectrophotometer could also perform spectral scans, the measure of absorbance of a sample over a desired range of wavelengths.

The second type of spectrophotometer was a Spectronic™ Helios™ Gamma UV-Vis spectrophotometer. This type of spectrophotometer measured the absorbance of one sample at a time, in a cuvette. Usually quartz cuvettes are used for spectrophotometry, though for this experiment disposable methacrylate cuvettes were used to minimize contamination. A new, clean cuvette was used for each sample.

4.12 Reliability of Polymethacrylate Cuvettes

The absorbance of samples containing zoledronate was measured at 290 nm. Methacrylate cuvettes can be used for wavelengths greater than 275 nm. The percent of transmittance of methacrylate cuvettes at 290 nm is 80%. To ensure that measurements at 290 nm were not compromised by reduced transmittance or proximity to the lowest wavelength indicated for use, the variation between methacrylate cuvettes was tested. Four cuvettes were randomly selected and 1 ml of distilled water was pipetted into each one. The absorbance of the distilled water was measured once for each cuvette. The spectrophotometer was then recalibrated and the absorbance was measured again for each cuvette. These wavelength and transmittance limitations did not exist for the multi-well plates.

4.13 Ultraviolet spectrophotometry analysis of bisphosphonates

In order to determine the amount of bisphosphonate in elution samples, calibration curves had to be generated. To obtain a calibration curve for pamidronate in water, a standard solution of pamidronate was made. Pamidronate (7.1 mg) was weighed and placed in a 25 ml volumetric flask. The flask was filled to the line with distilled water, giving a $1.0x10^{-3}$ M pamidronate solution. Using this solution, the standard solution of copper (II) sulfate, and distilled water, four standard concentrations of pamidronate and a blank solution were made. The amounts of each solution used to make the standard concentrations are found in table 4.4.

Table 4.4 - Volumes of solutions used for pamidronate in water calibration curve and final concentration of pamidronate

Volume $CuSO_4$ sol.	Volume Pamidronate sol.	Volume distilled water	Total volume	Pamidronate concentration
1.00 ml	0 ml	24.00 ml	25 ml	0 M (blank)
1.00 ml	1.25 ml	22.75 ml	25 ml	5×10^{-5} M
1.00 ml	2.50 ml	21.50 ml	25 ml	1×10^{-4} M
1.00 ml	3.75 ml	20.25 ml	25 ml	1.5×10^{-4} M
1.00 ml	5.00 ml	19.00 ml	25 ml	2×10^{-4} M

When using the µ-Quant spectrophotometer, the standards were each pipetted in 200 µl increments into 8 wells of a 96 well UV-transparent plate (figure 4.10), and the plate was read at 240 nm wavelength. Plotting the absorbance against concentration gave a linear calibration curve. Using the equation of the line, the concentration of unknown samples was determined. A second pamidronate calibration curve was generated in a similar way, using saline as the solvent instead of distilled water. Only the µ-Quant spectrophotometer was used for the analysis of pamidronate.

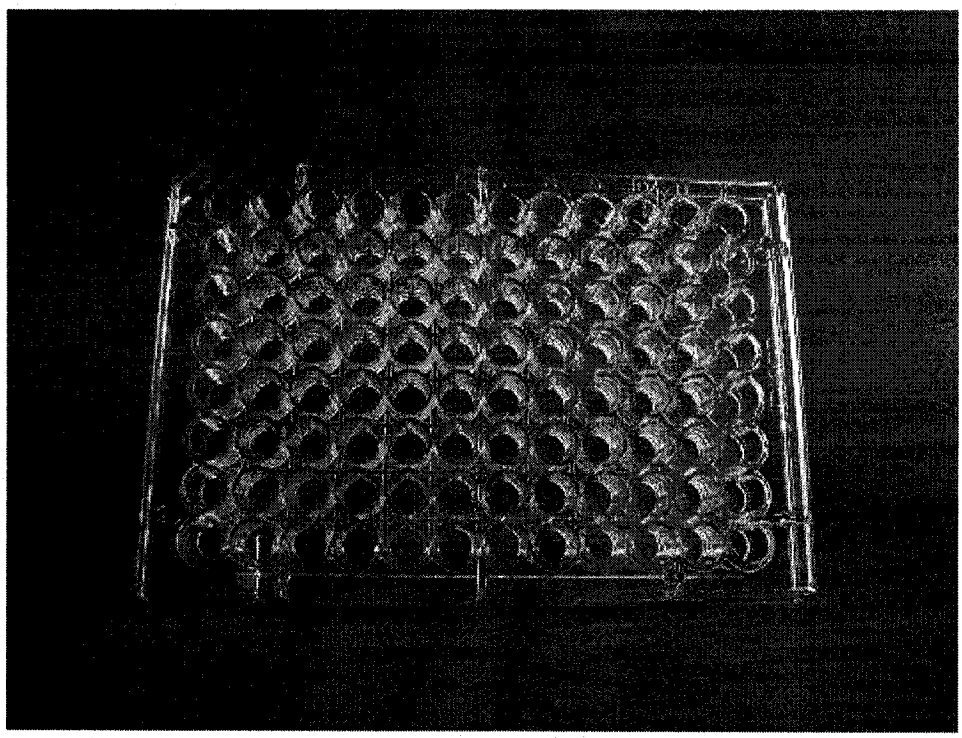

Figure 4.10 - A 96-well UV transparent well plate

Calibration curves were also created using zoledronate. First, a calibration curve of zoledronate in saline with copper (II) sulfate as the complexing agent was used. The zoledronate was used as reconstituted in its original vial. The first zoledronate vial had been reconstituted with 8 ml of distilled saline, giving a zoledronate concentration of 1.72×10^{-3} M. Using saline, reconstituted zoledronate and the standard copper (II) sulfate solution, four standard concentrations of zoledronate and a blank were made (table 4.5). The standard samples were placed into well plates and the absorbance was measured, as described above.

Because the pharmaceutical compilation of zoledronate (Zometa) also contained mannitol and sodium citrate, it was necessary to create calibration curves of both chemical compounds as well. Mannitol (220 mg) was weighed and placed in a beaker and dissolved in 4 ml of saline. Sodium citrate dihydrate (27.3 mg) was weighed and placed in a beaker and dissolved in 4 ml of saline. Each was diluted to concentrations that corresponded to the concentration found

in the standard zoledronate solutions. The calibration curves were compared to those to zoledronate to determine whether the additional chemical agents present in Zometa influenced the calibration curve.

Table 4.5 - Volumes of solutions used for zoledronate in saline calibration curve and final concentration of zoledronate

Volume $CuSO_4$ sol.	Volume Zoledronate sol.	Volume saline	Total volume	Zoledronate concentration
12.5 µl	0 µl	987.5 µl	1000 µl	0 M (blank)
12.5 µl	29 µl	958.5 µl	1000 µl	5×10^{-5} M
12.5 µl	43.5 µl	944 µl	1000 µl	7.5×10^{-5} M
12.5 µl	58 µl	929.5 µl	1000 µl	1.0×10^{-4} M
12.5 µl	87 µl	900.5 µl	1000 µl	1.5×10^{-4} M

Zoledronate was also calibrated in water and saline with iron (III) chloride standard solution. A 0.05 mg sample of zoledronate in 500 µl of water (1 vial) was used. The zoledronate was diluted with either water or saline and the standard iron (III) chloride solution was added to make four standard concentrations of zoledronate (table 4.6). The standard concentration samples were placed in well plates and the absorbance was measured at 290 nm.

When using the Thermospectronic™ spectrophotometer to create a calibration curve for zoledronate with iron (III) chloride, 1 ml of complexed solution was pipetted into each cuvette. Each standard was divided into two and the absorbance of each portion of the standard was measured twice, for a total of four readings per sample.

Table 4.6 - Volumes of solutions used for zoledronate in saline or water calibration curve with iron (III) chloride and final concentration of zoledronate

Volume $FeCl_3$ sol.	Volume Zoledronate sol.	Volume saline/water	Total volume	Zoledronate concentration
40 µl	0 µl	2000 µl	2080 µl	0 M (blank)
40 µl	60 µl	1940 µl	2080 µl	1×10^{-5} M
40 µl	150 µl	1850 µl	2080 µl	2×10^{-5} M
40 µl	302 µl	1698 µl	2080 µl	5×10^{-5} M
40 µl	450 µl	1550 µl	2080 µl	7.5×10^{-5} M

Mannitol and sodium citrate were analyzed in a similar manner. Mannitol (220 mg) was weighed in a beaker and 4 ml of distilled water was added. A 50 µl aliquot of that solution was removed and diluted to 500 µl with distilled water. That mannitol solution was then further diluted in the same ratios as zoledronate in table 6 and the absorbance was measured at 290 nm for each standard sample. Sodium Citrate (27.3 mg) was weighed and dissolved in 4 ml of distilled water. Standard solutions were made and analyzed by spectrophotometry in an identical manner as mannitol.

To analyze the solutions retrieved during the elution studies, the appropriate standard solution was added in the required amount immediately prior to measuring the absorbance of the solution. The sample solution was vortexed to ensure uniform distribution of the added standard solution. When using the µQuant™ spectrophotometer, the solution was pipetted into ultraviolet transparent 96-well microplates. Each elution solution was placed into eight wells, with 200 µl in each well. When the microplates were scanned at either 240 nm for those complexed with copper (II) ions, or 290 nm for those complexed with iron (III) ions, each solution had eight readings. When using the Thermospectronic™, 1 ml of the solution was pipetted into a 1.5 ml disposable polymethacrylate cuvette and the absorbance was measured twice. This was then repeated with the same sample for a total of four readings, to be averaged for calculations. From the absorbance readings, the concentration of each sample was determined, based on the calibration curve. Using the known

volume, the concentration was used to determine the mass of pamidronate and zoledronate eluted from the implant during each time interval.

Chapter 5. Results

5.1 Bisphosphonate Deposition

When the bisphosphonate solutions were pipetted onto the hydroxyapatite-coated porous tantalum implants, the solution was wicked into the implant pores and onto the struts by the hydrophilic hydroxyapatite. Prior to applying the drug solution, the implants were light gray. When the entire volume of solution had been applied, the implant appeared darker in colour and appeared to be wet, though the solution was entirely contained within the implant pores (figure 5.1). There was no liquid beaded on the implant outer surface.

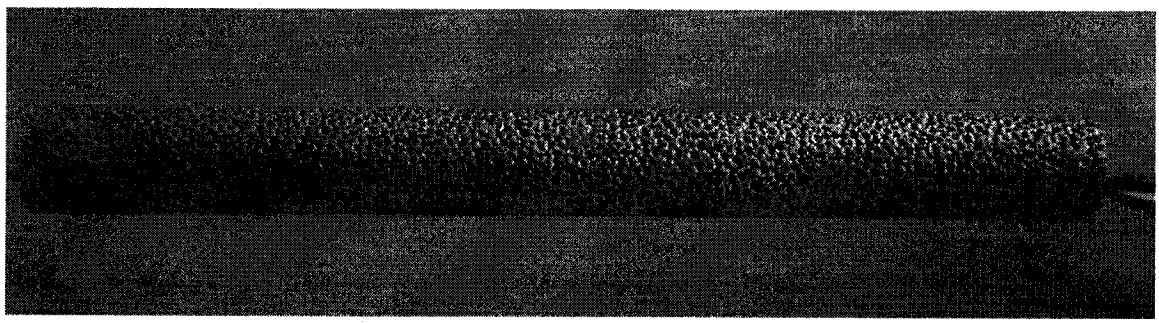

Figure 5.1 - Bisphosphonate solution on HA-coated porous tantalum implant

When the bisphosphonate solutions were pipetted onto the non-hydroxyapatite coated tantalum implants, the solution beaded on the surface of the tantalum and the solution was not readily wicked into the pores (figure 5.2). To ensure adequate coverage of the implant by the solution, the drug solution was rubbed with the pipette tip along the surface of the implant. Only part of the solution could be added at a time because the surface tension was not sufficient to hold the entire 500 µl on the implant surface.

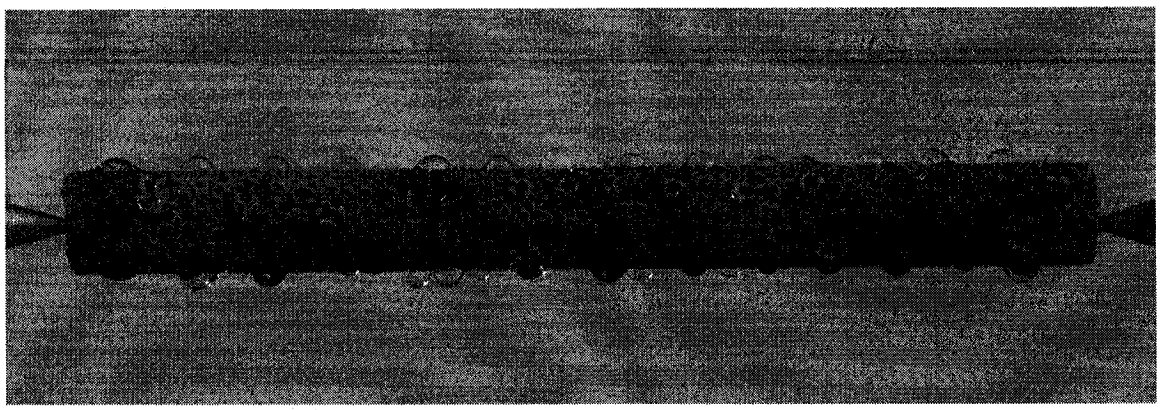

Figure 5.2 – Bisphosphonate solution beaded on a non-HA coated porous tantalum implant

When bisphosphonate solution was applied to the solid titanium rods, the solution could not easily be adsorbed by the implant because there were no pores for the solution to be wicked into. The solution pooled instead of beaded on the surface, and as with the non-hydroxyapatite coated tantalum implants, the solution was rubbed along the surface of the implant to ensure the even distribution of the bisphosphonate.

After drying in the oven for 48 hours, the implants were weighed to ensure that the drug had been deposited on the implant. An increase in mass of an appropriate amount indicated that the drug had been deposited onto the implant struts. Once dry, the hydroxyapatite-coated porous tantalum implants still appeared slightly darker in colour than prior to being coated with the bisphosphonate, though the bisphosphonate was not visible on the tantalum struts. The non-hydroxyapatite coated porous tantalum implants had a white residue after the bisphosphonate solution application, due to the absence of hydroxyapatite to absorb the bisphosphonate, mannitol and sodium citrate.

The mass of the implants before and after the application of the bisphosphonate solution is listed in tables 5.1-5.5. The implants were divided into six groups: HA-coated pamidronate dosed (P), non-HA coated pamidronate dosed (Ta), HA-coated zoledronate dosed (Z), ethylene oxide sterilized HA-

coated zoledronate dosed, non-HA coated zoledronate dosed (Ta), and HA-coated zoledronate dosed titanium (Ti).

The increase in mass of the zoledronate-coated implants was greater than the mass of bisphosphonate added because Zometa also contains mannitol and sodium citrate. These additional ingredients in the pharmaceutical composition also remained on the implant and contributed to the increase in mass. The Zometa-coated implants that had a 0.2 mg dose had a greater increase in implant mass than for the remainder of the implants, because of the larger dose of drug and respectively larger doses of mannitol and sodium citrate.

Table 5.1 - Hydroxyapatite coated porous tantalum implants for pamidronate elution studies

Implant	Mass of implant	Mass of pamidronate	Mass of dosed implant	Δ Mass
P1	3.7178 g	2.2 mg	3.7201 g	2.3 mg
P2	4.2567 g	2.1 mg	4.2593 g	2.6 mg
P3	5.6725 g	2.1 mg	5.6746 g	2.1 mg
P4	4.9646 g	2.0 mg	4.9663 g	1.7 mg
P5	5.1509 g	2.0 mg	5.1526 g	1.7 mg
P6	5.6083 g	2.2 mg	5.6101 g	1.8 mg
P7	5.9528 g	2.1 mg	5.9546 g	1.8 mg

Table 5.2 - Porous tantalum implants for pamidronate elution studies

Implant	Mass of implant	Mass of pamidronate	Mass of dosed implant	Δ Mass
Ta1	3.9589 g	2.1 mg	3.9607 g	1.8 mg
Ta2	4.0958 g	2.1 mg	4.0976 g	1.8 mg

Table 5.3 - Hydroxyapatite coated porous tantalum implants for zoledronate elution studies

Implant	Mass of implant	Mass of zoledronate	Mass of dosed implant	Δ Mass
Z1	7.0640 g	0.2 mg	7.0806 g	16.6 mg
Z2	4.9109 g	0.2 mg	4.9279 g	17.0 mg
Z3	3.1945 g	0.05 mg	3.1970 g	2.5 mg
Z4	3.8918 g	0.05 mg	3.8944 g	2.6 mg
Z5	3.6226 g	0.05 mg	3.6251 g	2.5 mg
Z6	3.4296 g	0.05 mg	3.4314 g	1.8 mg
Z7	5.1661 g	0.05 mg	5.1691 g	3.0 mg
Z8	3.5018 g	0.05 mg	3.5046 g	2.8 mg
Z9	4.0438 g	0.05 mg	4.0463 g	2.5 mg
Z10	4.1096 g	0.05 mg	4.1125 g	2.9 mg

Table 5.4 - Porous tantalum implants for zoledronate elution studies

Implant	Mass of implant	Mass of zoledronate	Mass of dosed implant	Δ Mass
Ta3	3.8492 g	0.05 mg	3.8516 g	2.4 mg
Ta4	3.7332 g	0.05 mg	3.7360 g	2.8 mg
Ta5	3.2161 g	0.2 mg	3.2268 g	10.7 mg
Ta6	3.0466 g	0.2 mg	3.0576 g	11.0 mg

Table 5.5 - HA-coated solid titanium implants for zoledronate elution studies

Implant	Mass of implant	Mass of zoledronate	Mass of dosed implant	Δ Mass
Ti1	4.3467 g	0.2 mg	4.3550 g	8.3 mg
Ti2	4.2887 g	0.2 mg	4.2975 g	8.8 mg
Ti3	4.3432 g	0.2 mg	4.3520 g	8.8 mg

5.2 Pamidronate Calibration in Water

When first attempting to calibrate pamidronate in water, the standard solutions were prepared the day prior to ultra-violet spectrophotometric analysis. However, the absorbance readings of the solutions at 240 nm with respect to concentration were not linear. During the next attempt at calibrating pamidronate in water, the copper (II) sulfate solution was added to the standard solutions immediately before pipetting the solutions into the well plates. The copper (II) solution was added with a pipette and then the vial of solution was swirled to ensure that the copper (II) sulfate was distributed evenly. The plates were read at 240 nm. The raw data are listed in table 5.6 and the blank data, obtained by subtracting the average absorbance of the eight blank solutions, are listed in table 5.7. This resulted in a linear calibration curve, appropriate for calculating the concentration of unknown samples. The calibration curves are plotted using blanked data. Plotting the blanked absorbance of each standard solution versus concentration and determining the line of best fit gave a calibration curve (figure 5.3).

Table 5.6 - Absorbance of known concentrations of pamidronate in water, at 240 nm

Concentration	0 M	0.00005 M	0.0001 M	0.00015M	0.0002 M
Absorbance	0.268	0.309	0.349	0.395	0.444
	0.275	0.304	0.351	0.401	0.456
	0.253	0.31	0.352	0.4	0.437
	0.254	0.304	0.354	0.399	0.434
	0.256	0.302	0.356	0.396	0.435
	0.257	0.303	0.353	0.391	0.445
	0.256	0.302	0.356	0.386	0.441
	0.26	0.311	0.361	0.4	0.441

Table 5.7 - Blanked absorbance of known concentrations of pamidronate in water, at 240 nm

Concentration	0 M	0.00005 M	0.0001 M	0.00015 M	0.0002 M
Absorbance	0.008	0.049	0.089	0.135	0.184
	0.015	0.044	0.091	0.141	0.196
	-0.007	0.05	0.092	0.14	0.177
	-0.006	0.044	0.094	0.139	0.174
	-0.004	0.042	0.096	0.136	0.175
	-0.003	0.043	0.093	0.131	0.185
	-0.004	0.042	0.096	0.126	0.181
	0	0.051	0.101	0.14	0.181

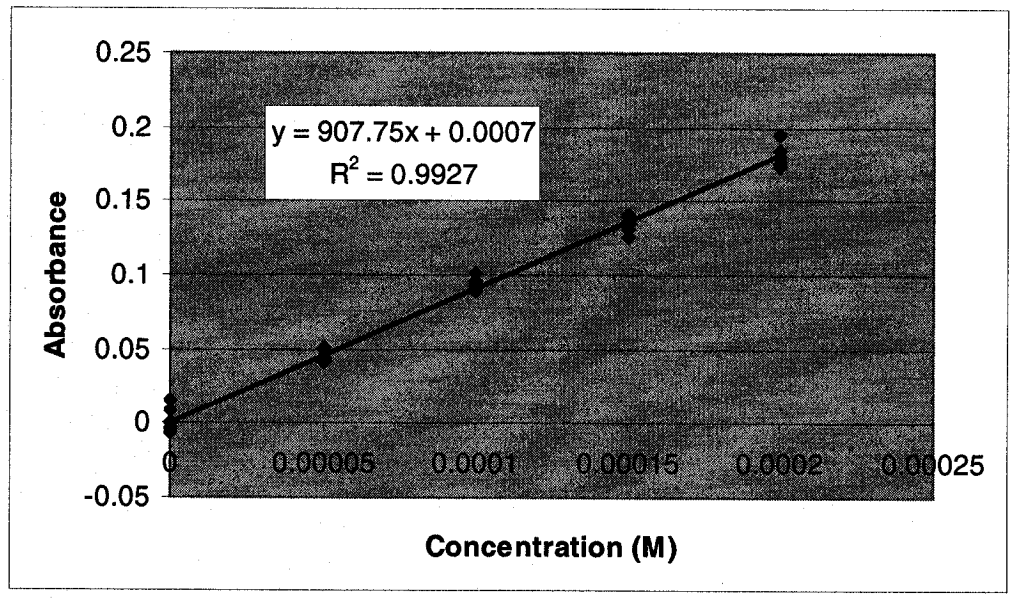

Figure 5.3 - Calibration of pamidronate in water

5.3 Pamidronate Calibration in saline

The calibration of pamidronate in saline was completed using the same method as the calibration of pamidronate in water. The complexing solution used for the calibration had saline as a solvent instead of water. The raw and blanked data are listed in tables 5.8 and 5.9. The resulting curve (figure 5.4) was linear and suitable for calibration.

Table 5.8 - Absorbance of known concentrations of pamidronate in saline, at 240 nm

Concentration	0 M	0.00005 M	0.0001 M	0.00015 M	0.0002 M	0.0004 M
Absorbance	0.492	0.529	0.515	0.551	0.586	0.715
	0.487	0.511	0.517	0.548	0.583	0.714
	0.494	0.511	0.528	0.551	0.592	0.716
	0.494	0.505	0.523	0.552	0.592	0.713
	0.497	0.513	0.52	0.554	0.597	0.714
	0.495	0.514	0.519	0.551	0.591	0.712
	0.5	0.513	0.521	0.558	0.595	0.715
	0.5	0.521	0.525	0.562	0.594	0.719

Table 5.9 - Blank absorbance of known concentrations of pamidronate in saline, at 240 nm

Concentration	0 M	0.00005 M	0.0001 M	0.00015 M	0.0002 M	0.0004 M
Absorbance	-0.003	0.034	0.02	0.056	0.091	0.220
	-0.008	0.016	0.022	0.053	0.088	0.219
	-0.001	0.016	0.033	0.056	0.097	0.221
	-0.001	0.01	0.028	0.057	0.097	0.218
	0.002	0.018	0.025	0.059	0.102	0.219
	0	0.019	0.024	0.056	0.096	0.217
	0.005	0.018	0.026	0.063	0.1	0.22
	0.005	0.026	0.03	0.067	0.099	0.224

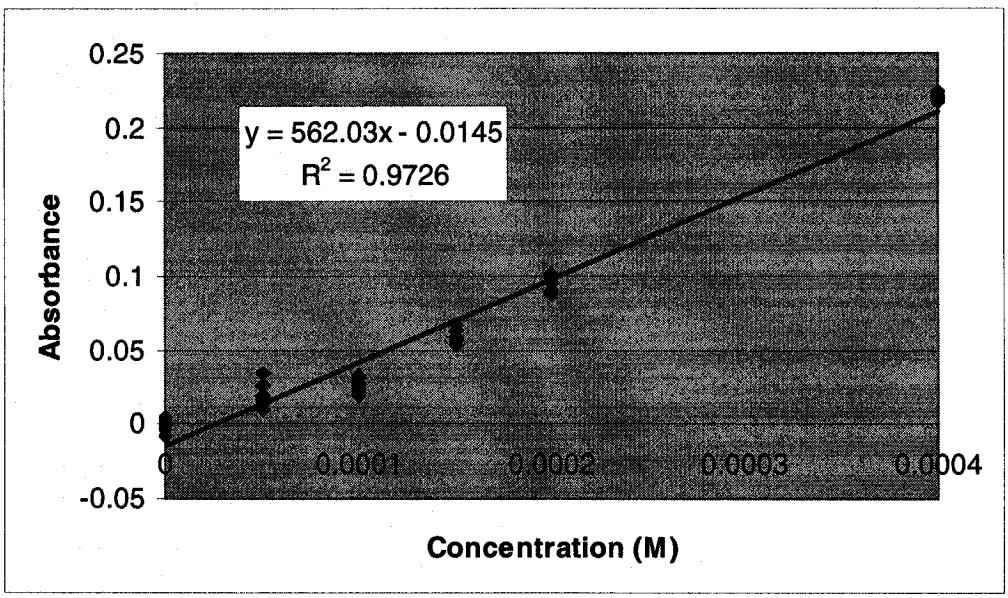

Figure 5.4 - Calibration of pamidronate in saline

5.4 Zoledronate Calibration in Water with Copper (II) Sulfate

Zoledronate was calibrated using the copper (II) sulfate solution as the complexing agent. The raw and blanked data appear in tables 5.10 and 5.11. The resulting calibration curve (figure 5.5) was linear, with a positive slope, so it appeared to be appropriate for measuring the concentration of unknown zoledronate solutions.

Table 5.10 - Absorbance of known concentrations of zoledronate in water, at 240 nm

Concentration	0 M	0.00005 M	0.000075 M	0.0001 M	0.00015 M
Absorbance	0.497 0.495 0.5 0.5	0.773 0.768 0.751 0.774	0.873 0.865 0.876 0.88	0.932 0.93 0.954 0.945	1.383 1.353 1.359 1.251

Table 5.11 - Blanked absorbance of known concentrations of zoledronate in water, at 240 nm

Concentration	0 M	0.00005 M	0.000075 M	0.0001 M	0.00015 M
Absorbance	-0.001	0.275	0.375	0.434	0.885
	-0.003	0.270	0.367	0.432	0.855
	0.002	0.253	0.378	0.456	0.861
	0.002	0.276	0.382	0.447	0.753

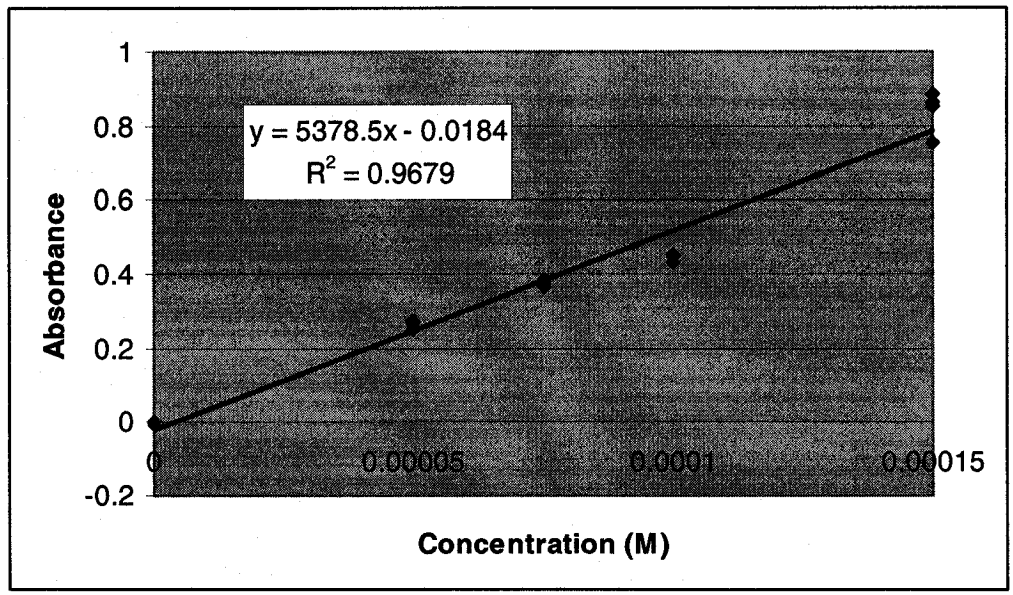

Figure 5.5 - Calibration of zoledronate in water with copper (II) ions, at 240 nm

When the elution data were calculated following the first 24 hours of elution using the calibration of Zometa with copper (II) sulfate, the results indicated that far more zoledronate had eluted than was actually applied to the implant. This impossibility led to further spectrophotometric analyses. Calibrations and spectral scans of sodium citrate solutions (figures 5.6-5.8) and mannitol solutions (figures 5.9-5.11) were run to determine the cause of the excess absorbance readings. Figures 5.6 and 5.9 are the calibration curves of sodium citrate and mannitol, respectively. Figure 5.7 is a spectral scan from 200 nm to 999 nm of sodium citrate in water. Figure 5.8 is a spectral can of sodium citrate in water with copper (II) sulfate. The same spectral scans with mannitol appear in figures 5.10 and 5.11. Figure 5.12 is a spectral scan of Zometa, sodium citrate, and mannitol, each in water with copper (II) sulfate.

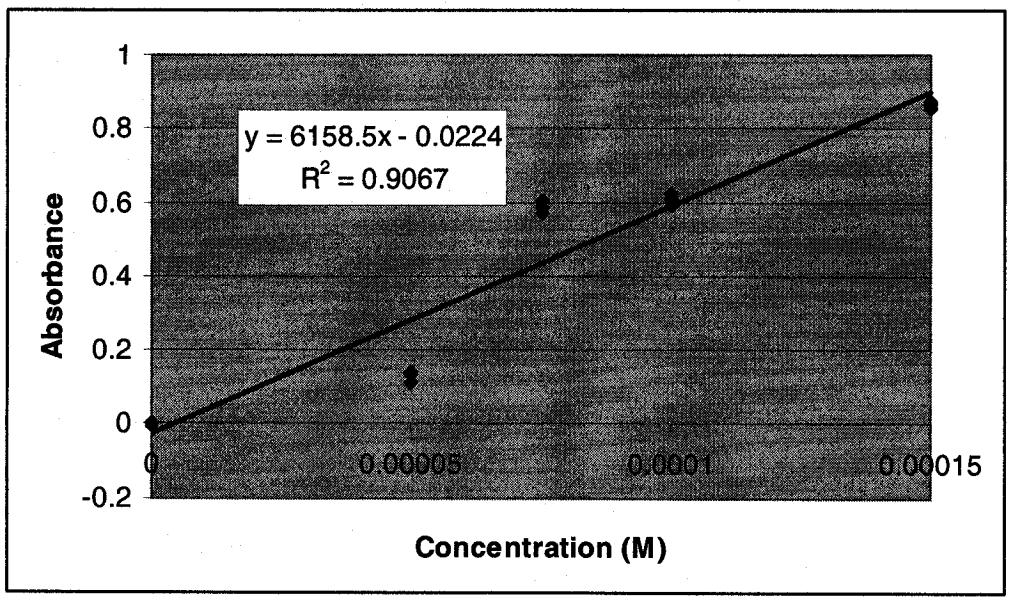

Figure 5.6 - Calibration of sodium citrate in water with copper (II) sulfate solution, at 240 nm

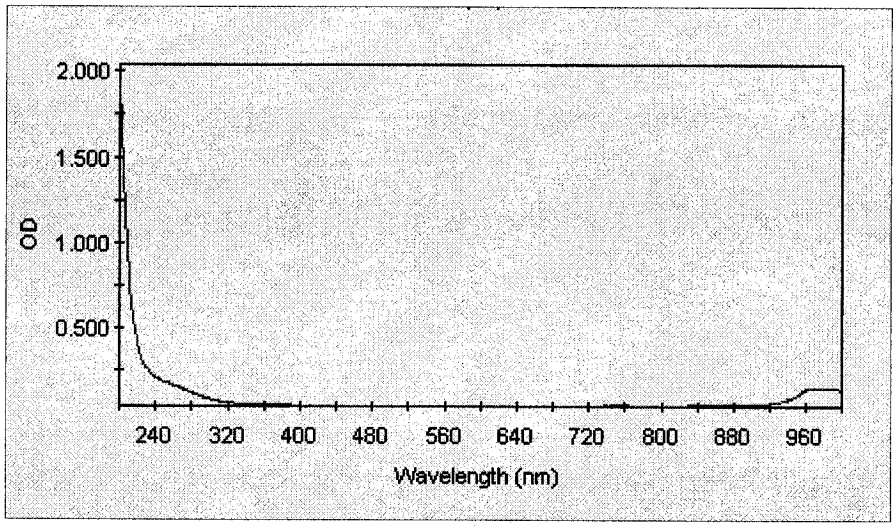

Figure 5.7 - Spectral scan of sodium citrate in water

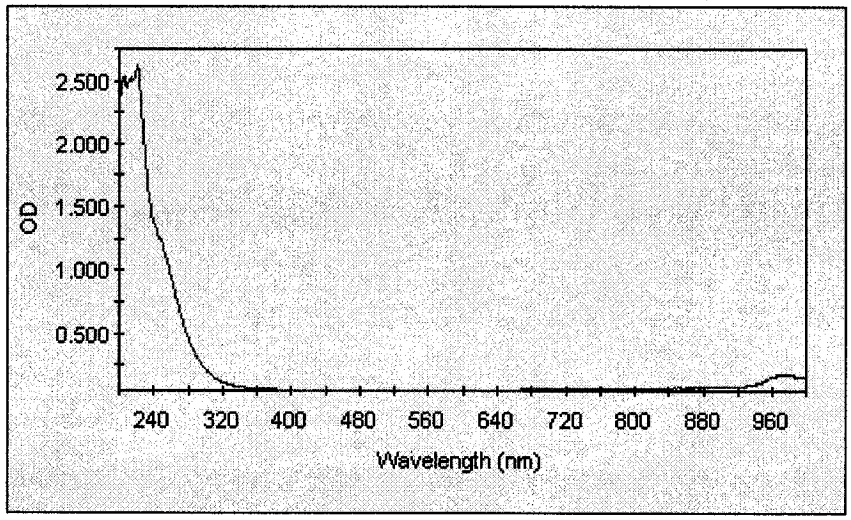

Figure 5.8 - Spectral scan of sodium citrate in water with copper (II) sulfate

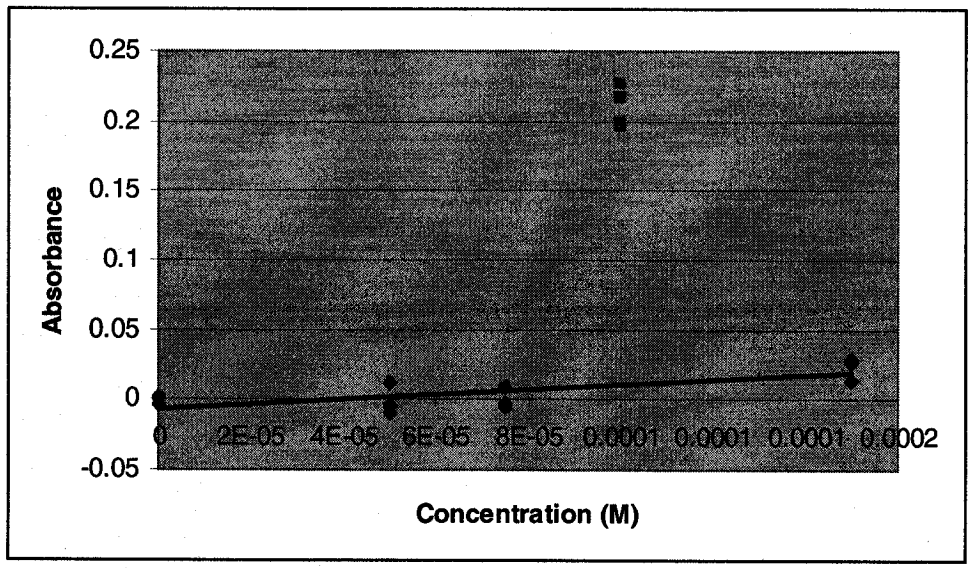

Figure 5.9 - Calibration of mannitol in water with copper (II) sulfate solution

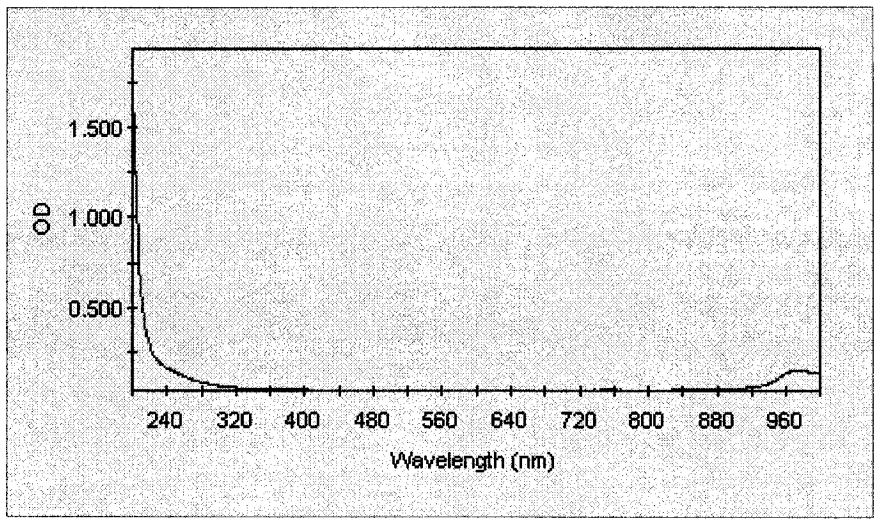

Figure 5.10 - Spectral scan of mannitol in water

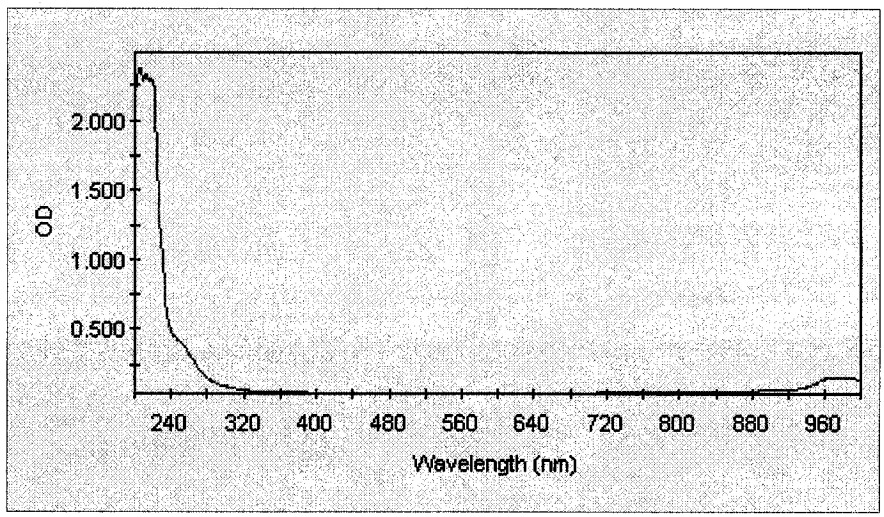

Figure 5.11 - Spectral scan of mannitol in water with copper (II) sulfate

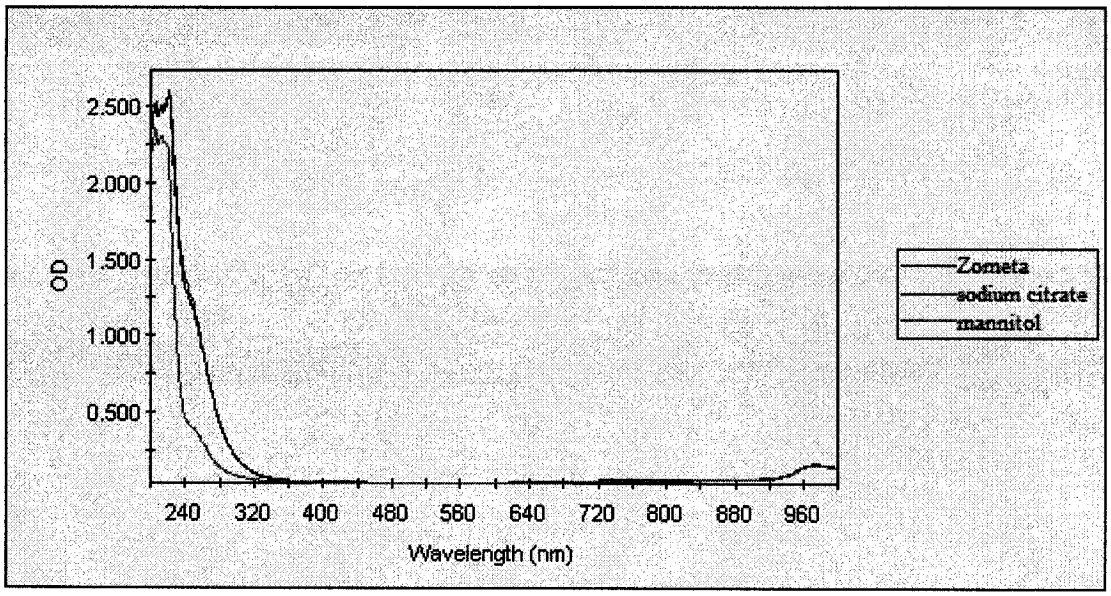

Figure 5.12 - Spectral scans of Zometa, sodium citrate, and mannitol, each in water with copper (II) sulfate.

From the mannitol calibration curve, it was seen that the calibration of mannitol (figure 5.9) had a slope close to zero. The absorbance of mannitol in solution appeared to be dependent on concentration, though it was not making a significant contribution to the excess absorbance readings. The square points on the mannitol calibration graph were not used in determining the trendline and equation of the line because that group of points did not seem to be consistent with the other points. The addition of copper (II) sulfate to mannitol did alter the absorbance of the solution (figure 5.10 & 5.11), though the spectral scan was quite different than that of Zometa (figure 5.12). The calibration of sodium citrate (figure 5.6) resulted in a trendline with a positive slope, showing that at 240 nm an increase in sodium citrate concentration resulted in an increase in absorbance. The spectral scans reinforced that sodium citrate (figure 5.7 & 5.8) was also complexing with copper (II) ions to absorb at 240 nm. The spectral scan of sodium citrate with copper (II) ions was nearly identical to that of Zometa with copper (II) ions (figure 5.12). This indicated that when sodium citrate was present in the elution sample, the sodium citrate was complexing with the copper (II) ions to form a species that absorbs light between 200 nm and 350 nm, which resulted in an increase of the absorbance readings at 240 nm. It was not

possible to determine what portion of the absorbance reading was due to the zoledronate and which portion was due to sodium citrate. In fact, it was possible that the entire reading was due to the complexation of copper (II) to sodium citrate because of the similarity of the spectral scans of sodium citrate and Zometa. Since the elution rate of sodium citrate from hydroxyapatite coated tantalum implants was unknown, this experiment revealed that it was not possible to determine the elution of zoledronate using copper (II) sulfate as a complexing agent for spectrophotometric analysis. As it was impossible to differentiate between the sodium citrate and the zoledronate during the elution, a different chemical assay needed to be used for determining the concentration of zoledronate.

5.5 Zoledronate Calibration in Saline with Iron (III) Chloride

Zoledronate calibration was repeated, this time using a solution of iron (III) chloride and perchloric acid as the complexing agent. Iron (III) was previously successfully used to calibrate and measure a pharmaceutical compilation of alendronate [99]. The presence of perchloric acid is necessary because the binding of iron (III) to zoledronic acid requires an acidic medium. Calibration was repeated with sodium citrate and mannitol to ensure that the two additional components of Zometa were not interfering with the measurement of zoledronate within the pharmaceutical composition, as occurred with copper (II). The raw data and blanked data for Zometa in saline with iron (III) chloride are in tables 5.12 and 5.13. Absorbance was plotted against concentration to obtain a calibration curve in figure 5.13. The raw and blanked absorbance data at 290 nm for sodium citrate with iron (III) chloride in saline appear in table 5.14 and table 5.15 and the calibration curve appears in figure 5.14. The raw and blanked absorbance data at 290 nm for mannitol with iron (III) chloride in saline appear in table 5.16 and table 5.17 and the calibration curve is depicted in figure 5.15.

Table 5.12 - Absorbance of standard solutions of Zometa in saline with Fe(III), at 290 nm

Concentration	0 M	0.00001 M	0.000025 M	0.00005 M	0.000075 M
Absorbance	0.178	0.198	0.211	0.243	0.258
	0.179	0.194	0.213	0.236	0.266
	0.178	0.196	0.216	0.242	0.262
	0.176	0.198	0.214	0.236	0.266

Table 5.13 - Blanked absorbance of standard solutions of Zometa in saline with Fe(III), at 290 nm

Concentration	0 M	0.00001 M	0.000025 M	0.00005 M	0.000075 M
Absorbance	0	0.020	0.033	0.065	0.080
	0.001	0.016	0.035	0.058	0.088
	0	0.018	0.038	0.064	0.084
	-0.002	0.020	0.036	0.058	0.088

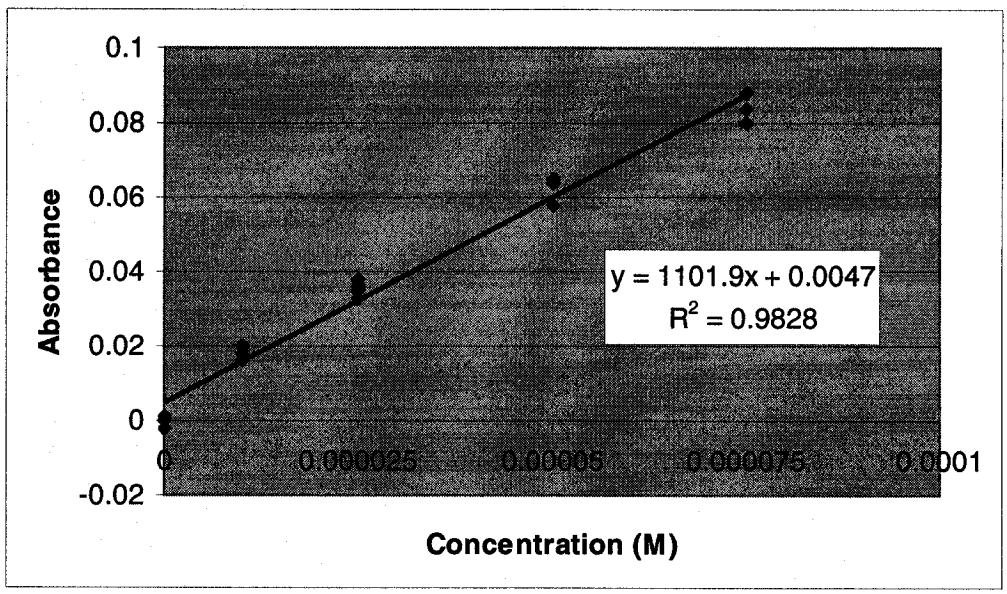

Figure 5.13 – Calibration of Zometa in saline with iron (III) chloride solution

Table 5.14 - Absorbance of standard solutions of sodium citrate in saline with Fe(III), at 290 nm

Concentration	0 M	0.00001 M	0.000025 M	0.00005 M	0.000075 M
Absorbance	0.187	0.183	0.193	0.187	0.185
	0.185	0.178	0.193	0.180	0.182
	0.185	0.179	0.178	0.181	0.180
	0.185	0.175	0.186	0.180	0.180

Table 5.15 - Blanked absorbance of standard solutions of sodium citrate in saline with Fe(III), at 290 nm

Concentration	0 M	0.00001 M	0.000025 M	0.00005 M	0.000075 M
Absorbance	0.002	-0.002	0.008	0.002	0
	0	-0.007	0.008	-0.005	-0.003
	0	-0.006	-0.007	-0.004	-0.005
	0	-0.01	0.001	-0.005	-0.005

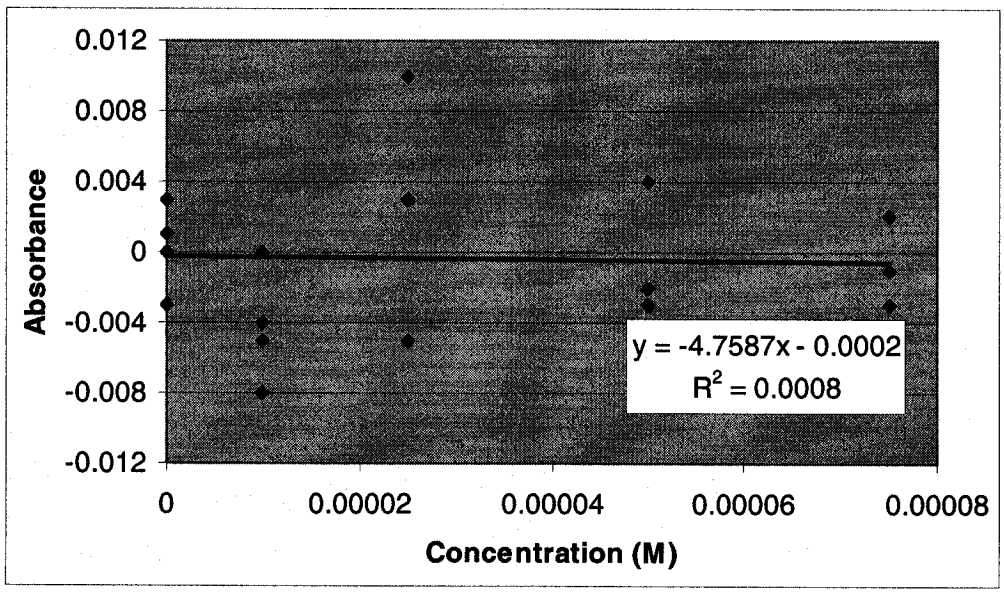

Figure 5.14 - Calibration of sodium citrate in saline with iron (III) chloride solution at 290 nm

Table 5.16 - Absorbance of standard solutions of mannitol in saline with Fe(III), at 290 nm

Concentration	0 M	0.00001 M	0.000025 M	0.00005 M	0.000075 M
Absorbance	0.183	0.179	0.179	0.181	0.189
	0.184	0.181	0.184	0.184	0.183
	0.18	0.181	0.181	0.184	0.178
	0.186	0.185	0.189	0.184	0.181

Table 5.17 - Blanked absorbance of standard solutions of mannitol in saline with Fe(III), at 290 nm

Concentration	0 M	0.00001 M	0.000025 M	0.00005 M	0.000075 M
Absorbance	0	-0.004	-0.004	-0.002	0.006
	0.001	-0.002	0.001	0.001	0
	-0.003	-0.002	-0.002	0.001	-0.005
	0.003	0.002	0.006	0.001	-0.002

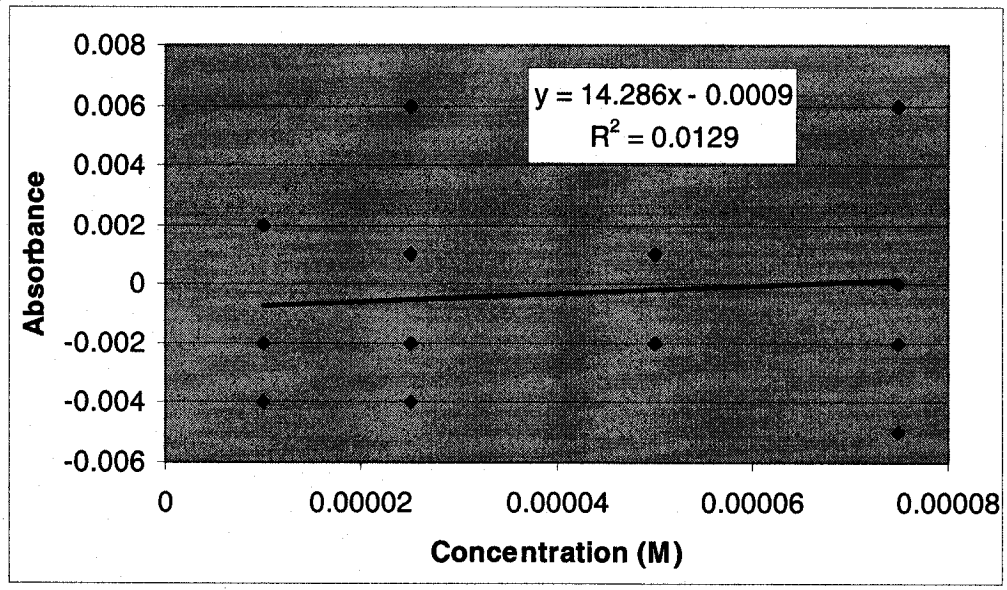

Figure 5.15 – Calibration of mannitol in saline with iron (III) chloride solution at 290 nm

From the calibrations, it appeared that neither mannitol (figure 5.15) nor sodium citrate (figure 5.14) in saline and iron (III) chloride solution contributed to the absorbance measurement of Zometa at 290 nm. This indicated that only zoledronic acid was absorbing at 290 nm, so the calibration of the Zometa with iron (III) chloride in saline (figure 5.13) truly represented a calibration of zoledronic acid in saline. The absorbance of both the mannitol and the sodium citrate was constant over multiple concentrations at the specified wavelength. Therefore, absorbance of Zometa at 290 nm was not dependent on the concentration of mannitol or sodium citrate in solution. As the concentration of mannitol and sodium citrate increased in solution, the absorbance remained the same and was equal to the absorbance of the blank solution (saline with iron (III) ions). However, the absorbance did change when the concentration of Zometa changed. As the concentration increased, the absorbance increased. The

absorbance increase was linear and directly proportional to the concentration of Zometa. Because the absorbance did not change with a change in the concentration for two of the three components in the pharmaceutical compilation of Zometa, it was concluded that zoledronic acid was causing the change in absorbance. To further confirm that the Zometa and iron (III) calibration was accurate, spectral scans were performed for each of the solutions and the blank solution, as depicted in figures 5.16-5.21. Figures 5.16 and 5.17 show spectral scans of standard solutions of Zometa and saline. Figure 5.18 shows spectral scans of standard solutions of sodium citrate and figure 5.19 shows spectral scans of standard solutions of mannitol. Figures 5.20 and 5.21 depict spectral scans of equivalent concentrations of Zometa, sodium citrate, mannitol and saline.

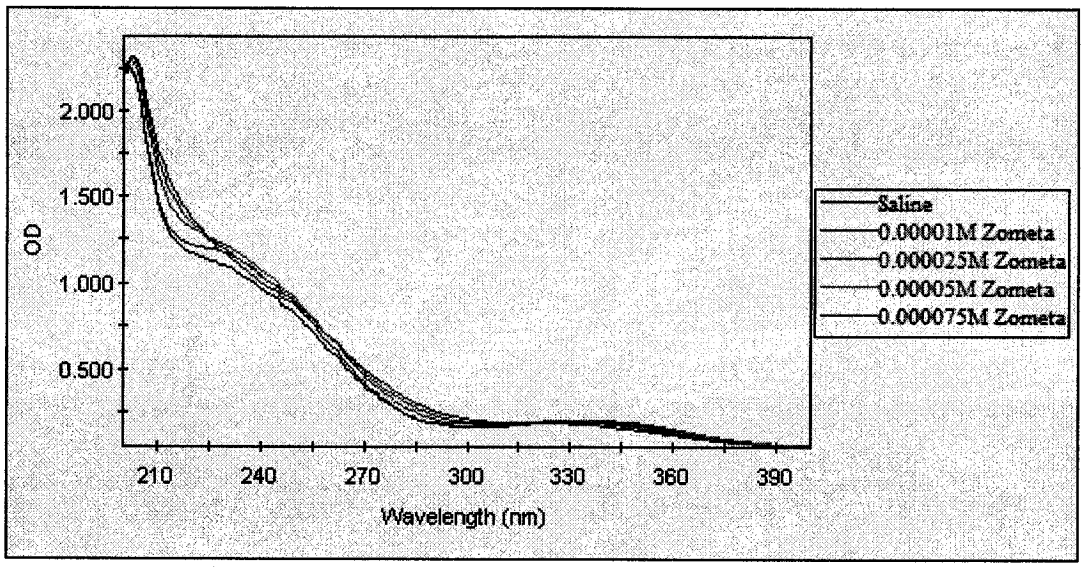

Figure 5.16 - Spectral scans of standard solutions of Zometa in saline with iron (III) chloride, from 200 nm to 999 nm

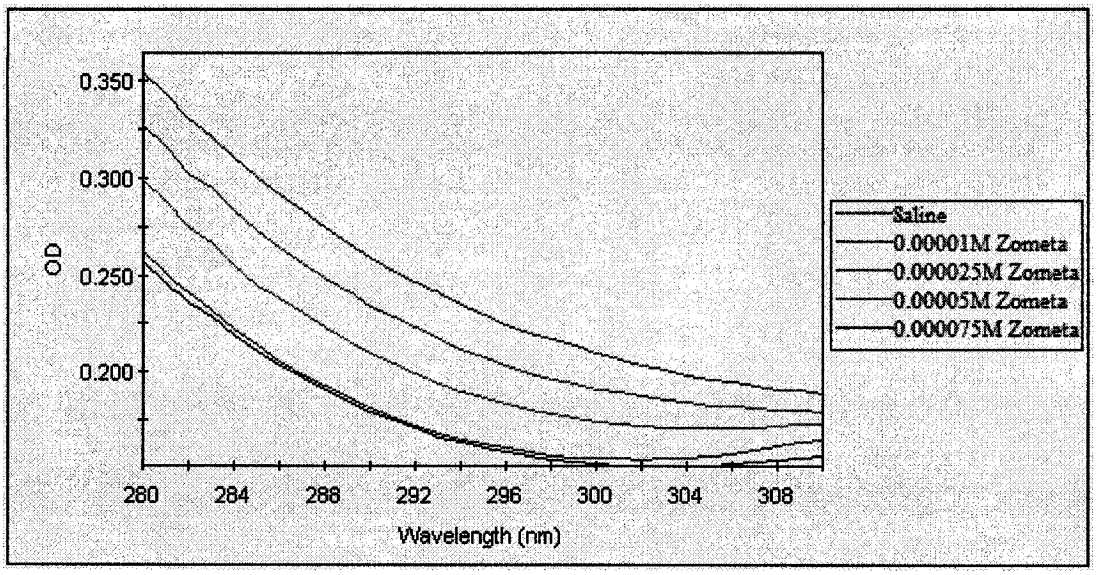

Figure 5.17 - Spectral scans of Zometa in saline with iron (III) chloride, from 280 nm to 310 nm

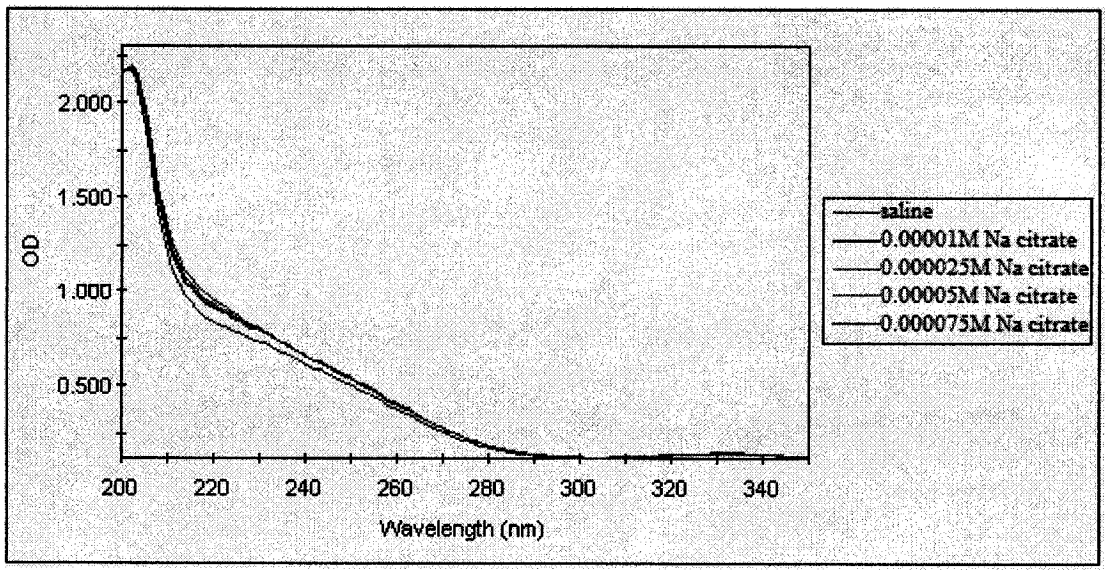

Figure 5.18 - Spectral scans of sodium (Na) citrate in saline with iron (III) chloride, from 200nm to 350nm. The concentrations represent the concentration Zometa that corresponds to the concentration of sodium citrate

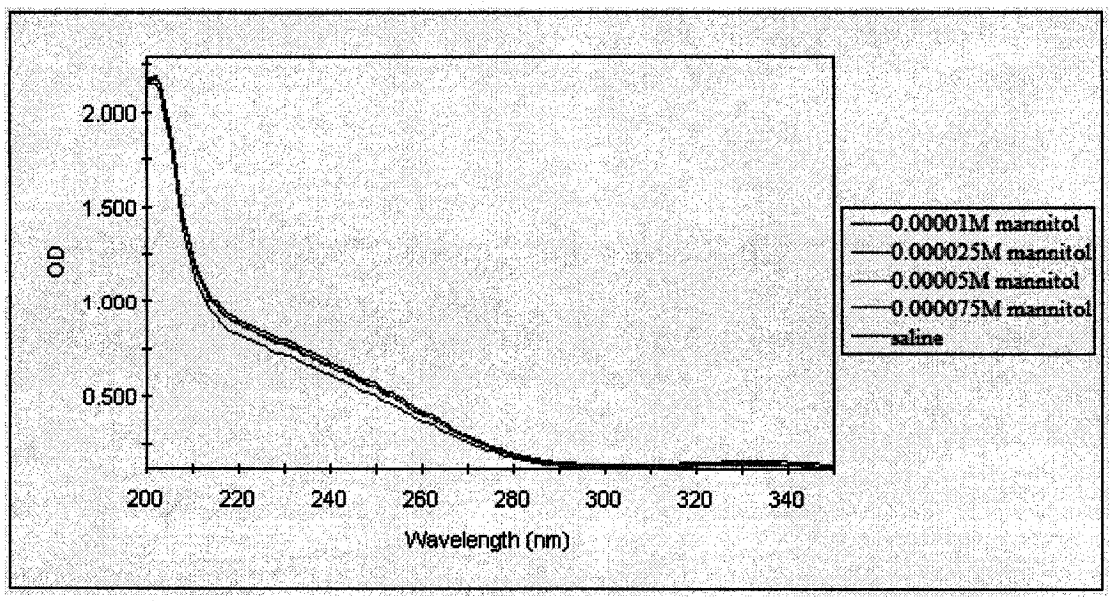

Figure 5.19 - Spectral scans of mannitol in saline with iron (III) chloride, from 200nm to 350 nm. The concentrations represent the concentration of Zometa that corresponds to the concentration of mannitol

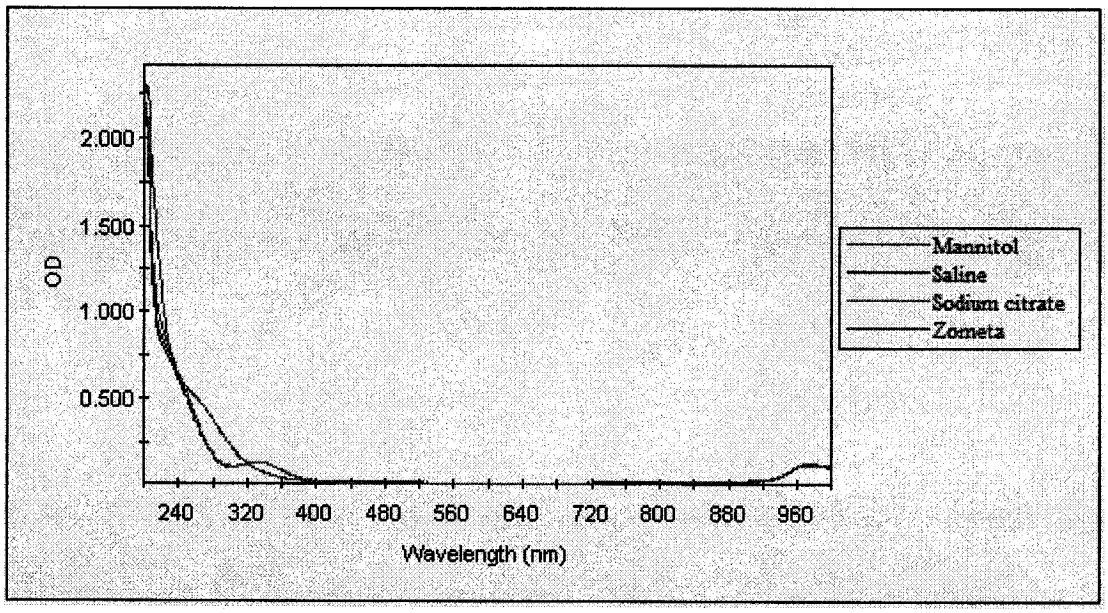

Figure 5.20 - Spectral scans of Zometa, saline, mannitol, and sodium citrate in saline with iron (III) chloride. All concentrations are equivalent

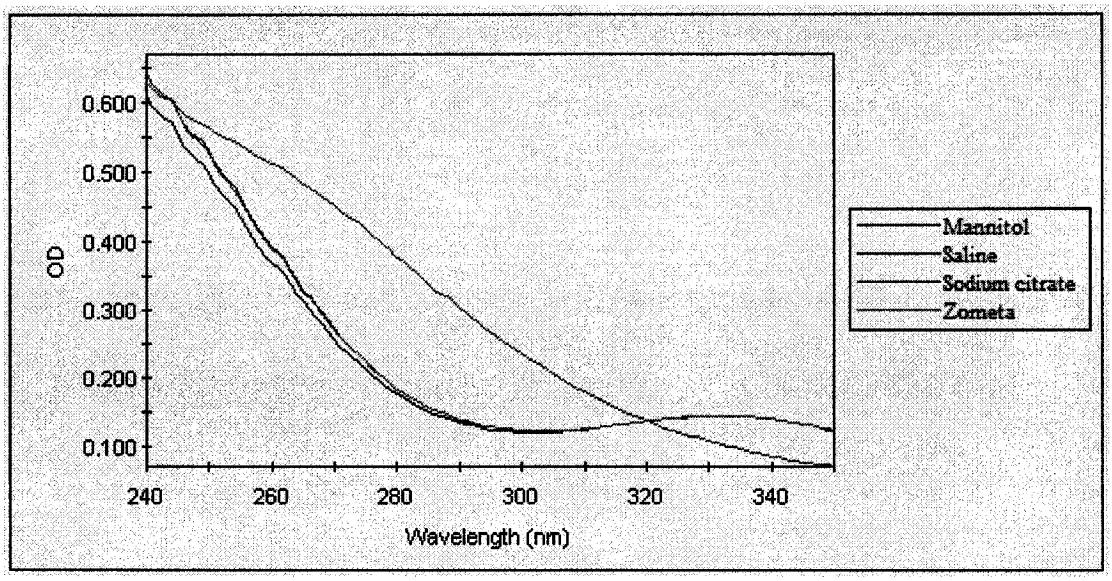

Figure 5.21 - Spectral scans of Zometa, saline, mannitol, and sodium citrate in saline with iron (III) chloride. All concentrations are equivalent

The spectral scans (figures 5.16-5.21) confirmed that it was zoledronic acid that was absorbing light at 290 nm. When the spectral scans of mannitol and sodium citrate with iron (III) chloride and perchloric acid were compared to that of saline with iron (III) chloride and perchloric acid, it was observed that they were all identical. Furthermore, the spectral scans of various concentrations of mannitol and sodium citrate were identical to each other. This seemed to indicate that iron (III) chloride and perchloric acid in saline did not interact with either mannitol or sodium citrate, as they both had the same spectral scan as saline with iron (III) chloride and the spectral scan was not affected by changes in concentration. The spectral scan of the Zometa solution, though, was different from those of mannitol, sodium citrate and saline. From 200 nm to approximately 380 nm, the spectral scan of Zometa was quite different from that of the other three solutions, especially between 260 nm and 350 nm, which includes the wavelength of interest for the calibration. Also, the spectral scan of Zometa, as anticipated, did vary with concentration. At 290 nm, the curves separated completely and the separation was proportional to the difference in concentration between samples.

As previously mentioned, the calibration of zoledronate in bovine serum was also attempted, because it represented a better biological analog than water or saline. However, when the complexing solution iron (III) chloride in perchloric acid was added to zoledronate-bovine serum solutions, the solutions coagulated. The acid content of the complexing solution combined with the proteins of the serum and formed a white precipitate the rendered the solution unusable for ultraviolet spectrophotometry.

5.6 Pamidronate elution from Hydroxyapatite coated implants

The absorbance of each sample was measured 8 times, and calculations were performed using the average of the eight readings. Each of the eight wells was filled with 200 µl of solution. From the absorbance readings, the concentration of each sample was determined, based on the linear equation obtained from the calibration curve. Using the known volume, which is the total of the volume of sample solution removed and the complexing agent solution volume, the concentration was used to determine the mass of pamidronate eluted from the implant during each time interval. Elution from all of the pamidronate-dosed implants was analyzed using the first method for removal of solution.

5.6.1 Elution Results for Implant P1

The absorbance data and calculated quantities of eluted pamidronate for implant P1 are found in table 5.18. The cumulative percent of pamidronate eluted is plotted against time in figure 5.22. Upon calculating the results of the first implant elution, it was observed that a large percentage of the pamidronate was eluted during the first 24 hours (figure 5.22). During the first day over 12% of the deposited amount of pamidronate eluted, which was a greater amount of drug elution than occurred during the remainder of the first six weeks. Therefore, the first 24 hours needed to be investigated more closely to determine the rate of elution during this time.

Table 5.18 - Elution data and calculated values of pamidronate elution from implant P1

Time (days)	**1**	**3**	**7**	**10**	**14**
Absorbance	0.467 0.492 0.488 0.487 0.545 0.488 0.476 0.469	0.265 0.27 0.267 0.28 0.272 0.266 0.262 0.281	0.273 0.273 0.268 0.270 0.270 0.271 0.280 0.277	0.265 0.273 0.278 0.281 0.278 0.278 0.277 0.279	1.57 0.274 0.278 0.282 0.281 0.283 0.278 0.273
Average	0.489	0.270	0.273	0.276	0.278
Blank average	0.229	0.010	0.013	0.016	0.018
Concentration (M)	0.0002516	0.0000107	0.0000132	0.0000170	0.0000196
Volume (L)	0.0039286	0.0039286	0.0037755	0.0040817	0.00306
Moles (n)	9.883×10^{-7}	4.209×10^{-8}	4.998×10^{-8}	6.958×10^{-8}	5.993×10^{-8}
Mass (g)	0.0002758	0.00001174	0.00001395	0.00001941	0.00001672
Mass (mg)	0.2758	0.0117	0.0139	0.0194	0.0167
Cumulative mass	0.2758	0.2875	0.3015	0.3209	0.3376
Initial mass (mg)	2.2	2.2	2.2	2.2	2.2
% mass Released	12.4%	13.07%	13.7%	14.59%	15.34%
Time (days)	**21**	**28**	**36**	**43**	**49**
Absorbance	0.276 0.256 0.267 0.258 0.261 0.262 0.259 0.265	0.295 0.260 0.271 0.270 0.274 0.273 0.275 0.271	0.302 0.300 0.298 0.311 0.310 0.309 0.308 0.316	0.365 0.375 0.373 0.369 0.373 0.364 0.361 0.379	0.255 0.255 0.256 0.252 0.257 0.263 0.254 0.259
Average	0.263	0.274	0.307	0.369875	0.256375
Blank average	0.003	0.014	0.047	0.110	-0.004
Concentration (M)	0.0000026	0.0000143	0.0000508	0.0001203	0
Volume (L)	0.003468	0.003927	0.003927	0.003672	0.003672
Moles (n)	8.98×10^{-9}	5.61×10^{-8}	1.994×10^{-7}	4.418×10^{-7}	0
Mass (g)	0.00000251	0.0000157	0.00005565	0.0001233	0
Mass (mg)	0.0025	0.0157	0.0556	0.1233	0.0000
Cum. Mass (mg)	0.3401	0.3558	0.4114	0.5347	0.5347
Initial mass (mg)	2.2	2.2	2.2	2.2	2.2
% mass released	15.46%	16.17%	18.70%	24.30%	24.30%

Time (days)	56	63	70	77	91
Absorbance	0.302 0.307 0.284 0.301 0.338 0.306 0.315 0.295	0.361 0.341 0.344 0.392 0.369 0.385 0.388 0.400	0.287 0.292 0.292 0.293 0.300 0.305 0.304 0.282	0.296 0.294 0.293 0.303 0.320 0.309 0.295 0.304	0.303 0.292 0.291 0.295 0.307 0.306 0.290 0.292
Average	0.306	0.3725	0.294375	0.30175	0.297
Blank average	0.046	0.113	0.034	0.042	0.037
Concentration (M)	0.0000500	0.0001232	0.0000372	0.0000453	0.0000400
Volume (L)	0.003774	0.00357	0.003825	0.003723	0.003876
Moles (n)	1.8854×10^{-7}	4.3988×10^{-7}	1.4211×10^{-7}	1.6857×10^{-7}	1.5521×10^{-7}
Mass (g)	0.000052611	0.00012275	0.000039654	0.000047037	0.00004331
Mass (mg)	0.0526	0.1227	0.0397	0.0470	0.0433
Cumulative mass	0.5873	0.7101	0.7497	0.7967	0.8401
Initial mass (mg)	2.2	2.2	2.2	2.2	2.2
% mass released	26.70%	32.28%	34.08%	36.21%	38.19%

Time (days)	98	112	126
Absorbance	0.302 0.290 0.304 0.293 0.348 0.292 0.293 0.296	0.402 0.386 0.393 0.408 0.430 0.404 0.416 0.403	0.309 0.320 0.304 0.300 0.328 0.306 0.303 0.298
Average	0.30228571	0.40525	0.3085
Blank average	0.042	0.145	0.049
Concentration (M)	0.0000459	0.0001593	0.0000527
Volume (L)	0.003927	0.003774	0.003927
Moles (n)	1.8012×10^{-7}	6.0118×10^{-7}	2.07×10^{-7}
Mass (g)	0.000050261	0.00016775	0.000057762
Mass (mg)	0.0503	0.1678	0.0578
Cumulative mass	0.8903	1.0581	1.1158
Initial mass (mg)	2.2	2.2	2.2
% mass released	40.47%	48.10%	50.72%

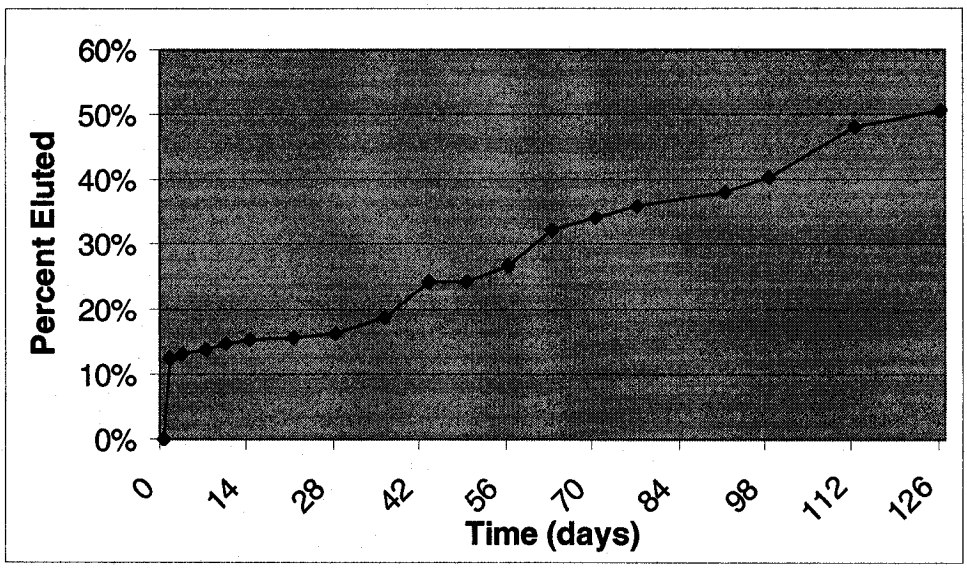

Figure 5.22 - Percent of pamidronate eluted from implant P1 against time

5.6.2 Elution Results for Implant P2

The cumulative mass and corresponding percent of eluted pamidronate are tabulated in table 5.19. The percent of mass eluted was plotted against time in figures 5.23 and 5.24. Figure 5.23 presents the time axis as time-scaled to represent the relative release over time. The time axis in figure 5.24 is not time-scaled, to expand the graph during the first hour of elution. The pamidronate elution from implant P2 (figures 5.23 and 5.24) was measured at three more intervals during the first 12 hours of elution than P1. At 15 minutes, already 25% had eluted and after 3 hours 33% had eluted. Over the next 9 weeks, only an additional 7% of the initial pamidronate eluted. By 14 weeks, 50% of the pamidronate had eluted from implant P2.

Table 5.19 - Elution results for implant P2

Time	Cumulative mass eluted	Percent mass eluted
15 minutes	0.5241 mg	24.96%
3 hours	0.6797 mg	32.37%
12 hours	0.6973 mg	33.20%
1 day	0.7068 mg	33.66%
3 days	0.7259 mg	34.57%
10 days	0.7286 mg	34.70%
2 weeks	0.7435 mg	35.40%
3 weeks	0.7435 mg	35.40%
4 weeks	0.7464 mg	35.54%
5 weeks	0.7648 mg	36.42%
6 weeks	0.7855 mg	37.40%
7 weeks	0.8027 mg	38.22%
9 weeks	0.8482 mg	40.39%
10 weeks	0.8950 mg	42.62%
12 weeks	1.0055 mg	47.88%
14 weeks	1.0279 mg	48.95%

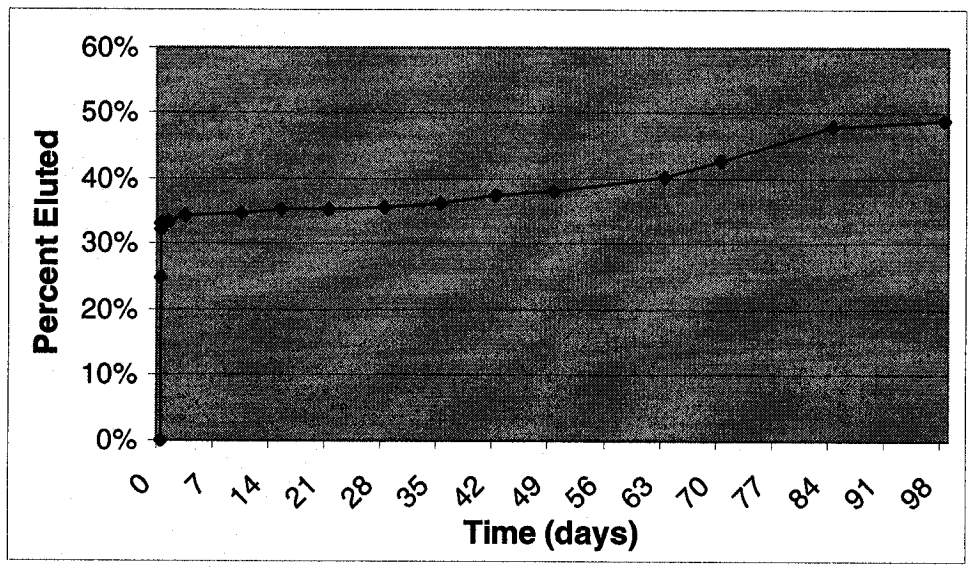

Figure 5.23 - Percent elution of pamidronate over time from implant P2, time scaled

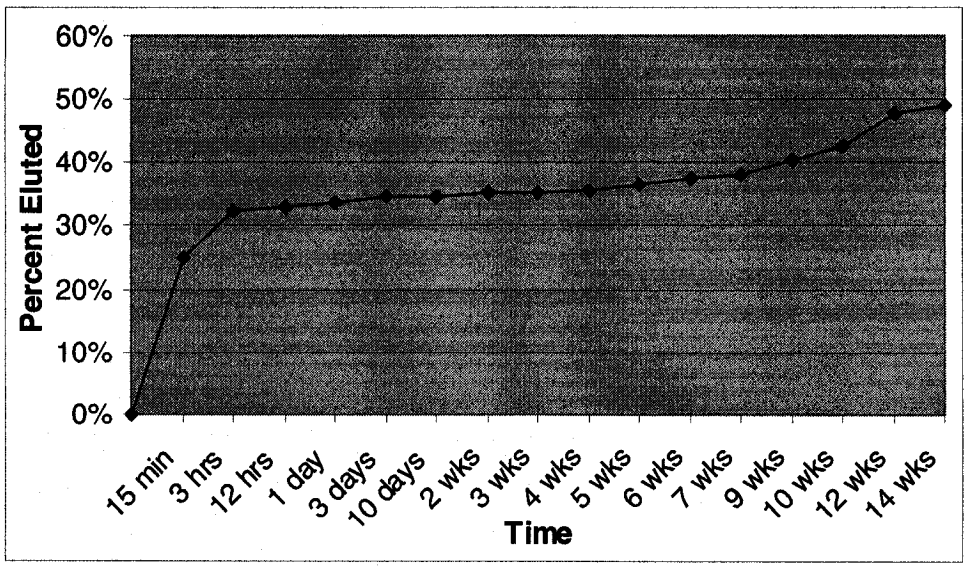

Figure 5.24 - Percent elution from implant P2, not time scaled

5.6.3 Elution Results for Implant P3

The cumulative mass of and the corresponding percent of eluted pamidronate are tabulated in table 5.20. The percent of pamidronate eluted was plotted against time in figures 5.25 and 5.26. Figure 5.25 has a time-scaled x-axis, whereas figure 5.26 does not. The elution from implant P3 was measured at the same intervals as implant P2. The release profile over the first 5 weeks of implant P3 was similar to that of P2, though during the first 15 minutes 40% of the pamidronate was eluted and 50% had eluted after 3 hours. An additional 10% was eluted between 3 hours and 5 weeks. From 5 weeks to 14 weeks, a further 30% of the pamidronate was eluted. Based on the elution results from P2 and P3 during the first 3 hours, that time period needed to be broken down into smaller intervals to determine how quickly the initial elution of pamidronate was occurring.

Table 5.20 - Elution results for implant P3

Time	Cumulative mass eluted	Percent mass eluted
15 minutes	0.8439 mg	40.19%
3 hours	1.0608 mg	50.86%
12 hours	1.0847 mg	51.65%
1 day	1.1178 mg	53.23%
3 days	1.1397 mg	54.27%
10 days	1.1525 mg	54.88%
2 weeks	1.1771 mg	56.05%
3 weeks	1.1810 mg	56.24%
4 weeks	1.2115 mg	57.69%
5 weeks	1.2299 mg	58.57%
6 weeks	1.4935 mg	71.12%
7 weeks	1.5853 mg	75.49%
9 weeks	1.6178 mg	77.04%
10 weeks	1.6417 mg	78.18%
12 weeks	1.8900 mg	90.00%
14 weeks	1.9175 mg	91.31%

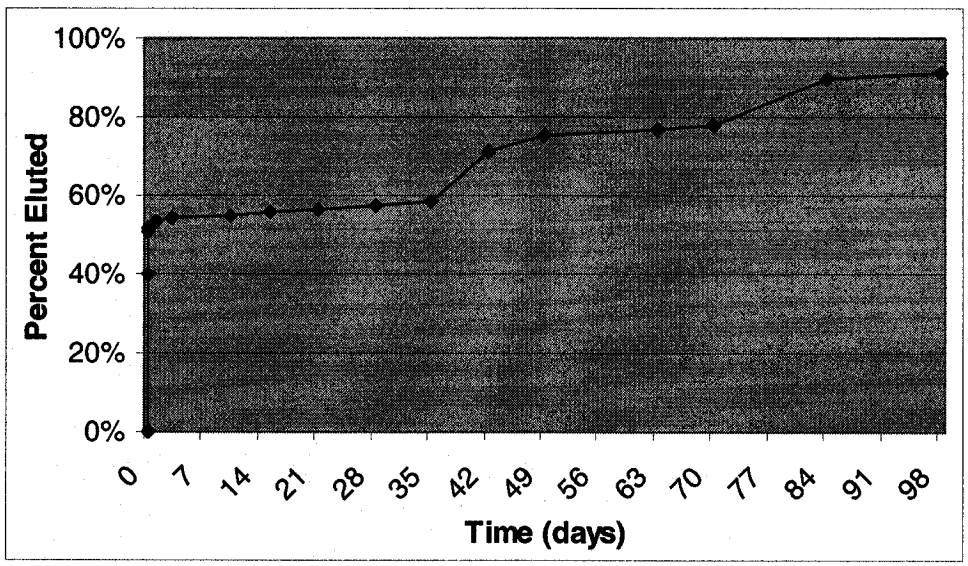

Figure 5.25 - Percent elution of pamidronate against time from implant P3, with time-scaled x-axis

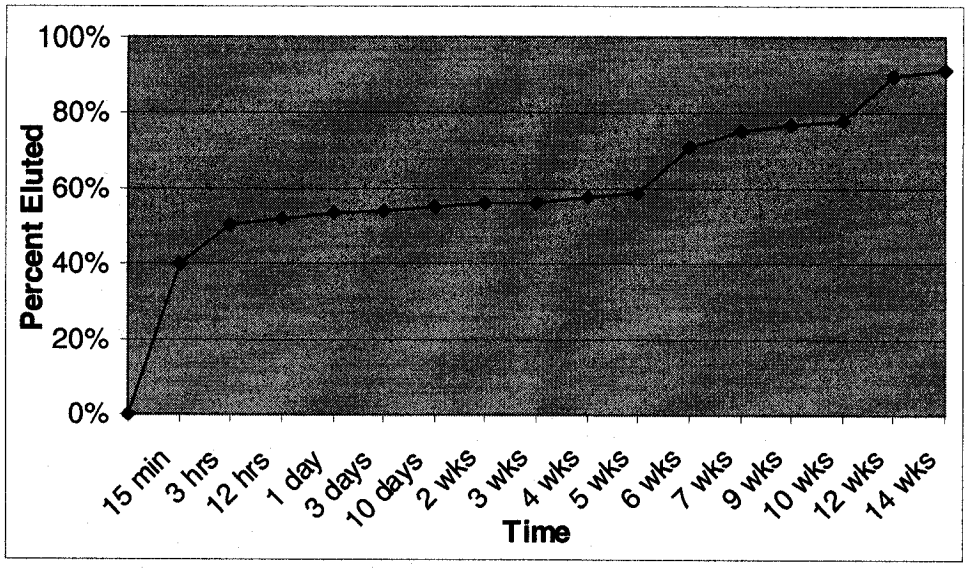

Figure 5.26 - Percent elution of pamidronate against time from implant P3, not time-scaled

5.6.4 Elution Results for Implant P4

The cumulative mass and the corresponding percent of eluted pamidronate are in table 5.21. The percent of pamidronate eluted was plotted against time in figure 5.27. In the first 5 minutes, 45% of the pamidronate was eluted from implant P4, and an additional 19% was eluted over the next 24 hours, for a total of 64% of the initial pamidronate eluted after the first day. Drug elution from 24 hours to 14 weeks was gradual and the percent eluted increased from 64% to 86% during that time.

Table 5.21 - Elution results for implant P4

Time	Cumulative mass eluted	Percent mass eluted
5 minutes	0.7920 mg	46.59%
15 minutes	0.9285 mg	54.62%
30 minutes	0.9769 mg	57.46%
1 hour	1.0213 mg	60.08%
3 hours	1.0696 mg	62.92%
12 hours	1.0924 mg	64.26%
24 hours	1.0980 mg	64.59%
5 days	1.0980 mg	64.59%
1 week	1.0980 mg	64.59%
2 weeks	1.1175 mg	65.73%
4 weeks	1.1408 mg	67.11%
6 weeks	1.1860 mg	69.76%
8 weeks	1.2388 mg	72.87%
10 weeks	1.3120 mg	77.18%
12 weeks	1.4004 mg	82.38%
14 weeks	1.4669 mg	86.29%

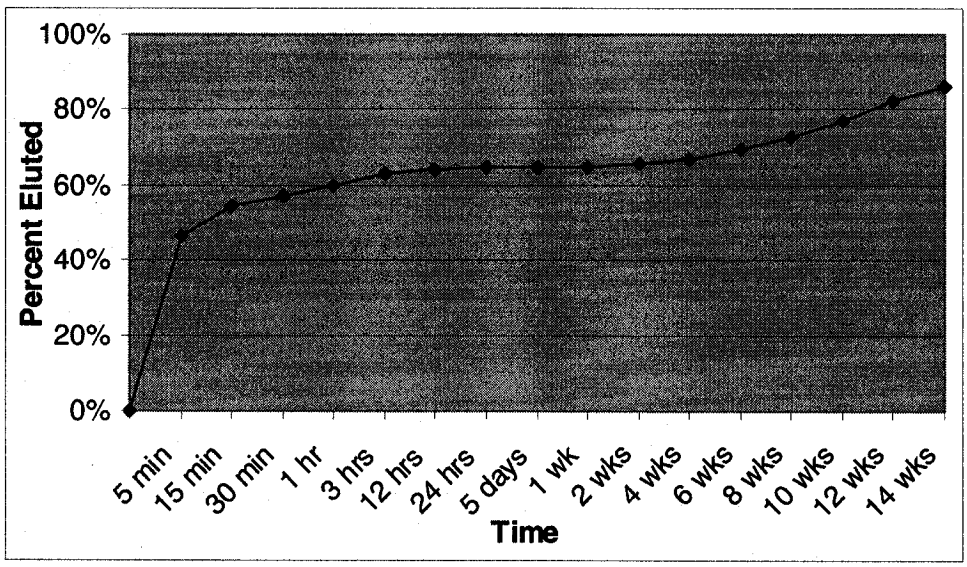

Figure 5.27 - Percent elution of pamidronate against time for implant P4

5.6.5 Elution Results for Implant P5

The cumulative mass of pamidronate eluted and the corresponding percent of mass eluted are found in table 5.22. The percent of pamidronate eluted was plotted against time in figure 5.28. Implant P5 had eluted 55% of the deposited pamidronate after 5 minutes, and had eluted 64% after 15 minutes.

Unlike P4, which had gradual elution from 5 minutes to 12 hours, implant P5 had very little elution between the 15 minutes sample and the 12 hour sample, an amount that represented only an increased amount of elution of 2%. From 24 hours to 14 weeks pamidronate eluted gradually and the percent eluted increased from 64% to 90%.

Table 5.22 - Elution results for implant P5

Time	Cumulative mass eluted	Percent mass eluted
5 minutes	0.9341 mg	54.95%
15 minutes	1.0652 mg	62.66%
30 minutes	1.0781 mg	63.42%
1 hour	1.0795 mg	63.50%
3 hours	1.0853 mg	63.84%
12 hours	1.0886 mg	64.04%
24 hours	1.0888 mg	64.05%
5 days	1.0940 mg	64.35%
1 week	1.0969 mg	64.52%
2 weeks	1.1204 mg	65.91%
4 weeks	1.2030 mg	70.76%
6 weeks	1.3052 mg	76.78%
8 weeks	1.3777 mg	81.04%
10 weeks	1.4053 mg	82.66%
12 weeks	1.4993 mg	88.19%
14 weeks	1.5301 mg	90.00%

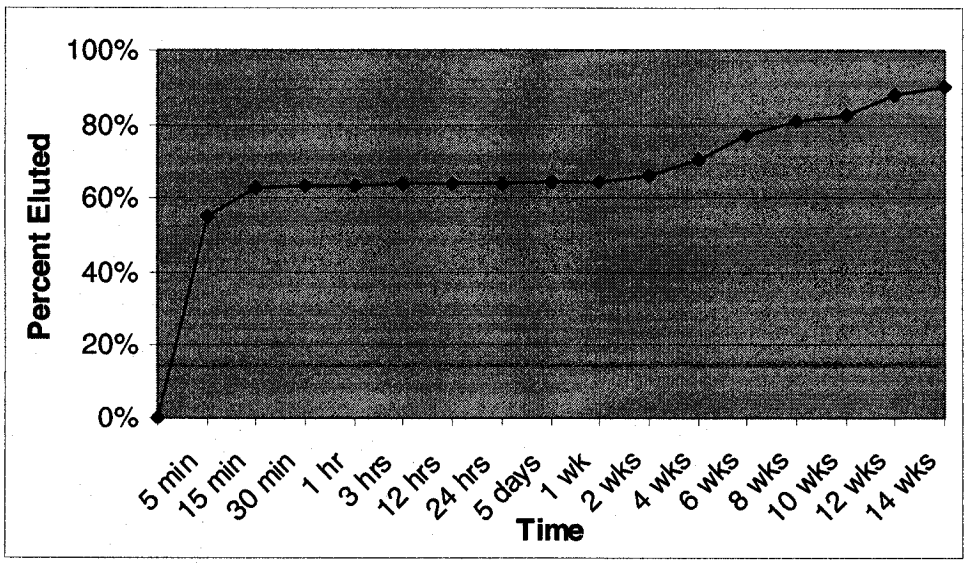

Figure 5.28 - Percent elution of pamidronate against time for implant P5

5.6.6 Average Pamidronate Elution in Water from HA-coated Implants

Calculation of the average pamidronate elution from HA-coated implants P2, P3, P4, and P5, as depicted graphically in figure 5.29, showed that there was a large percent of pamidronate eluted during the first 15 minutes of implant submersion in water, followed by a slow rate of elution over the next 6 weeks. After 6 weeks, the rate of elution increased. The error bars in figure 37 represent the standard deviation of the four samples. The standard deviation remained fairly constant over 14 weeks, just below 20%. However, most of the difference in elution appeared to occur during the first 15 minutes. During this time the percent of pamidronate eluted varied from 24% to 66%. Following this time, all of the elutions took place at nearly the same rate, so the error derives from the difference in the 15 minute starting point. Implant P1 was excluded from the average because of the lack of measurements during the first 24 hours.

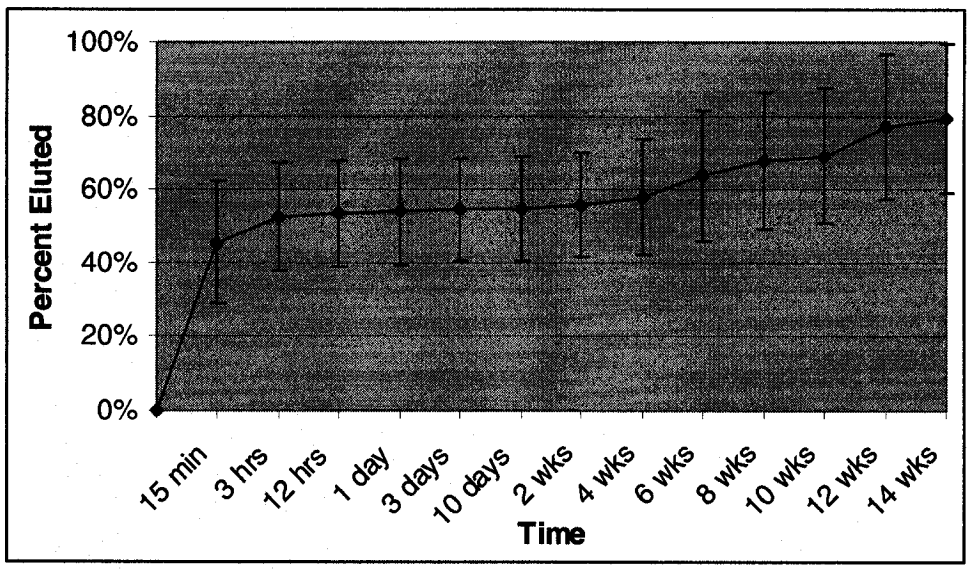

Figure 5.29 - Average percent of pamidronate elution from HA-coated implants against time

5.7 Pamidronate Elution from non-HA Coated Porous Tantalum Implants

The elution of pamidronate from non-HA coated implants was measured to compare with the elution from HA-coated implants to determine if the HA coating was causing a difference in elution rates. Because bisphosphonates have a natural chemical affinity for HA, it was anticipated that the bisphosphonate elution from non-HA coated tantalum implants would occur much more quickly than elution from HA-coated implants. Drug elution from all pamidronate-dosed non-HA coated porous tantalum implants was measured using the first method.

5.7.1 Elution Results for Implant Ta1

The cumulative mass of pamidronate elution and the corresponding percent of mass eluted are in table 5.23. The percent of pamidronate eluted was plotted against time in figure 5.30. After 5 minutes, over 80% of the pamidronate had eluted from implant Ta1, 94% after 15 minutes, and all of the pamidronate had eluted after one hour.

Table 5.23 - Elution results for Implant Ta1

Time	Cumulative mass eluted	Percent mass eluted
5 minutes	1.4823 mg	82.35%
15 minutes	1.6988 mg	94.38%
30 minutes	1.7217 mg	95.65%
1 hour	1.8130 mg	100.72%

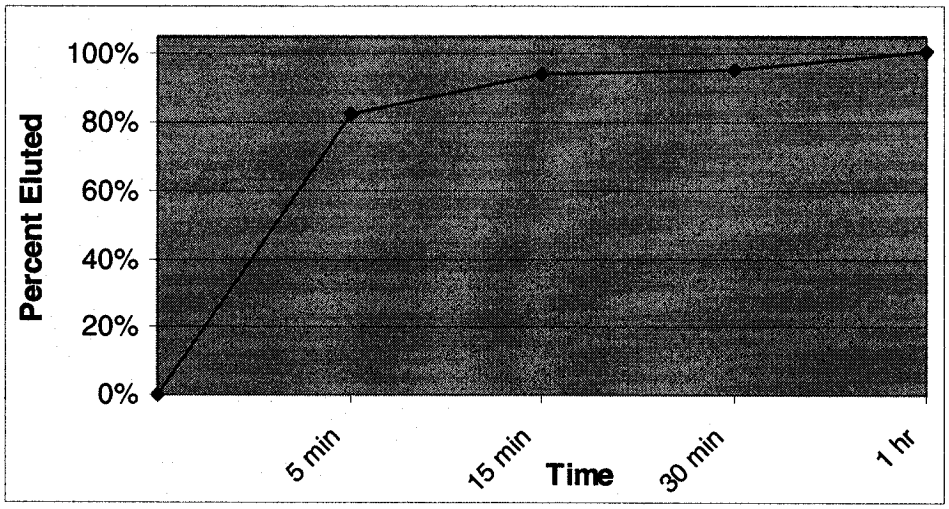

Figure 5.30 - Percent of pamidronate eluted against time for implant Ta1

5.7.2 Elution Results for Implant Ta2

The cumulative mass of pamidronate eluted and the corresponding percent of mass eluted are tabulated in table 5.24. The percent of pamidronate eluted was plotted against time in figure 5.31. Pamidronate elution profile from Ta2 was almost identical to that from Ta1. Over 80% eluted during the first 5 minutes and by one hour 99% of the pamidronate had eluted.

Table 5.24 - Elution results for implant Ta2

Time	Cumulative mass eluted	Percent mass eluted
5 minutes	1.5026 mg	83.48%
15 minutes	1.7374 mg	96.52%
30 minutes	1.7542 mg	97.46%
1 hour	1.7783 mg	98.79%

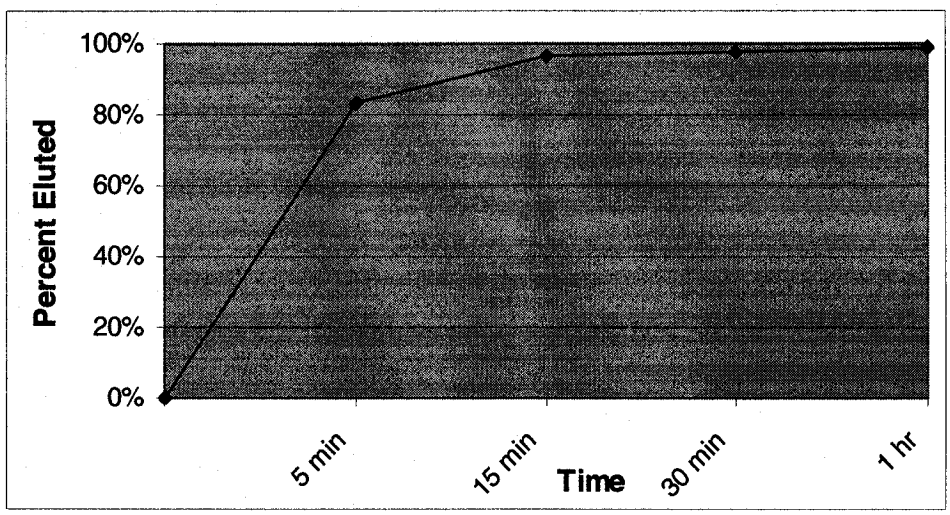

Figure 5.31 - Percent elution of pamidronate against time for implant Ta2

5.7.3 Average Pamidronate Elution from non-HA coated implants

Taking the average of the pamidronate elution from the two non-HA coated tantalum implants and plotting the data against time (figure 5.32) showed that the elution profile of both of the implants were nearly identical. The standard deviation, as shown by the error bars, was less than 2% for all times. Both of the implants had eluted 99% of the pamidronate after one hour. The profile of drug release from non-HA coated implants was significantly different from the pamidronate release from HA-coated implants, showing that hydroxyapatite does bind pamidronate and delay its elution from a tantalum implant into water.

The elution profile of pamidronate from tantalum implants not coated with hydroxyapatite was different than those coated with hydroxyapatite. The implants coated with hydroxyapatite were still eluting pamidronate after 10 weeks, whereas those without an HA coating eluted the entire dose of pamidronate in one hour (figure 5.33). The average of implants P4 and P5 was used for figure 48 because samples were taken at the same time intervals as for implants Ta1 and Ta2. The standard deviation for implants P4 and P5 was less than 6% for all time intervals.

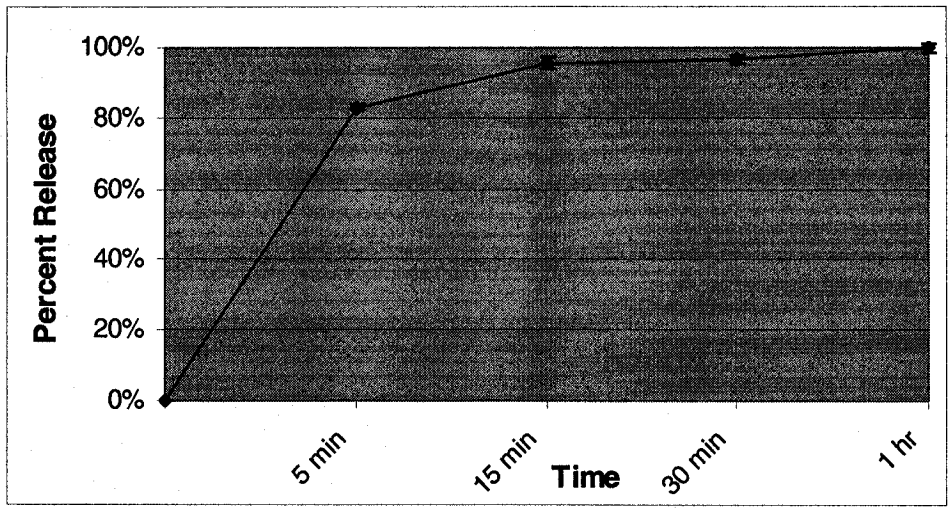

Figure 5.32 - Average percent of pamidronate elution from non-HA coated implants against time

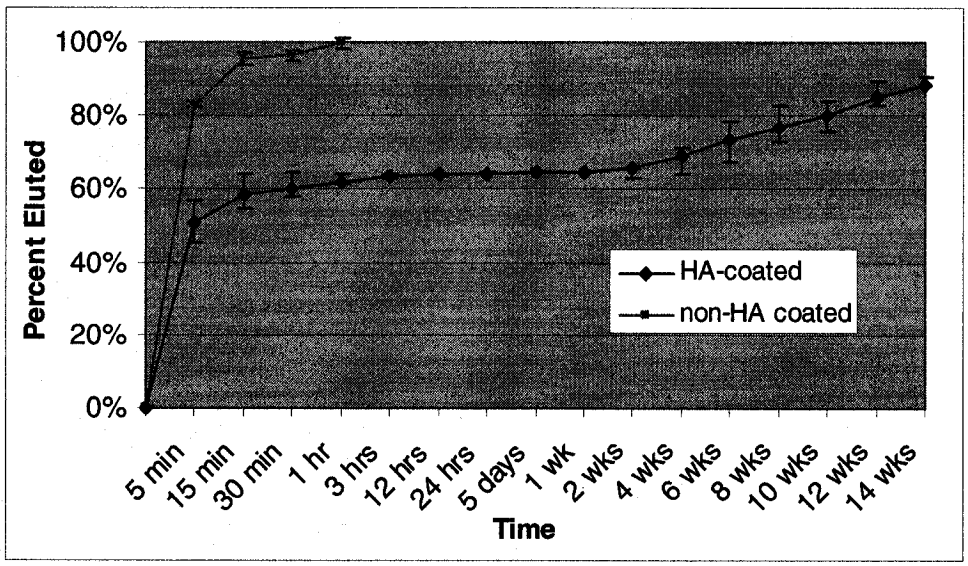

Figure 5.33 - Average percent of pamidronate elution from HA-coated and non-HA coated implants against time

5.8 Pamidronate Elution in Saline

The cumulative mass pamidronate eluted and the corresponding percent of elution for implant P6 is found in table 5.25. Initially, the results for the elution of pamidronate in saline from HA coated implants appeared to be similar to elution of pamidronate in water. However, at four weeks 100% of the

pamidronate appeared to have eluted, and following that the absorbance measurements still indicated that drug was being eluted. By 14 weeks, the amount of pamidronate measured was more than twice as great as the amount of drug deposited on the implant. Similar results were obtained from a second HA-coated implant dosed with pamidronate and soaked in saline. This indicated that there was a difference in how the pamidronate is being measured between the water and saline elutions. The only difference between the two solutions was the presence of sodium chloride.

Table 5.25 - Elution results for implant P6

Time	Cumulative mass eluted	Percent mass eluted
5 minutes	0.5295 mg	29.42%
15 minutes	0.6558 mg	36.43%
30 minutes	0.6953 mg	38.63%
1 hour	0.6953 mg	38.63%
3 hours	0.6953 mg	38.63%
12 hours	0.7895 mg	43.86%
24 hours	0.8173 mg	45.41%
5 days	0.9221 mg	51.23%
1 week	0.9883 mg	54.91%
2 weeks	1.1887 mg	66.04%
4 weeks	1.8225 mg	101.25%
6 weeks	2.6077 mg	144.87%
8 weeks	2.9726 mg	165.15%
10 weeks	3.3391 mg	185.51%
12 weeks	3.5225 mg	195.69%
14 weeks	3.9693 mg	220.52%

5.9 Zoledronate Elution in Saline

The first set of zoledronate-dosed implants, Z1, Z2, Z3, and Z4, were analyzed using the first method for elution measurement. The second method was used for the elution measurements of zoledronate-dosed implants Z5 and Z6. Zoledronate belongs to a newer generation of bisphosphonate than

pamidronate and has greatly increased potency, so the doses of zoledronate applied to the implants were much lower than those of pamidronate.

5.9.1 Zoledronate Elution from Implant Z1 and Z2

The samples of solution taken from the elution studies for implant Z1 were complexed with copper (II) sulfate solution, like the pamidronate. The results are found in table 5.26. Using copper (II) sulfate as the complexing agent, the calculated amount of zoledronate eluted at 5 minutes was greater than the amount of zoledronate deposited on the implant. The calculated amount of zoledronate eluted continued to increase with time. This was repeated with a second implant, Z2, with similar results. These results, combined with the spectrophotometric results described earlier, clearly indicated that copper (II) sulfate was not a suitable complexing agent for the measurement of zoledronate in Zometa.

Table 5.26 - Elution results for implant Z1

Time	Cumulative mass eluted	Percent mass eluted
5 minutes	0.2452 mg	122.62%
15 minutes	0.2680 mg	134.01%
30 minutes	0.2771 mg	138.54%
1 hour	0.2868 mg	143.39%
3 hours	0.2939 mg	146.95%
12 hours	0.3044 mg	152.21%
24 hours	0.3112 mg	155.58%
1 week	0.3896 mg	194.79%
2 weeks	0.4649 mg	232.45%
3 weeks	0.5017 mg	250.86%
4 weeks	0.5188 mg	259.42%
5 weeks	0.5291 mg	264.57%
6 weeks	0.5523 mg	276.15%
8 weeks	0.5718 mg	285.91%

5.9.2 Elution Results for Implant Z3

The elution of zoledronate from HA-coated implants was successfully measured using iron (III) chloride as the complexing agent. Zoledronate elution from implant Z3, and all subsequent zoledronate elutions, was measured using iron (III) chloride. The elution data are compiled in table 5.27 and the percent of mass eluted is plotted against time in figure 5.34. The initial zoledronate release from implant Z3 was very high; over 80% was eluted during the first 5 minutes. This high amount of elution was followed by almost no zoledronate release over the first 4 weeks of elution. By 14 weeks, all of the zoledronate had eluted from the implant.

Table 5.27 - Elution results for implant Z3

Time	Cumulative mass eluted	Percent mass eluted
5 minutes	0.0430 mg	82.06%
15 minutes	0.0433 mg	82.63%
30 minutes	0.0433 mg	82.63%
1 hour	0.0433 mg	82.63%
3 hours	0.0433 mg	82.63%
12 hours	0.0433 mg	82.63%
1 weeks	0.0433 mg	82.63%
2 weeks	0.0433 mg	82.63%
3 weeks	0.0433 mg	82.63%
4 weeks	0.0433 mg	82.63%
5 weeks	0.0460 mg	87.79%
6 weeks	0.0460 mg	87.79%
8 weeks	0.0460 mg	87.79%
9 weeks	0.0460 mg	87.79%
10 weeks	0.0460 mg	87.79%
11 weeks	0.0477 mg	91.03%
12 weeks	0.0487 mg	92.94%
13 weeks	0.0511 mg	97.52%
14 weeks	0.0523 mg	99.81%

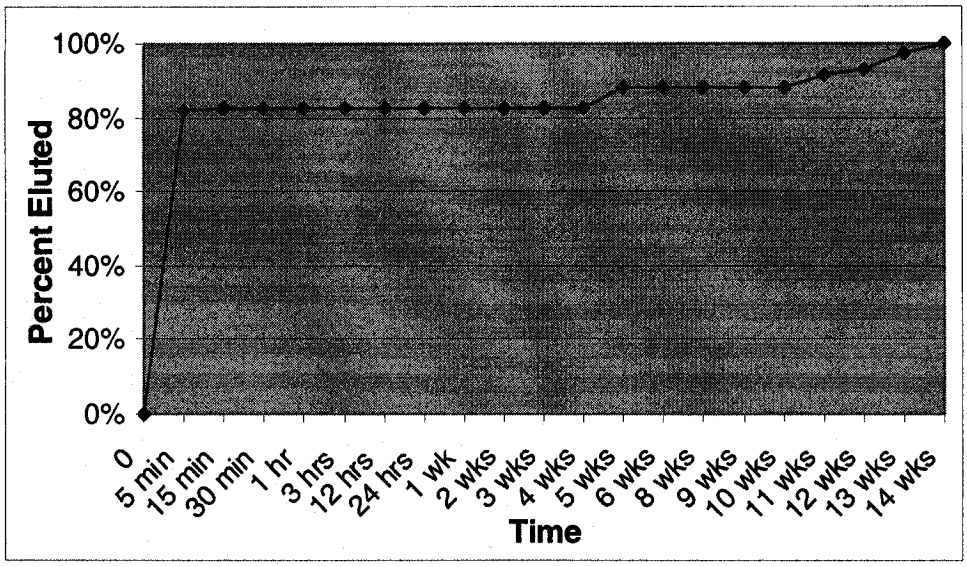

Figure 5.34 - Percent elution of zoledronate against time for implant Z3

5.9.3 Elution results for implant Z4

The elution data for implant Z4 are found in table 5.28 and the percent of mass eluted from implant Z4 over time is plotted in figure 5.35. During the first 5 minutes, 45% of the zoledronate had eluted. The amount of zoledronate eluted increased to 62% during the first 24 hours. By 6 weeks, 100% of the initial dose of zoledronate had eluted.

Table 5.28 - Elution data for implant Z4

Time	Cumulative mass eluted	Percent mass eluted
5 minutes	0.0238 mg	44.43%
15 minutes	0.0259 mg	48.29%
1 hour	0.0279 mg	52.15%
3 hours	0.0320 mg	59.63%
12 hours	0.0332 mg	61.88%
24 hours	0.0332 mg	61.88%
1 week	0.0457 mg	85.29%
3 weeks	0.0482 mg	89.95%
4 weeks	0.0502 mg	93.72%
6 weeks	0.0536 mg	100.00%
8 weeks	0.0536 mg	100.00%
10 weeks	0.0536 mg	100.00%
12 weeks	0.0536 mg	100.00%
14 weeks	0.0536 mg	100.00%

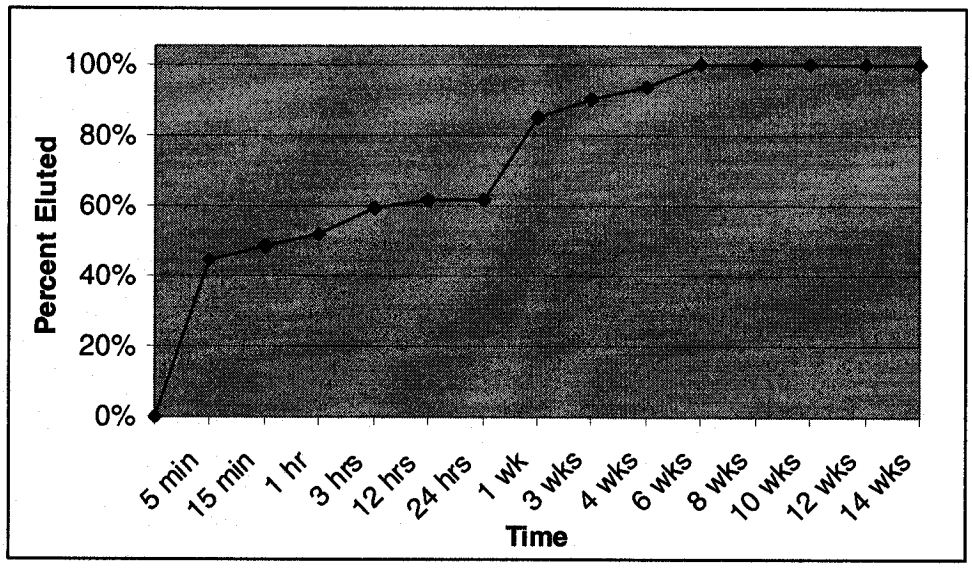

Figure 5.35 - Percent elution of zoledronate against time from implant Z4

5.9.4 Elution results for implant Z5

The elution data for implant Z5 are found in table 5.29 and the percent of mass eluted from implant Z5 over time is plotted in figure 5.35. During the first 5 minutes, 63% of the zoledronate had eluted. The amount of zoledronate eluted increased to 78% during the first 24 hours. By 4 weeks, 104% of the initial dose of zoledronate had eluted.

Table 5.29 - Elution results for implant Z5

Time	Cumulative mass eluted	Percent mass eluted
5 minutes	0.0314 mg	62.91%
15 minutes	0.0314 mg	62.91%
1 hour	0.0314 mg	62.91%
3 hours	0.0349 mg	69.80%
24 hours	0.0390 mg	78.06%
1 week	0.0390 mg	78.06%
2 weeks	0.0425 mg	84.95%
3 weeks	0.0467 mg	93.39%
4 weeks	0.0522 mg	104.41%
6 weeks	0.0522 mg	104.41%

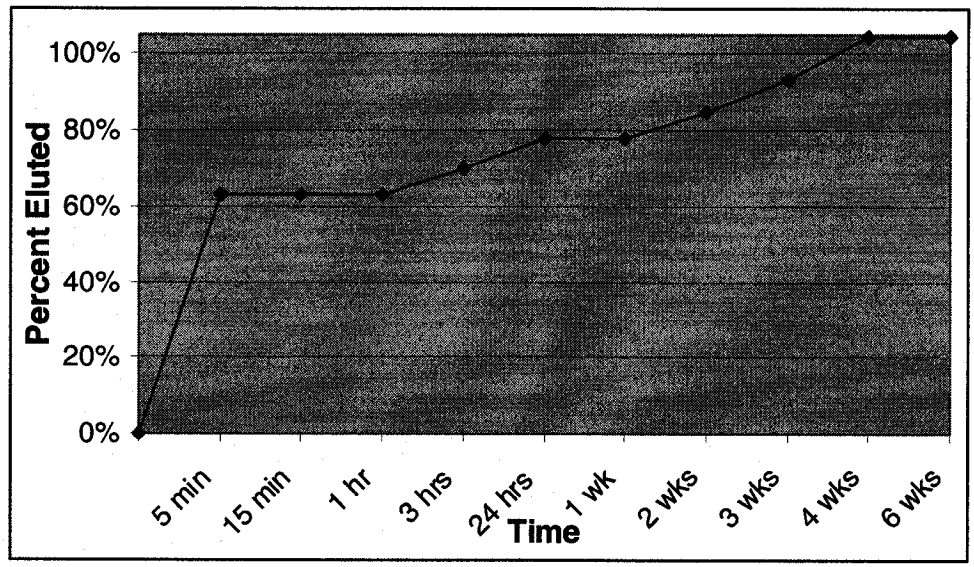

Figure 5.36 – Percent elution of zoledronate against time from implant Z5

5.9.5 Elution results for implant Z6

The elution data for implant Z6 are found in table 5.30 and the percent of mass eluted from implant Z6 over time is plotted in figure 5.37. During the first 5 minutes, 46% of the zoledronate had eluted, though the amount eluted increased to 61% during the next 10 minutes. A further 4%, for a total percent eluted of 65%, had eluted after 24 hours of elution time. By 4 weeks, 98% of the initial dose of zoledronate had eluted, and no more drug had eluted by 6 weeks.

Table 5.30 - Elution results for implant Z6

Time	Cumulative mass eluted	Percent mass eluted
5 minutes	0.0228 mg	45.65%
15 minutes	0.0304 mg	60.82%
1 hour	0.0326 mg	65.11%
3 hours	0.0326 mg	65.11%
24 hours	0.0326 mg	65.11%
1 week	0.0445 mg	89.09%
2 weeks	0.0445 mg	89.09%
3 weeks	0.0445 mg	89.09%
4 weeks	0.0488 mg	97.52%
6 weeks	0.0488 mg	97.52%

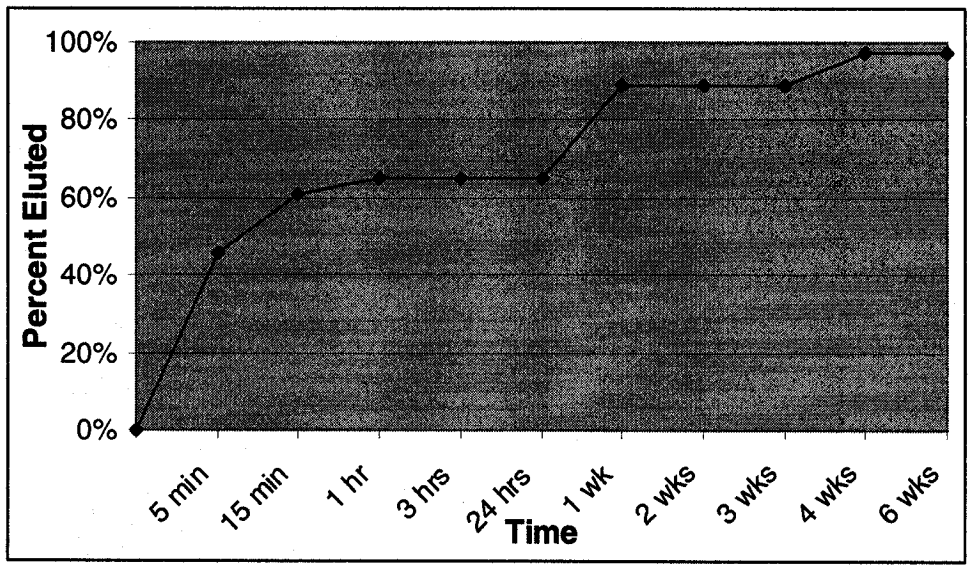

Figure 5.37 - Percent elution of zoledronate against time from implant Z6

5.9.6 Average Zoledronate elution from HA-coated implants

The average zoledronate elution from implants Z3, Z4, Z5, and Z6 was plotted against time in figure 5.38. The implants were plotted based on which measurement method was used during the elution study. Implants Z3 and Z4 were measured using method 1 and implants Z5 and Z6 were measured using method 2. The error bars represent the standard deviation of the sample. The standard deviation was largest during the first 24 hours, due to the difference in

the extent of elution at 5 minutes between the implants. The elution for the two methods was similar, especially during the first 24 hours. After the first day of elution, the elution from implants measured using method 2 was relatively constant until the entire dose of zoledronate had eluted by 4 weeks. The implants measured using method 1 also had fairly constant elution, though it took longer for the whole dose to elute from the implants and the elution was complete at 14 weeks. However, the differences between the two methods were not substantial.

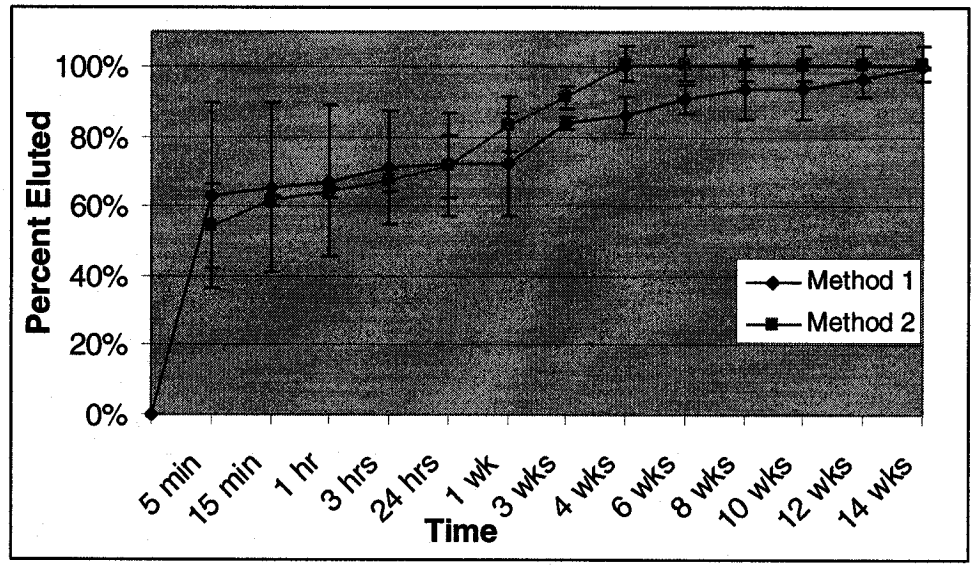

Figure 5.38 - Average percent of zoledronate elution from HA-coated implants

5.10 Zoledronate Elution from Ethylene Oxide Sterilized HA-Coated Implants

Three HA-coated, zoledronate dosed implants were sterilized with ethylene oxide prior to the elution studies to determine if the sterilization process changed the elution profile. Since the implants are for eventual use as orthopaedic implants, they will need to be sterilized prior to surgical implantation, and ethylene oxide is a common method of sterilization. Zoledronate elution measurements from all EtO sterilized implants were conducted using the first method.

5.10.1 Elution Results for Implant Z7

The cumulative mass of zoledronate eluted and the corresponding percent of mass eluted from implant Z7 are tabulated in table 5.31, and the percent of mass eluted is plotted against time in figure 5.39. Implant Z7 eluted 30% of the initial zoledronate after 5 minutes and over 50% after 15 minutes. The rest of the elution took place between the end of the first week and the third week. By 3 weeks 100% of the zoledronate had eluted and the subsequent measurements indicated that this was true because the absorbance of the sample solutions remained constant and equal to a blank solution.

Table 5.31 - Elution results for implant Z7

Time	Cumulative mass eluted	Percent mass eluted
5 minutes	0.0152 mg	29.01%
15 minutes	0.0275 mg	52.48%
30 minutes	0.0281 mg	53.63%
1 hour	0.0281 mg	53.63%
3 hours	0.0281 mg	53.63%
12 hours	0.0281 mg	53.63%
24 hours	0.0281 mg	53.63%
1 week	0.0284 mg	54.20%
2 weeks	0.0401 mg	76.53%
3 weeks	0.0500 mg	100.00%
4 weeks	0.0500 mg	100.00%
5 weeks	0.0500 mg	100.00%
6 weeks	0.0500 mg	100.00%
7 weeks	0.0500 mg	100.00%
8 weeks	0.0500 mg	100.00%
9 weeks	0.0500 mg	100.00%

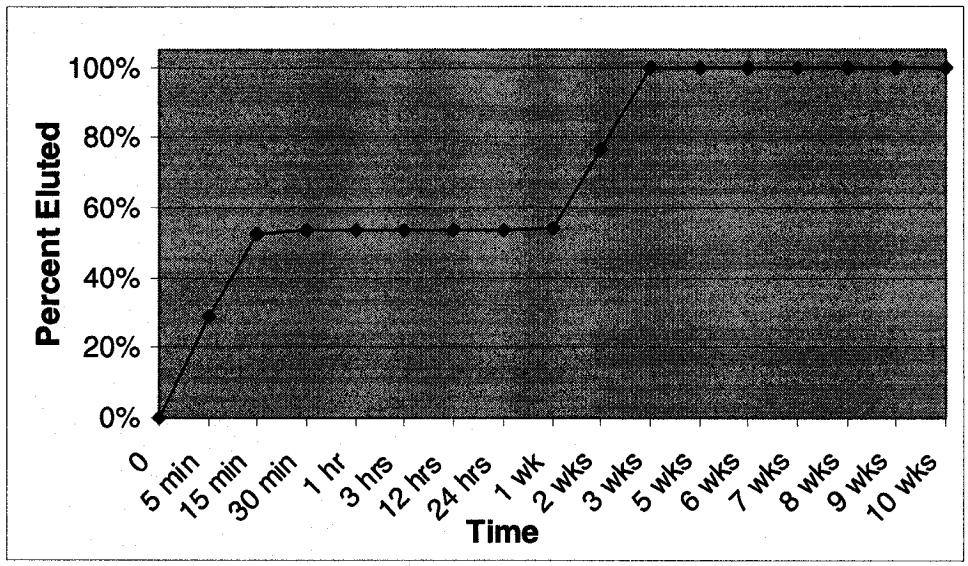

Figure 5.39 - Percent elution of zoledronate against time from implant Z7

5.10.2 Elution Results for Implant Z8

The cumulative mass of zoledronate elution and the percent of mass eluted from implant Z8 are found in table 5.32. The percent of mass eluted was plotted against time in figure 5.40. Implant Z8, eluted 28% of the zoledronate after 5 minutes and 32% of the drug after 15 minutes. There was no further elution during the remainder of the first day. Between 24 hours and 3 weeks, the drug eluted at a rapid rate and the percent of eluted zoledronate increased from 32% to 80%. The amount of eluted drug then stayed constant until the eighth week, when the rest of the drug was eluted between the 8 week and 10 week measurements.

Table 5.32 - Elution results for implant Z8

Time	Cumulative mass eluted	Percent mass eluted
5 minutes	0.0147 mg	27.95%
15 minutes	0.0169 mg	32.13%
30 minutes	0.0169 mg	32.13%
1 hour	0.0169 mg	32.13%
3 hours	0.0169 mg	32.13%
12 hours	0.0169 mg	32.13%
24 hours	0.0169 mg	32.13%
1 week	0.0182 mg	34.60%
2 weeks	0.0271 mg	51.52%
3 weeks	0.0424 mg	80.61%
5 weeks	0.0424 mg	80.61%
6 weeks	0.0424 mg	80.61%
7 weeks	0.0424 mg	80.61%
8 weeks	0.0424 mg	80.61%
9 weeks	0.0481 mg	91.44%
10 weeks	0.0500 mg	100.00%

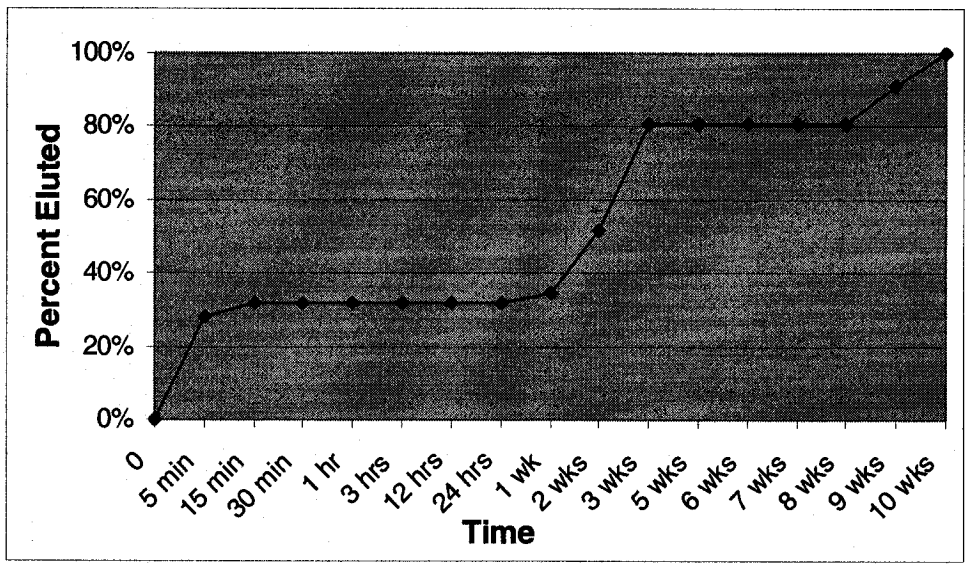

Figure 5.40 - Percent elution of zoledronate against time from implant Z8

5.10.3 Elution Results for Implant Z9

The cumulative mass of zoledronate eluted and the percent of mass eluted from implant Z9 are found in table 5.33 and the percent of mass eluted versus time was plotted in figure 5.41. During the first 5 minutes 17% of the initial dose of zoledronate eluted from implant Z9. The amount of zoledronate

eluted increased to 21% after 3 hours, and remained at 21% for until 24 hours. From one week to eight weeks, the elution was fairly constant, increasing from 35% to 100%, averaging slightly less than 10% per week.

Table 5.33 - Elution results for implant Z9

Time	Cumulative mass eluted	Percent mass eluted
5 minutes	0.0088 mg	16.67%
15 minutes	0.0088 mg	16.67%
1 hour	0.0094 mg	17.94%
3 hours	0.0112 mg	21.35%
12 hours	0.0112 mg	21.35%
24 hours	0.0112 mg	21.35%
1 week	0.0186 mg	35.46%
3 weeks	0.0323 mg	61.36%
4 weeks	0.0386 mg	73.42%
6 weeks	0.0487 mg	92.65%
8 weeks	0.0526 mg	100.08%
10 weeks	0.0526 mg	100.08%

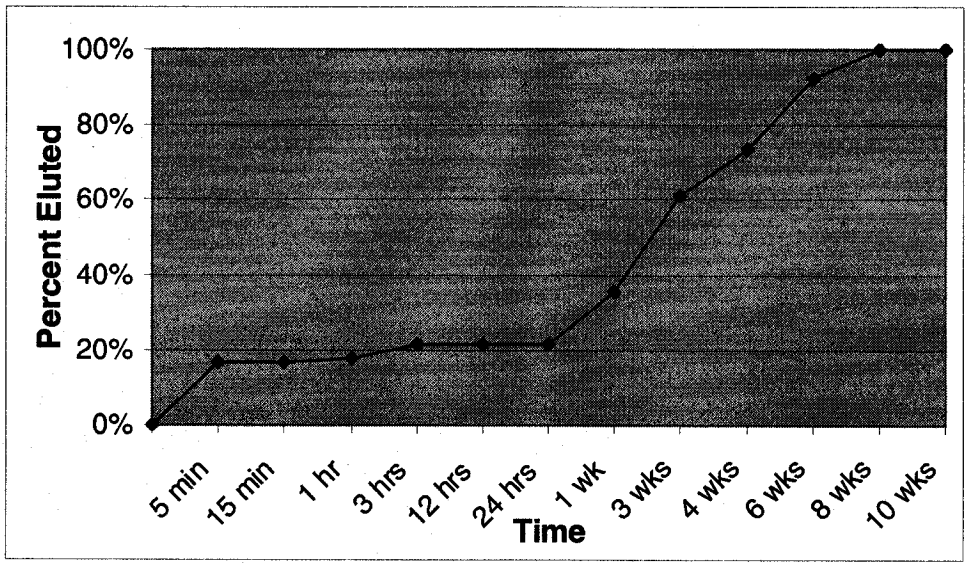

Figure 5.41 - Percent elution of zoledronate against time for implant Z9

5.10.4 Average Zoledronate Elution from HA-coated, EtO-sterilized implants

The average elution from the EtO-sterilized was plotted in figure 5.42. The error bars represent the standard deviation of the sample. The elution of zoledronate from ethylene oxide sterilized implants spiked during the first five minutes, and then remained fairly constant until the end of the first 24 hours. The standard deviation of the sample also remained fairly constant from 15 minutes to 24 hours, indicating that most of the difference between the elution from the three implants occurred at the 5 minute and 15 minute readings. Between 1 week and 3 weeks there was a large increase in the amount of zoledronate eluted, followed by a steady rate of elution until week 10, when 100% of the zoledronate had eluted.

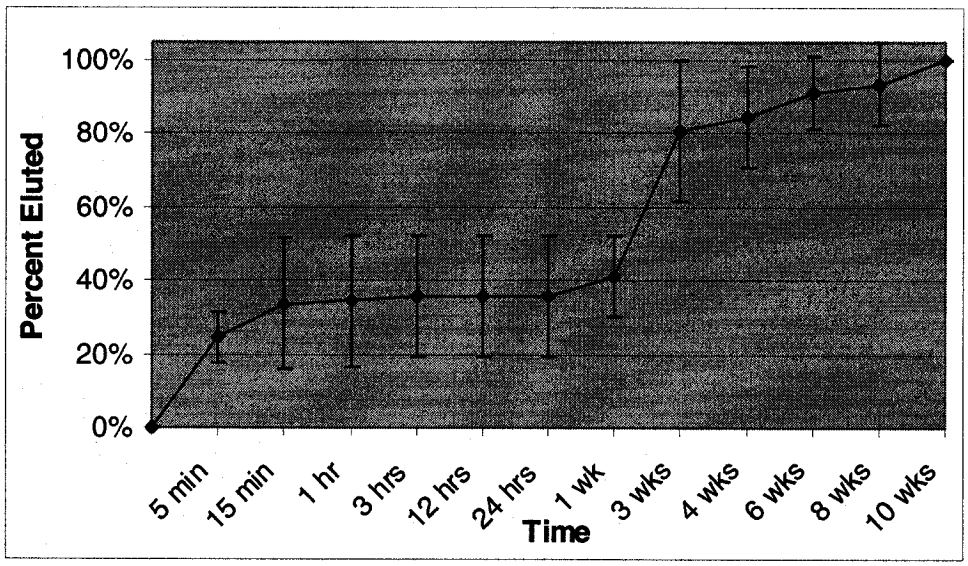

Figure 5.42 - Average percent of zoledronate eluted from HA-coated, ethylene oxide sterilized implants over time

5.11 Zoledronate Elution from Autoclave Sterilized, HA-coated implant

The cumulative mass of zoledronate eluted and the percent of mass eluted for implant Z10 are listed in table 5.34, and the results are plotted in figure 58. After 5 minutes, 46% of the zoledronate had eluted, followed by an additional

2% of elution over the first 12 hours. By 24 hours, 57% of the zoledronate had eluted. The zoledronate eluted gradually from 24 hours to 10 weeks, until 100% of the zoledronate had eluted.

Table 5.34 - Elution results for implant Z10

Time	Cumulative mass eluted	Percent mass eluted
5 minutes	0.0242 mg	46.29%
15 minutes	0.0242 mg	46.29%
1 hour	0.0243 mg	46.54%
3 hours	0.0253 mg	48.39%
12 hours	0.0253 mg	48.39%
24 hours	0.0298 mg	57.11%
1 week	0.0338 mg	64.58%
3 weeks	0.0355 mg	67.93%
4 weeks	0.0370 mg	70.75%
6 weeks	0.0436 mg	83.39%
8 weeks	0.0494 mg	94.48%
10 weeks	0.0522 mg	99.89%

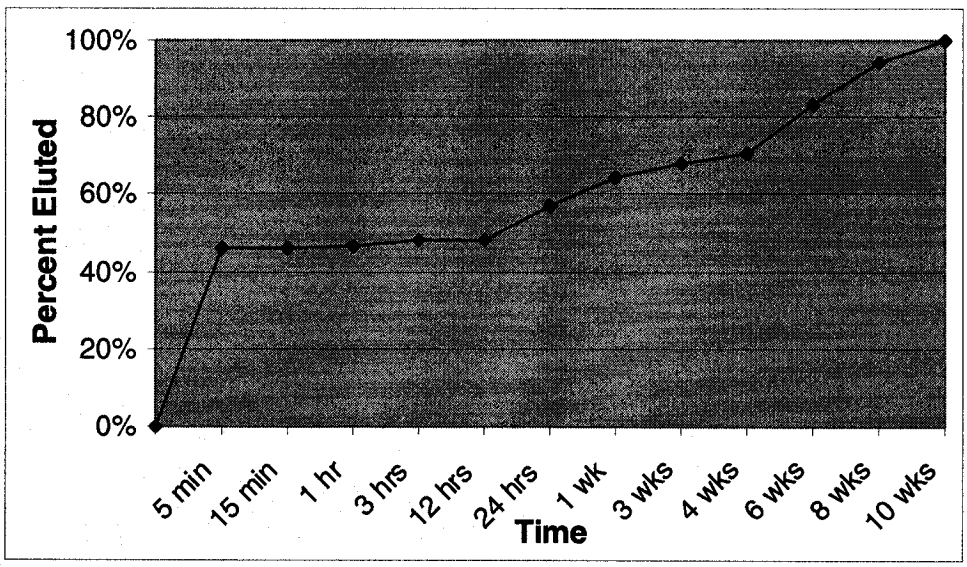

Figure 5.43 – Percent of zoledronate eluted from implant Z10

Comparing zoledronate elution from HA-coated implants to zoledronate elution from HA-coated, autoclave sterilized implants (figure 5.44) showed that the elution rates were almost the same. Most of the points fall within the standard deviation of the sample of the non-sterilized implants. Autoclaving did

not appear to affect the elution of zoledronate from HA-coated implants, so elution was only measured for one autoclaved implant.

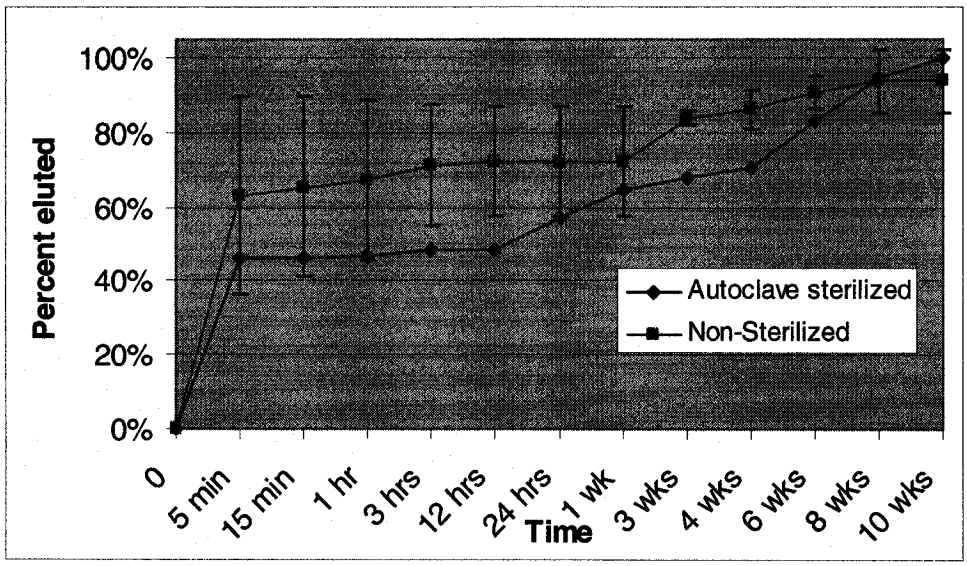

Figure 5.44 - Zoledronate elution from autoclave sterilized implant and non-sterilized implants

5.12 Zoledronate Elution from non-HA Coated Implants

Zoledronate elution was measured from non-HA coated implants for comparison with elution from HA-coated implants. Based on the pamidronate elution results, it was expected that the elution from non-HA coated implants would be more rapid than the elution from HA-coated implants and that all the zoledronate would be eluted from the implants within hours. The zoledronate elution from implants Ta3 and Ta4 was measured using the first technique of removing all of the solution around the implant. The zoledronate elution from implants Ta5 and Ta6 was measured using the second technique of removing only 2 ml of the elution solution at each interval.

5.12.1 Elution Results from Implant Ta3

The elution results for implant Ta3 are found in table 5.35, and the results are plotted in figure 5.45. Implant Ta3 eluted 87% of the zoledronate after 5 minutes, nearly 102% after 1 hour and 102% after 3 hours. At the 12 hour and 24 hour measurements, no further zoledronate had been eluted.

Table 5.35 - Elution results for implant Ta3

Time	Cumulative mass eluted	Percent mass eluted
5 minutes	0.0434 mg	86.80%
15 minutes	0.0434 mg	86.80%
30 minutes	0.0509 mg	101.80%
1 hour	0.0509 mg	101.80%
3 hours	0.0510 mg	102.00%
12 hours	0.0510 mg	102.00%
24 hours	0.0510 mg	102.00%

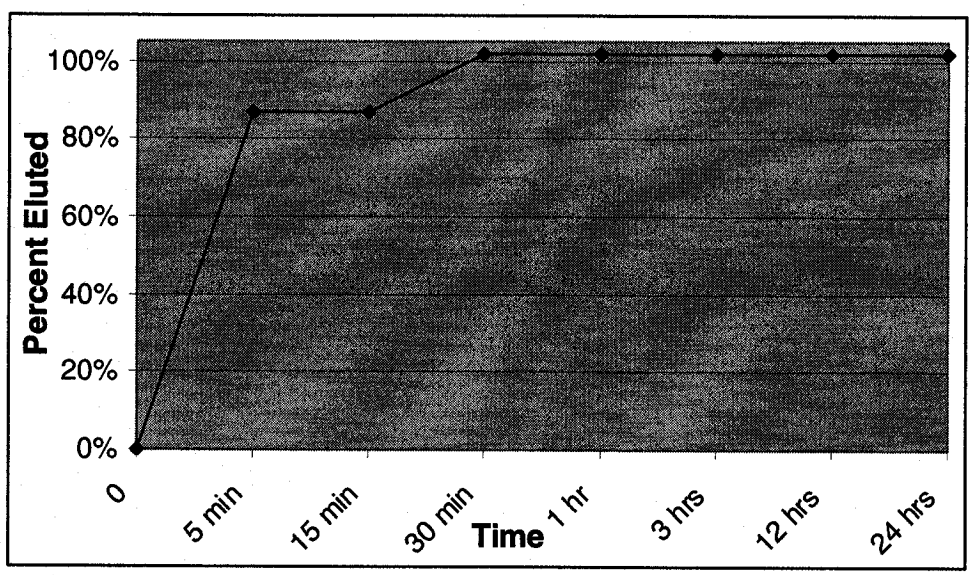

Figure 5.45 - Zoledronate elution from implant Ta3 against time

5.12.2 Elution Results for Implant Ta4

The cumulative mass of zoledronate eluted and the percent of mass eluted are tabulated in table 5.36, and the percent of mass eluted is plotted against time in figure 5.46. Implant Ta4 eluted 93% of the dose of zoledronate during the first 5 minutes. By 15 minutes, 100% of the zoledronate dose had eluted and the next sample measurements, until 24 hours, showed that no further zoledronate had eluted.

Table 5.36 - Elution results for implant Ta3

Time	Cumulative mass eluted	Percent mass eluted
5 minutes	0.0414 mg	82.80%
15 minutes	0.0493 mg	98.60%
30 minutes	0.0493 mg	98.60%
1 hour	0.0493 mg	98.60%
3 hours	0.0493 mg	98.60%
12 hours	0.0493 mg	98.60%
24 hours	0.0493 mg	98.60%

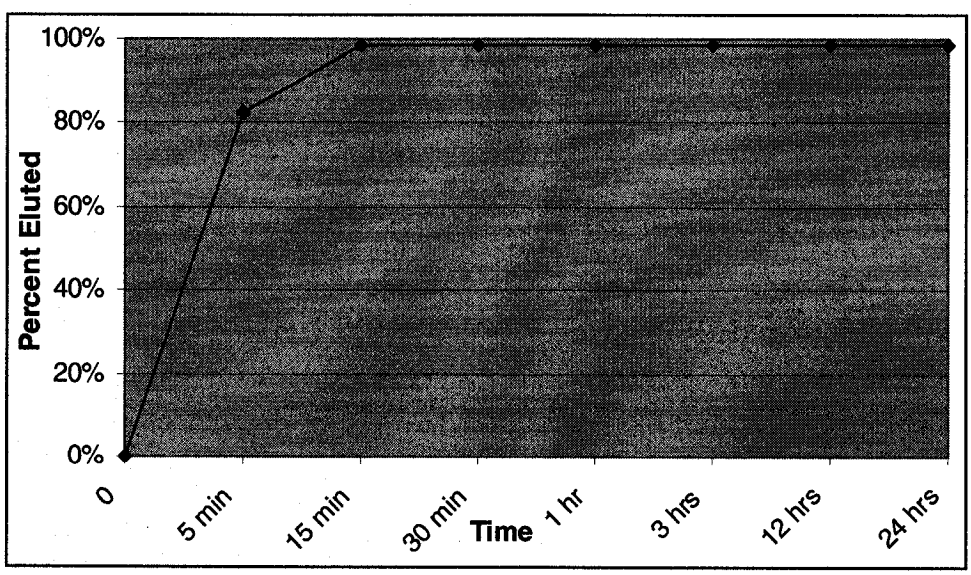

Figure 5.46 - Zoledronate elution from implant Ta4 against time

5.12.3 Elution Results from Implant Ta5

The elution results for implant Ta5 are listed in table 5.37 and the results are plotted in figure 5.47. After 5 minutes 97% of the zoledronate had eluted from implant Ta5. When 1 hour had elapsed, 105% of the zoledronate had eluted and by 24 hours no further zoledronate had eluted.

Table 5.37 - Elution results for implant Ta5

Time	Cumulative mass eluted	Percent mass eluted
5 minutes	0.1948 mg	97.40%
15 minutes	0.1948 mg	97.40%
1 hour	0.2090 mg	104.52%
3 hours	0.2090 mg	104.52%
12 hours	0.2090 mg	104.52%
24 hours	0.2111 mg	105.53%

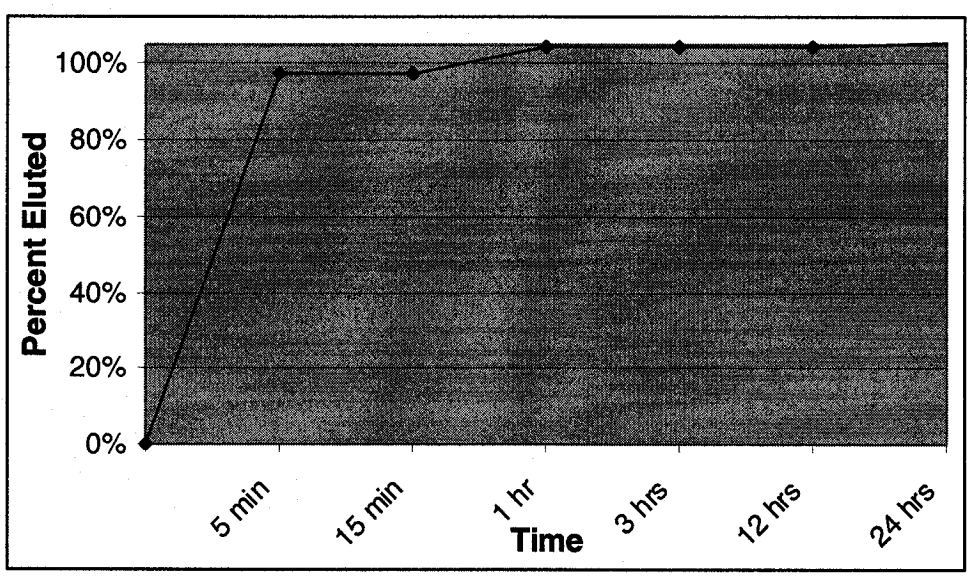

Figure 5.47 - Zoledronate elution from implant against time

5.12.4 Elution Results for Implant Ta6

The cumulative mass and percent of mass of zoledronate eluted from implant Ta6 are listed in table 5.38 and the percent of mass eluted is plotted against time in figure 5.48. After implant Ta6 had been immersed in saline for 5 minutes 103% of the zoledronate dose had been eluted. Over the next 3 hours the measured amount of zoledronate eluted increased to 114%.

Table 5.38 - Elution results for implant Ta6

Time	Cumulative mass eluted	Percent mass eluted
5 minutes	0.2058 mg	102.91%
15 minutes	0.2286 mg	114.31%
1 hour	0.2286 mg	114.31%
3 hours	0.2286 mg	114.31%
12 hours	0.2286 mg	114.31%
24 hours	0.2391 mg	119.55%

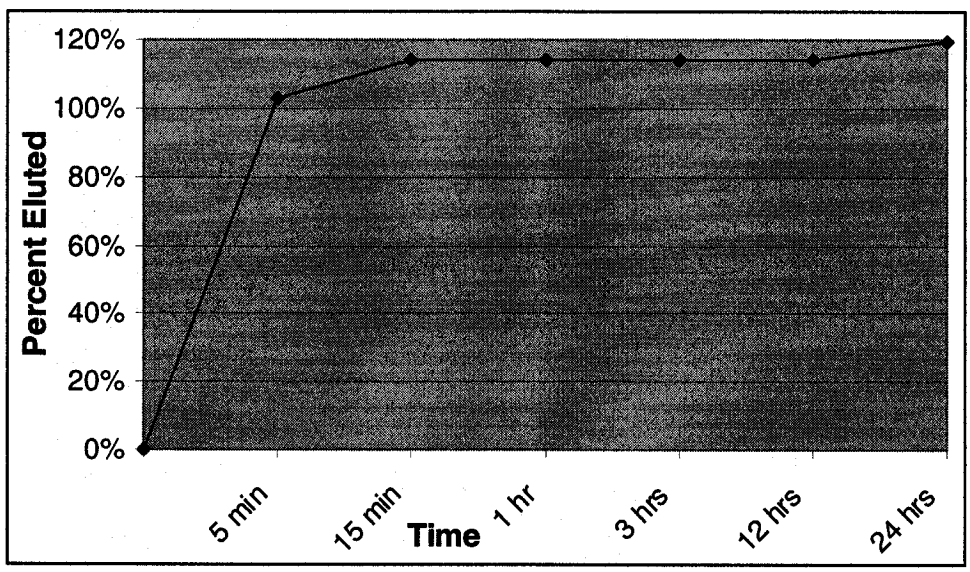

Figure 5.48 - Zoledronate elution from implant Ta6 against time

5.12.5 Average Zoledronate Elution from non-HA Coated Implants

The average zoledronate elution from non-HA coated implants (figure 5.49) shows that all of the zoledronate eluted from the implants by 30 minutes with both methods of measuring elution. Elution from implants Ta3 and Ta4 was measured using method 1 and elution from implants Ta5 and Ta6 was measured using method 2. The error bars represent the standard deviation of the samples. There was little difference between the elution profiles using the two methods. Method 2 resulted in greater values, with some of the results yielding a cumulative percent of mass eluted greater than 100%. The elution profile of zoledronate from non-HA coated implants was similar to that from the pamidronate-dosed non-HA coated implants. This further confirmed that HA was causing prolonged elution of bisphosphonate because the zoledronate was eluted rapidly and was not retained on the implant.

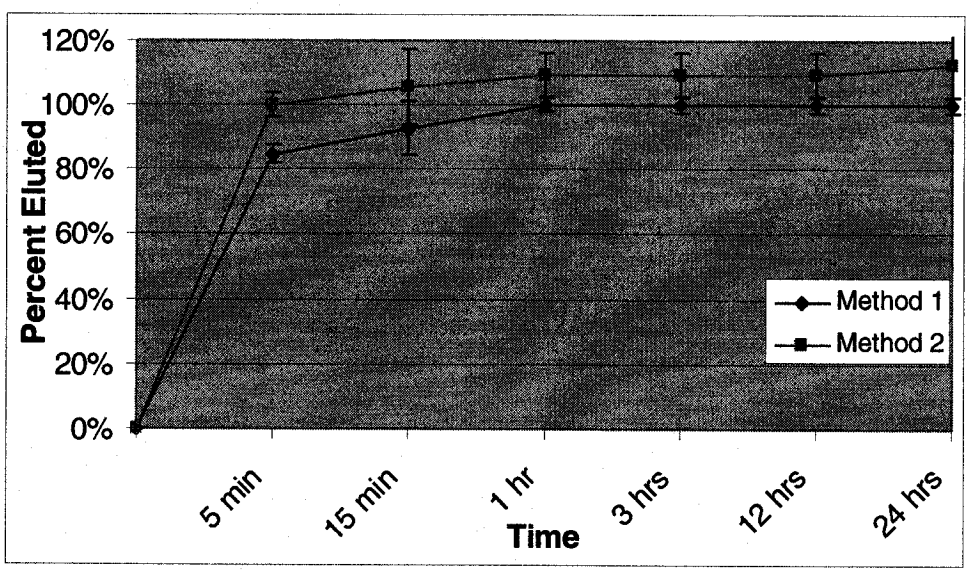

Figure 5.49 - Average zoledronate elution from non-HA coated implants

5.13 Zoledronate Elution from HA-coated Solid Titanium Implants

Three HA-coated solid titanium implants were dosed with zoledronate and the drug elution was measured. The elution was measured using the second method of removing 2 ml aliquots at each time interval and replacing 2 ml of saline.

5.13.1 Zoledronate Elution from Implant Ti1

The cumulative mass and percent of mass of zoledronate eluted from implant Ti1 are found in table 5.39 and the percent of mass eluted versus time was plotted in figure 5.50. During the first 5 minutes, 56% of the initial dose of zoledronate had eluted. Over the following three hours an additional 6% eluted and 73% had eluted after the first 24 hours. At the end of one week 75% of the zoledronate dose had eluted. By 10 weeks, 99% of the bisphosphonate dosed had eluted and no more bisphosphonate had eluted from the implant.

Table 5.39 - Elution results for implant Ti1

Time	Cumulative mass eluted	Percent mass eluted
5 minutes	0.1127 mg	56.37%
15 minutes	0.1174 mg	58.69%
1 hour	0.1235 mg	61.74%
3 hours	0.1235 mg	61.74%
24 hours	0.1456 mg	72.78%
1 week	0.1496 mg	74.78%
2 weeks	0.1496 mg	74.78%
3 weeks	0.1503 mg	75.16%
4 weeks	0.1538 mg	76.88%
6 weeks	0.1753 mg	87.65%
8 weeks	0.1753 mg	87.65%
10 weeks	0.1979 mg	98.97%
12 weeks	0.1979 mg	98.97%

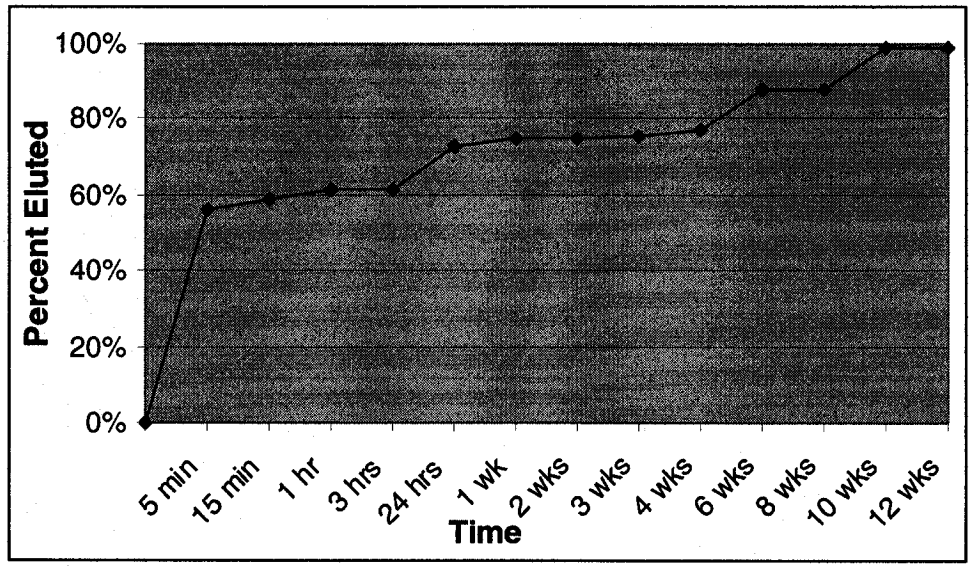

Figure 5.50 - Zoledronate elution from implant Ti1 against time

5.13.2 Zoledronate Elution from Implant Ti2

The cumulative mass and percent of mass of zoledronate eluted from implant Ti2 are listed in table 5.40 and the percent of mass eluted is plotted against time in figure 5.51. During the first 5 minutes 32% of the zoledronate dose eluted and an additional 16% eluted over the next ten minutes. After the first 24 hours 52% of the zoledronate had eluted and 75% had eluted after the first week. Zoledronate continued to elute until week 10, when 105% had eluted, and at 12 weeks no further zoledronate had eluted. Though a measured amount of 105% indicates that more zoledronate eluted than actually exists, and additional 5% was within a reasonable amount of experimental error.

Table 5.40 - Zoledronate elution from implant Ti2 against time

Time	Cumulative mass eluted	Percent mass eluted
5 minutes	0.0631 mg	31.56%
15 minutes	0.0960 mg	47.98%
1 hour	0.0960 mg	47.98%
3 hours	0.0960 mg	47.98%
24 hours	0.1046 mg	52.32%
1 week	0.1492 mg	74.58%
2 weeks	0.1492 mg	74.58%
3 weeks	0.1635 mg	81.76%
4 weeks	0.1686 mg	84.31%
6 weeks	0.1828 mg	91.40%
8 weeks	0.1850 mg	92.48%
10 weeks	0.2114 mg	105.68%
12 weeks	0.2114 mg	105.68%

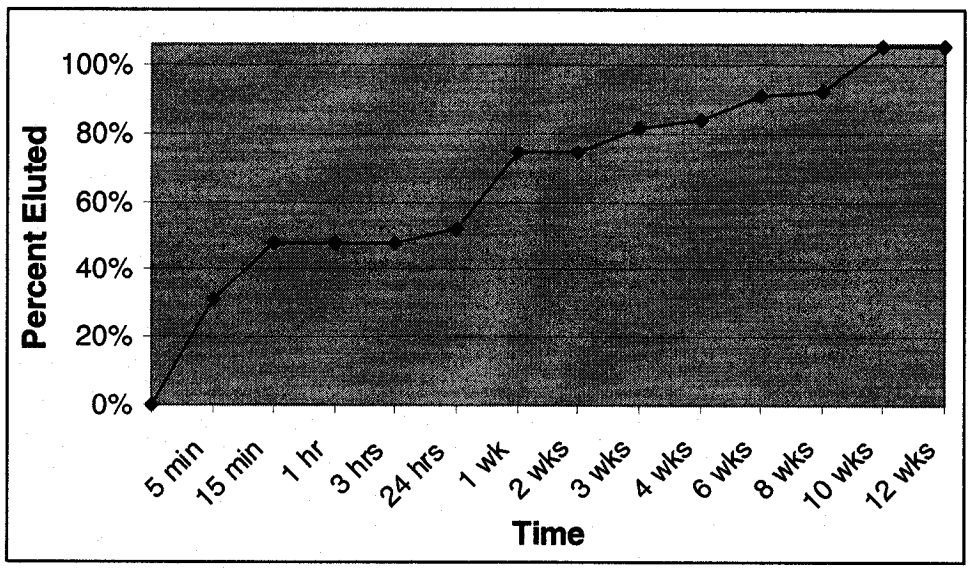

Figure 5.51 - Zoledronate elution from implant Ti2 against time

5.13.3 Zoledronate Elution from Implant Ti3

The cumulative mass and percent of mass of zoledronate eluted from implant Ti3 can be found in table 5.41 and the percent of mass eluted is plotted against time in figure 5.51. During the first 5 minutes of implant immersion in saline 63% of the zoledronate dose had eluted. An additional 8% had eluted after 3 hours. By 24 hours 78% of the zoledronate dose had eluted, and this

amount did not increase during the first 2 weeks. Between 3 weeks and 10 weeks, the remaining zoledronate eluted, so that 105% of the dose had eluted. No further bisphosphonate had eluted by 12 weeks.

Table 5.41 - Elution results from implant Ti3

Time	Cumulative mass eluted	Percent mass eluted
5 minutes	0.1261 mg	63.04%
15 minutes	0.1343 mg	67.14%
1 hour	0.1414 mg	70.70%
3 hours	0.1424 mg	71.18%
24 hours	0.1558 mg	77.90%
1 week	0.1558 mg	77.90%
2 weeks	0.1558 mg	77.90%
3 weeks	0.1584 mg	79.21%
4 weeks	0.1584 mg	79.21%
6 weeks	0.1876 mg	93.79%
8 weeks	0.1876 mg	93.79%
10 weeks	0.2107 mg	105.34%
12 weeks	0.2107 mg	105.34%

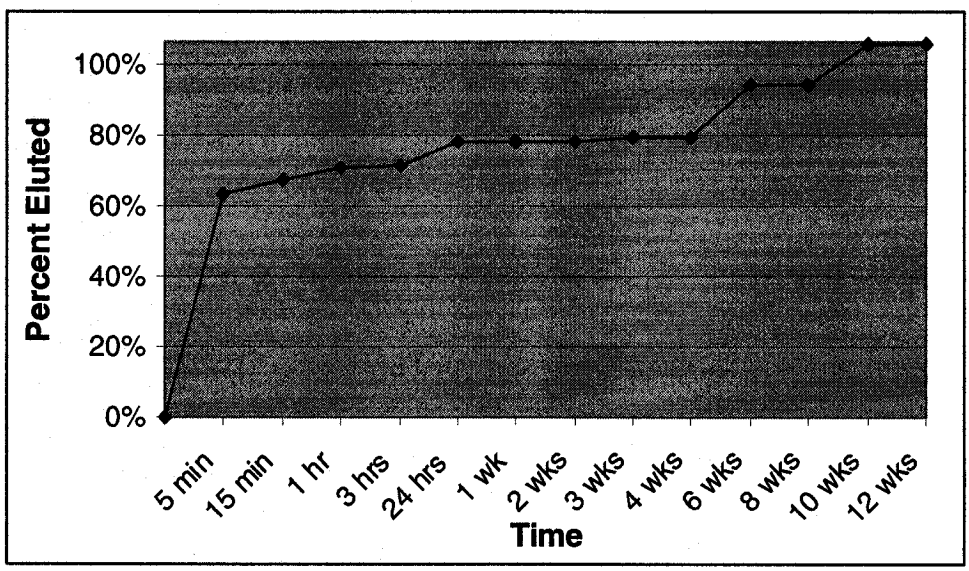

Figure 5.52 - Zoledronate elution from implant Ti3 against time

5.13.4 Average Zoledronate Elution from HA-coated Titanium Implants

The zoledronate elution from the hydroxyapatite-coated solid titanium implants showed that the hydroxyapatite coating was binding the bisphosphonate to the surface coated and causing the zoledronate to elute into solution slowly over time. The average zoledronate elution from HA-coated titanium implants is shown in figure 5.53. The error bars represent the standard deviation of the three samples. The standard deviation is greatest during the first 24 hours and then declines over time. Implant Ti2 had a much lower percent of elution than the other two titanium implants during the first 5 minutes, eluting only half of the zoledronate eluted by Ti3, but by one week the percent of elution from all three implants was within 3% of each other.

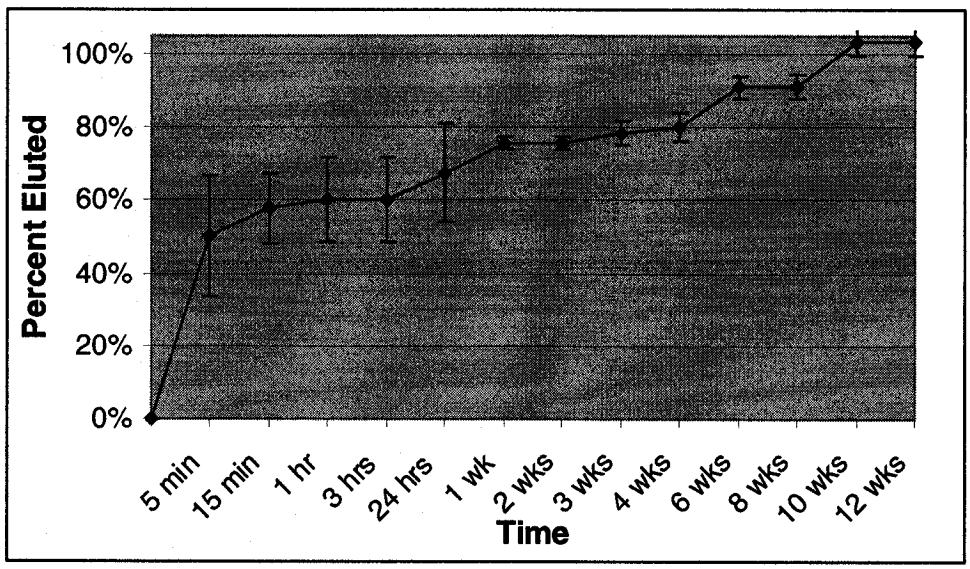

Figure 5.53 - Average zoledronate elution from HA-coated titanium implants

5.14 Average Zoledronate Elution

A comparison of the three types of zoledronate-coated implants (figure 5.54) showed that zoledronate was eluted much more rapidly from the non-hydroxyapatite coated implants than from the hydroxyapatite coated implants.

Sterilization by ethylene oxide appeared to decrease the initial peak in elution during the first hour, when compared to the hydroxyapatite implants that were not sterilized. However, by three weeks the amount of zoledronate eluted from the ethylene oxide sterilized implants reached the same amount of zoledronate eluted from the non-sterilized implants. For the remainder of the elution after 3 weeks, the elution profiles of zoledronate from ethylene oxide sterilized and non-sterilized were similar. The non-HA coated implants had all eluted the entire dose of zoledronate within the first hour of immersion in saline, whereas the HA-coated implants eluted the dose of zoledronate over several weeks. The profile of zoledronate elution from HA-coated solid titanium implants was very similar to the elution profile from HA-coated porous tantalum implants indicating that the base substrate did not affect the rate of zoledronate elution and that the hydroxyapatite surface coating was responsible for the prolonged elution observed from the HA-coated implants.

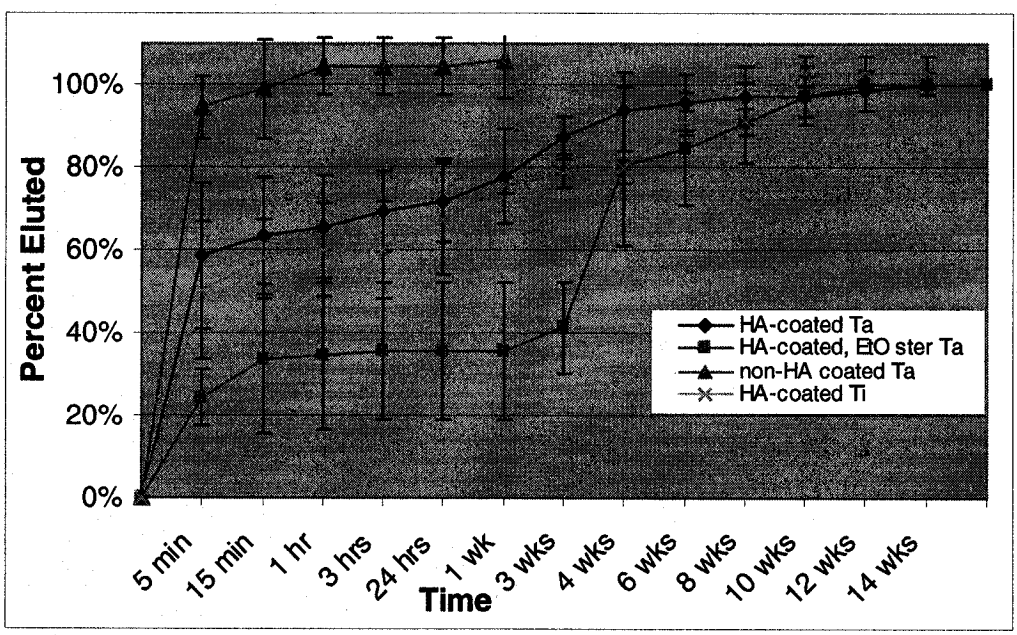

Figure 5.54 - Average zoledronate elution

5.15 Spectrophotometric Results for Non-Bisphosphonate Dosed Implants

A non-HA coated porous tantalum implant was immersed in saline and the absorbance of the solution was measured by UV spectrophotometry as described for the bisphosphonate dosed implants. The absorbance of a blank solution of saline with iron chloride was measured both before and after the samples were measured, and the values were averaged. The blank average absorbance was 0.425. The average absorbance measurements of the elution samples over 24 hours ranged between 0.423 and 0.426, which showed that porous tantalum did not alter the absorbance measurements and therefore did not affect the calculated amount of bisphosphonate eluted over time.

The above was repeated with an HA-coated porous tantalum implant. A blank solution of saline with iron chloride was measured both before and after the samples and averaged. The average absorbance of the blank solution was 0.184. The average absorbance measurements of the elution samples over 24 hours ranged between 0.182 and 0.185, which was consistent with the anticipated result that the HA coating also did not affect the absorbance readings and therefore did not alter the calculated amount of bisphosphonate eluted.

5.16 Reliability of Methacrylate Cuvettes

To ensure that the polymethacrylate cuvettes were giving reproducible results, the variability of the cuvettes was tested by randomly selecting four cuvettes, filling them with water and measuring the absorbance at 290 nm (table 5.42). The spectrophotometer was calibrated between the first and second measurements.

Table 5.42 – Absorbance at 290 nm for cuvettes with distilled water

Cuvette	1st Absorbance	2nd Absorbance	Average Absorbance
1	0.301	0.302	0.3015
2	0.304	0.303	0.3035
3	0.304	0.305	0.3045
4	0.306	0.306	0.306

Assuming that all of the distilled water samples were identical, differences in absorbance were due to differences between the cuvettes. Three of the four cuvettes had a difference in absorbance of 0.001 between readings. Since the distilled water sample did not change between measurements, this difference was due to the precision of the spectrophotometer. There was an absolute difference in absorbance of 0.005 between the highest and the lowest reading. This difference was due to variability between cuvettes. Each sample was measured using two separate cuvettes, which decreased the impact of cuvette disparity on the calculations.

Chapter 6. Discussion

This study was aimed at measuring the release of bisphosphonate compounds from porous orthopaedic implants into solutions of water or 0.9% saline. This necessitated the development of appropriate chemical assays using complexing agents and UV spectrophotometry to measure the absorbance of the bisphosphonates in solution as a function of time. The studies were conducted using two bisphosphonate compounds, pamidronate and zoledronate. Some of the porous implants were coated with hydroxyapatite (HA) to delay the elution of bisphosphonate. Release profiles were recorded for both HA-coated and non-HA coated implants.

6.1 Deposition of bisphosphonate onto implants

Deposition of solution containing bisphosphonate was technically easier for implants coated with HA because of the hydrophilic nature of the material. It was also easier for porous implants compared with solid implants because of the additional space for solution to adsorb and collect. Should this concept reach clinical application a more sophisticated deposition method will likely need to be developed to ensure accuracy and reproducibility.

The post-deposition masses of implants did not always produce a perfect correlation with the pre-deposition mass and added mass of bisphosphonate. One source of error was the fact that the bisphosphonate solution in the vial could not be completely removed by pipetting. Another source of error was possibly that the hydroxyapatite coating would have some moisture content prior to deposition, due to its hydrophilic nature, and a variable amount would have been lost once implants were dried in the oven prior to the final weighing. There may also have been some variability in the extent of drying from one implant to the next. It is also possible that minute amounts of tantalum were removed from implants as they were turned in the apparatus during deposition.

6.2 Assay Method

A copper (II) sulfate solution had been previously used by Ostovic et al [97] to assay alendronate. For the studies in this thesis a copper (II) sulfate solution was used to successfully assay pamidronate in water. Measuring the absorbance of known concentrations of pamidronate, comparing them to a blank solution and plotting the absorbance against concentration resulted in a linear relationship. However, this method was not successful for measuring the concentration of pamidronate in saline. By comparing the calibration curve of pamidronate in water to the calibration curve of pamidronate in saline, it was apparent that the saline caused a positive increase in both the absorbance and the slope of the calibration curve. This must have been due to the Na and/or the Cl content because it was the only difference between the water-based solutions and the saline solutions. It is hypothesized that using iron (III) chloride solution as the complexing agent would be successful for measuring pamidronate in saline because it was successful for measuring zoledronate in saline.

During the spectrophotometry measurements, there was a small amount of error in the absorbance readings. The absorbance measurements, when using the μ-Quant spectrophotometer, were an average of eight values. The values were examined for consistency and anomalous readings, but there was always a small variation in the measured absorbance values. An inaccuracy in absorbance of only 0.001 (the smallest value measured) would have altered the calculated mass by approximately 0.0016 mg, a difference of 0.8% for a 0.2 mg dose of bisphosphonate and 3.2% for 0.05 mg dose of bisphosphonate. When using the Thermospectronic spectrophotometer, the average of four absorbance values was used to calculate the eluted mass of zoledronate. Two cuvettes were used for each sample and two measurements were taken for each cuvette. There was also variation in the absorbance readings using this method. The difference between the measurements using the same cuvette was generally

0.002 or less, while the difference in absorbance between cuvettes for the same sample was often greater than that. Testing the variability between cuvettes showed that the transmittance of the cuvettes was variable and could result in some disparity between absorbance measurements. Using two cuvettes neutralized some of this error, though the random selection of the cuvettes did not guarantee that the transmittance of the cuvettes averaged to a median value. This may explain why some of the total bisphosphonate elution masses were calculated to be greater than the initial deposited masses.

6.3 Release Profiles

In the first experiments, because the bisphosphonate release profile was unknown, the first interval examined was 24 hours after the initial soaking in water. It was clear that a large portion of the dose was being eluted over this time period and so subsequent implant elution trials used shorter time intervals during the first 24 hours, especially during the first hour, in order to better understand the elution profile during the time period that would immediately follow implantation in a surgical setting. The first implant used for the pamidronate elution studies demonstrated the smallest amount of elution during the first 24 hours. However, by not sampling and exchanging solutions at earlier time periods, it is likely that eluted pamidronate was able to re-bind with available hydroxyapatite; this would explain the lower 24 hour reading compared with other implants that were sampled at earlier intervals as well. In the dental literature it is reported that the method of immobilizing bisphosphonate onto a hydroxyapatite coated implant is to soak the implant overnight in a bisphosphonate solution. This lends support to the notion that eluted bisphosphonate could re-bind with available hydroxyapatite given sufficient time.

The release profiles of both pamidronate and zoledronate from the non-hydroxyapatite coated implants as compared to the hydroxyapatite coated implants indicates that the hydroxyapatite chemically binds the bisphosphonates,

and therefore retards their elution. This renders it an attractive method for controlled delivery of bisphosphonate from an orthopaedic implant, especially since hydroxyapatite coatings already have a long history of successful clinical use. It still took at least an hour for all the bisphosphonate to be eluted from non-coated implants, despite the fact that it would have quickly hydrated once an implant was immersed. This is probably because of the diffusion rate of the bisphosphonate from within the constricted implant pores and surface tension effects of water on the tantalum struts. Another factor in the release rate may have been the solubility of bisphosphonates in water. While both bisphosphonates are quite soluble in water, when making the pamidronate solution to apply to the implant, it did take approximately 15 minutes to dissolve 2 mg of pamidronate in 500 µl of water.

As can be seen from the graphs of the elution of the bisphosphonates against time, there was an initial peak during the first 15 to 30 minutes, wherein approximately half of the applied bisphosphonate was released. This was likely due to the fact that the hydroxyapatite coating on the porous tantalum was only superficial due to the line-of-sight nature of the plasma spray process. As bisphosphonates have an affinity for hydroxyapatite, but not for tantalum, the bisphosphonate chemically bonded only to the hydroxyapatite-coated struts. During the bisphosphonate-coating process, the entire implant became wet and the bisphosphonate solution permeated the struts deep within the implant. Any bisphosphonate that remained on the inner, uncoated tantalum struts would understandably have eluted into solution quickly.

Zoledronate elution from solid titanium implants was investigated to determine the release profile from bisphosphonate bound to HA, without the confounding factor of inner, non-HA coated tantalum struts. In other words, the solid titanium rods were studied to ascertain the characteristic elution of bisphosphonate from HA alone. The entire surface of the titanium implants was HA-coated and, therefore it was presumed that all of the bisphosphonate dose

would have been bound to the HA. However, the zoledronate elution observed from HA-coated solid titanium implants had a similar release profile to zoledronate elution from HA-coated porous tantalum implants. Both types of implants had a burst of release during the first 15 to 30 minutes of soaking, followed by drug release sustained over several weeks. This was unexpected and suggested that perhaps not all of the zoledronate had chemically bound to the HA coating, leaving some free for fast release upon hydration. The HA-coated solid titanium implants were dosed with 0.2 mg of zoledronate whereas the HA-coated porous tantalum implants were dosed with 0.05 mg of zoledronate. Therefore, it was possible that the amount of hydroxyapatite on the struts became saturated with bisphosphonate and could not chemically bind the entire 0.2 mg dose of zoledronate. If not chemically bound to HA, the excess bisphosphonate would sit on the implant surface and elute quickly from the implant. Further experiments with a smaller dose of zoledronate on HA-coated titanium implants are needed to determine whether over-saturation of HA is responsible for the burst of release. This issue of how much bisphosphonate can be bound by how much hydroxyapatite is clearly important to determine prior to clinical development of the concept.

The initial burst of bisphosphonate release from hydroxyapatite coated implants may be a suitable profile given that systemic injection of bisphosphonate, analogous to a burst release, has proven to be effective for enhancing peri-implant bone formation in animal studies [73]. This would have to be explored in the context of in vivo studies that measure peri-implant bone formation as a function of time and different bisphosphonate release profiles. It is possible that different release profiles could be created by changing the chemistry and location of the calcium phosphate coating. For instance, tricalcium phosphate might behave differently than hydroxyapatite in terms of binding and releasing bisphosphonate. Also, the use of different types of calcium phosphate coating, such as biomimetic coatings that are not line-of-sight and can deposit onto the inner recesses of porous coatings, could be used to alter the

bisphosphonate release profile. It would also be of interest to examine the local bone response to bisphosphonate release from solid implants, as opposed to porous implants.

Two methods were developed to measure bisphosphonate elution. When the first method was employed, implants were immersed in 5 ml of water or saline. At each interval the entire volume of solution was removed and then the removed volume was replaced by fresh water or saline. This method was developed because all other groups that have dosed HA-coated implants with bisphosphonate have soaked the implants in a bisphosphonate solution for several hours. To avoid elution of bisphosphonate followed by rebinding of bisphosphonate, the entire volume of solution with eluted bisphosphonate was removed. Later elution studies had shorter intervals between samples, which made rebinding of bisphosphonate less likely. When the second method was employed, the implants were immersed in 10 ml of saline. At each interval a 2 ml aliquot of solution was removed from the test tube and 2 ml of saline were added to replace the removed solution and maintain a total volume of 10 ml. This method presented a more accurate physiological analog, with bisphosphonate being released into solution and remaining in the area surrounding the implant. When comparing the difference in results between the two methods for HA-coated porous tantalum implants, it was observed that the results were very similar. Both methods resulted in a burst of release of approximately 60% of the bisphosphonate dose during the first 5 minutes, followed by sustained elution of the remainder of the dose over several weeks. The primary difference observed was that when elution was measured using the second method the implants had eluted the entire bisphosphonate dose after 4 weeks, whereas when elution was measured using the first method, the implants eluted the entire bisphosphonate dose between 8 weeks and 12 weeks. The elution profiles for the two methods were also very similar for the non-HA coated porous tantalum implants. The main difference was that the total drug elution measured using the second

method was usually about 5% to 20% greater than 100%. This indicates that there was greater experimental error in the second method.

The greater error in the second method for measuring elution may have been that the calculated mass eluted at each interval was dependent on the calculated mass eluted at the previous interval. Most of the solution into which the bisphosphonate had eluted remained in the test tube at each interval, but the calculated mass of bisphosphonate eluted needed to be calculated based on the entire volume of solution. Therefore the amount of bisphosphonate remaining in the solution needed to be calculated and accounted for in subsequent calculations to determine the mass of bisphosphonate eluted for only the time period that had most recently elapsed. Inaccuracies in one calculation, therefore, affected the subsequent calculation. When performing calculations using the first method for measuring elution, each interval was discrete and only the amount eluted during each interval was measured because all of the solution surrounding the implant was removed. The calculations were only dependent upon each other in that the calculated mass eluted for each interval was added to the previously calculated cumulative eluted mass.

There were considerable differences in elution characteristics from implant to implant. The differences between individual implants could be explained by temperature fluctuations of the water bath in which the test tubes were immersed during elution studies. For most solids, temperature affects solubility and therefore fluctuation in temperature would affect the dissolution of bisphosphonate into water or saline. Initially the water bath was heated on a hot plate, but it was difficult to maintain the temperature at 37°C since the lowest setting of the hot plate gave a temperature around 45°C. This was improved by changing the heating method from a hot plate to an oven set at 37°C.

Even with some error in the calculated eluted mass, the results indicated a general trend in the elution characteristics. Bisphosphonate elution from HA-

coated implants spiked during the first 15 minutes, followed by very little elution during the first week and then a steady rate of elution to 14 weeks or completion.

Differences were observed between the zoledronate elution from ethylene oxide (EtO) sterilized implants and non-sterilized implants. The EtO sterilized HA-coated porous tantalum implants eluted an average of 34% of the zoledronate dose during the first 15 minutes of soaking. The HA-coated porous tantalum implants eluted an average of 64% during the same time period. Despite the slower initial elution of zoledronate from the EtO sterilized implants, by four weeks the sterilized and non-sterilized implants had eluted the same percent of the dose of zoledronate. During the sterilization process, the implants were heated to temperatures exceeding those that the implants were exposed to while drying in the oven. The higher temperatures may have enhanced the bonding between the HA and the zoledronate, slowing the initial elution of zoledronate from the implant. Alternatively, the extra time allowed for drying and the exposure to higher temperatures may have dried the implant more thoroughly, also reducing the initial burst of release. Further elution studies need to be performed using different sterilization techniques to more completely understand the various effects.

6.4 Future Directions

The spectrophotometric technique developed for measuring bisphosphonate elution was for the most part effective, once the parameters were understood. It might also be useful to investigate mass spectrometry as an assay tool as well. Mass spectrometry has the possible advantage of being used for quantifying bisphosphonate concentration in serum. This was not possible with the UV spectrometry technique because of the need to use acid solutions for chelation, a step that coagulated serum and invalidated measurements. Mass spectrometry could also identify the precise chemistry of the elution products and ascertain whether the bisphosphonate compound was altered during sterilization

and after elution. Future studies of this type would also benefit from more realistic elution scenarios, including bisphosphonate elution in serum and perhaps also with a modified elution protocol. The protocol of placing an implant in a test tube of saline and sampling aliquots at various time intervals was a reasonable first case approximation of what might occur *in vivo*. Use of a diffusion chamber could be an alternative method for measuring the bisphosphonate elution from orthopedic implants. A diffusion chamber consists of a solvent bath divided into two compartments by a semi-permeable membrane. The bisphosphonate-coated implant would be placed in one side of the chamber and measurement aliquots would be taken from the other side of the chamber. The concentration of the eluted bisphosphonate would equilibrate across the membrane and the measured absorbance of the sample would represent the total mass of bisphosphonate eluted.

These laboratory studies need to be complemented with *in vivo* experiments to assess the local bone response to elution of bisphosphonates from orthopaedic implants. This will enable insight into the optimum bisphosphonate dose for enhancing net bone formation around and within porous devices as well as study of the effect of different bisphosphonates on local bone formation. These studies are presently ongoing in the context of both ulnar and femoral intramedullary implant models.

Chapter 7. Conclusions

Based on the results of this study, it was concluded that a thin layer of hydroxyapatite coating on porous tantalum implants was suitable for initially binding a bisphosphonate compound and subsequently releasing it after immersion in an aqueous solution. The release profile was markedly different for implants without and with hydroxyapatite coating. Bisphosphonate that was present on non-hydroxyapatite coated surfaces hydrated and eluted into solution very quickly, typically within one to three hours of immersion. In contrast, bisphosphonate that was added to hydroxyapatite coated surfaces demonstrated a delayed release profile that required several weeks for complete elution. This was true for both pamidronate and zoledronate.

A method was developed to measure the mass of the drug eluted from the implants using ultraviolet spectrophotometry. The measurement of pamidronate in solution was possible using copper (II) sulfate as a complexing agent because it was obtained in its pure chemical form. It was not possible to measure zoledronate using this method because the only available zoledronate was in its pharmaceutical compilation, Zometa, which included sodium citrate that also complexed with copper (II) ions. It was, however, possible to measure zoledronate by ultraviolet spectrophotometry using iron (III) chloride as a complexing agent.

Prior to commercial development of this concept additional studies would have to be completed to understand the bone response to local delivery of bisphosphonates from orthopaedic devices. A more sophisticated technique for dosing an implant with bisphosphonate would also need to be developed to enable high volume production with the necessary quality control.

References

1. J.M. Wilkinson, I. Stockley, N.F.A. Peel, A.J. Hamer, R.A. Elson, N.A. Barrington, R. Eastell, Effect of pamidronate in preventing local bone loss after total hip arthroplasty: a randomized, double-blind, controlled trial. J. Bone Min. Res. 16 (2001) 556-564.

2. M. Iwase, K.J. Kim, Y. Kobayashi, M. Itoh, T. Itoh, A novel bisphosphonate inhibits inflammatory bone resorption in rat osteolysis model with continuous infusion of polyethylene particles. J. Orthop. Res. 20 (2002) 499-505.

3. H. Kienapfel, C. Sprey, A. Wilke, P. Griss. Implant fixation by bone ingrowth. J. Arthrop. 14 (1999) 355-368.

4. A.T. Moore. Metal hip joint: a new self-locking vitallium prosthesis. South Med. J. 45 (1952) 1015-1019.

5. J.S. Hirschhorn, J.T. Reynolds. Powder metallurgy fabrication of cobalt-chromium surgical implant. Research in Dental and Medical Materials. Ed: E. Korostoff. Plenum Press, New York, 1969. 137-150.

6. J.S. Hirschhorn, A.A. McBeath, M.R. Dustoor. Porous titanium surgical implant materials. J. Biomed. Mater. Res. Symp. II (part 1) (1971) 49-67.

7. R.A. Lueck, J.O. Galante, W. Rostoker, R.D. Ray. Development of an open pore metallic implant to permit attachment to bone. Surg. Forum 20 (1969) 456-457.

8. J.O. Galante, W. Rostoker, R. Lueck, R.D. Ray. Sintered metal fiber composites as a basis for attachment of implants to bone. J. Bone Joint Surg. Am 53 (1971) 101-114.

9. E. Lembert, J.O. Galante, W. Rostoker. Fixation of skeletal replacement by fiber metal composites. Clin. Orthop. 87 (1972) 303-310.

10. J. Galante, W. Rostoker. Fiber metal composites in the fixation of skeletal prosthesis. J. Biomed. Res. Symp. 4 (1973) 43-61.

11. R.M. Pilliar, H.U. Cameron, I. MacNab. Porous surface layered prosthetic devices. Biomed Eng. 10 (1975) 126-131.

12. H.U. Cameron, I. MacNab, R.M. Pilliar. A porous metal system for joint replacement surgery. Int. J. Artif. Organs. 1 (1978) 104-109.

13. H.U. Cameron, R.M. Pilliar, I. MacNab. The rate of bone ingrowth into porous metal. J. Biomed. Mater. Res. 10 (1976) 295-302.

14. R.P Welsh, R.M. Pilliar, I. MacNab. Surgical Implants – the role of surface porosity in fixation to bone and acrylic. J. Bone Joint Surg. 53A (1971) 963-977.

15. H. Hahn, W. Palich. Preliminary evaluation of porous metal surfaced titanium for orthopaedic implants. J. Biomed. Mater. Res. 4 (1970) 571-577.

16. R.B. Bourne, C.H. Rorabeck, B.C. Burkart, P.G. Kirk. Ingrowth surfaces: plasma spray coating to titanium alloy hip replacements. Clin. Orthop. 1994 (298) 37-46.

17. H. U. Cameron, I. MacNab, R. Pilliar. Porous surfaced vitallium staples. S. Afr. J. Surg. 10 (1972) 63-69.

18. H. U. Cameron, R.M. Pilliar, I. MacNab. The effect of movement on the bonding of porous metal to bone. J. Biomed. Mater. Res. 7 (1973) 301-311.

19. R.M. Pilliar, J.M. Lee, C. Maniatopoulos. Observations on the effect of movement on bone ingrowth into porous surfaced implants. Clin. Orthop. 208 (1986) 108-113.

20. H.U. Cameron, R.M. Pilliar, I. MacNab. The rate of bone ingrowth into porous metal. J. Biomed. Mater. Res. 10 (1976) 295-302.

21. J.D. Bobyn, R.M. Pilliar, H.U. Cameron, G.C. Weatherly. Osteogenic phenomena across endosteal bone-implant spaces with porous surfaced intramedullary implants. Acta. Orthop. Scand. 52 (1981) 145-153.

22. P.M. Sandborn, S.D. Cook, W.P. Spires, M.A. Kester. Tissue response to porous-coated implants lacking initial bone apposition. J. Arthroplasty. 3 (1988) 337-346.

23. J.D. Bobyn, R.M. Pilliar, H.U. Cameron, G.C. Weatherly. The optimum pore size for the fixation of porous-surfaced metal implants by the ingrowth of bone. Clin. Orthop. 150 (1980) 263-270.

24. S.D. Cook, K.A. Walsh, R.J. Haddad. Interface mechanics and bone growth into porous Co-Cr-Mo alloy implants. Clin. Orthop. 193 (1985) 271-280.

25. D.M. Robertson, L. St. Pierre, R. Chahal. Preliminary observations of bone ingrowth into porous materials. J. Biomed. Mater. Res. 10 (1976) 335-344.

26. A.J.T. Clemow, A.M. Weinstein, J.J. Klawitter, J. Koeneman, J. Anderson. Interface mechanics of porous titanium implants. J. Biomed. Mater. Res. 15 (1981) 73-82.

27. J. Pfeilschifter, I. Diel, B. Scheppach, A. Bretz, R. Krempien, J. Erdman, G. Schmid, N. Reske, H. Bismar, T. Seck, B. Krempien, R. Ziegler. Concentration of transforming growth factor beta in human bone tissue: relationship to age, menopause, bone turnover, and bone volume. J. Bone Miner. Res. 13 (1998) 716-730.

28. T. Seck, B. Scheppach, S. Scharla, I. Diel, W.F. Blum, H. Bismar, G. Schmid, B. Krempien, R. Ziegler, J. Pfeilschifter. Concetration of insulin-like growth factor (IGF)-I and –II in iliac crest bone matrix from pre- and post-menopausal women: relationship to age, menopause, bone turnover, bone volume, and circulating IGFs. J. Clin. Endocrinol. Metab. 83 (1998) 2331-2337.

29. T.C. Kwiatkowski, E.N. Hanley, W.K. Ramp. Cigarette smoking and its orthopedic consequences. Am. J. Orthop. 25 (1996) 590-597.

30. M. Jatsy, C.R. Bragdon, T. Haire, R.D. Mulroy, W.H. Harris. Comparison of bone ingrowth into cobalt chrome sphere and titanium fiber mesh porous coated cementless canine acetabular components. J. Biomed. Mater. Res. 27 (1993) 639-644.

31. H. Ronningen, P. Lereim, J. Galante, W. Rostoker, T. Turner, R. Urban. Total surface hip arthroplasty in dogs using a fiber metal composited as a fixation method. J. Biomed. Mater. Res. 17 (1983) 643-653.

32. A.K. Hedley, M. Kabo, W. Kim, I. Coster, H.C. Amstutz. Bony ingrowth fixation of newly designed acetabular components in a canine model. Clin. Orthop. 176 (1983) 12-23.

33. S.D. Cook, R.L. Barrack, K.A. Thomas, R.J. Haddad. Tissue growth into porous primary and revision femoral stems. J. Arthroplasty Suppl. 6 (1991) 37-46.

34. J.D. Bobyn, C.A. Engh, A.H. Glassman. Histologic analysis of a retrieved microporous-coated femoral prosthesis: a sever year case report. Clin. Orthop. 224 (1987) 303-310.

35. C.A. Engh, K.F. Zettl-Shaffer, Y. Kukita, D. Sweet, M. Jatsy, C. Bragdon. Histological and radiographic assessment of well functioning porous coated acetabular components: a human postmortem retrieval study. J. Bone Joint Surg. Am. 75 (1993) 814-824.

36. L.E. Pidhorz, R.M. Urban, J.J. Jacobs, D.R. Sumner, J.O. Galante. Histological study of the porous coating of the uncemented acetabulum: apropos of 11 implants removed at autopsy. Chiurgie. 119 (1994) 334-339.

37. C.A. Engh, J.P. Hooten, K.F. Zettl-Schaffer, M. Ghaffarpour, T.F. McGovern, J.D. Bobyn. Evaluation of bone ingrowth in proximally and extensively porous-coated anatomic medullary locking prostheses retrieved at autopsy. J. Bone Joint Surg. Am. 77 (1995) 903-910.

38. H. Kienapfel, D.R. Sumner, T.M. Turner, R.M. Urban, J.O. Galante. Efficacy of autograft and freeze-dried allograft to enhance fixation of porous coated implants in the presence of interface gaps. J. Orthop. Res. 10 (1992) 423-433.

39. P.E. Greis, J.D. Kang, V. Silvaggio, H.E. Rubash. A long term study of defect filling and bone ingrowth using a canine fiber metal total hip model. Clin. Orthop. 274 (1992) 47-59.

40. W.J. Shen, K.C. Chung, G.J. Wang, G. Balian, R.E. McLaughlin. Demineralized bone matrix in the stabilization of porous coated implants in bone defects in rabbits. Clin. Orthop. 293 (1993) 346-352.

41. S.D. Cook, S.L. Salkeld, L.P. Patron, R.L. Barrack. The effect of demineralized bone matrix gel on bone ingrowth and fixation of porous implants. J. Arthroplasty 17 (2002) 402-408.

42. J.M. Wozney, V. Rosen, A.J. Celeste, L.M. Mitsock, M.J. Whitters, R.W. Kriz, R.M. Hewick, E.A. Wang. Novel regulators of bone formation: molecular clones and activities. Science. 242 (1988) 1528-1534.

43. D.R. Sumner, T.M. Turner, A.F. Purchio, W.R. Gombotz, R.M. Urban, J.O. Galante. Enhancement of bone ingrowth by transforming growth factor-β. J. Bone Joint Surg. Am. 77 (1995) 1135-1147.

44. D.R. Sumner, T.M. Turner, R.M. Urban, T. Turek, H. Seeherman, J.M. Wozney. Locally delivered rhBMP-2 enhances bone ingrowth and gap healing in canine model. J. Orthop Res. 22 (2004) 58-65.

45. S. Itoh, M. Matubara, T. Kawauchi, H. Nakarura, S. Yukitake, S. Ichinose, K. Shinomiya. Enhancement of bone ingrowth in a titanium fiber mesh

implant by rhBMP-2 and hyaluronic acid. J. Mater. Sci. Mater. Med. 12 (2001) 575-581.

46. C.R. Bragdon, A.M. Doherty, H.E. Rubash, M. Jatsy, X.J. Li, H. Seeherman, W.H. Harris. The efficacy of BMP-2 to induce bone ingrowth in a total hip replacement model. Clin. Orthop. 417 (2003) 195-202.

47. M. Stewart, J.F. Welter, V.M. Goldberg. Effect of hydroxyapatite/tricalcium phosphate coating on osseointegration of plasma-sprayed titanium alloy implants. J. Biomed. Mater. Res. 69A (2004) 1-10.

48. R.G.T. Geesink. Osteoconductive coatings for total joint arthroplasty. Clin. Orthop. 395 (2002) 53-65.

49. E.Y. Kawachi, C.A. Bertran, L.T. Kubota. Interface potential of calcium phosphate in simulated body fluid. Biomaterials. 19 (1998) 2329-2333.

50. K.A. Gross, C.C. Berndt, D.D. Goldschlag, V.J. Iacono. In vitro changes of hydroxyapatite coatings. Int. J. Oral Maxillofac. Implants. 12 (1997) 589-597.

51. J. Weng, Q. Liu, J.G. Wolke, X. Zhang, K. de Groot. Formation and characteristics of the apatite layer on plasma-sprayed hydroxyapatite coatings in simulated body fluid. Biomaterials 18 (1997) 1027-1035.

52. R.G.T. Geesink, K. De Groot, C.P.A.T. Klein. Chemical implant fixation using hydroxyl-apatite coatings. Clin. Orthop. 225 (1987) 147-170.

53. W.H. Harris, R.E. White, J.C. McCarthy, P.S. Walker, E.H. Weingberg. Bony ingrowth fixation of the acetabular component in canine hip joint arthroplasty. Clin. Orthop. 176 (1983) 7-11.

54. H. Oonishi. Orthopedic applications of hydroxyapatite. Biomaterials. 12 (1991) 171-178.

55. S.D. Cook, K.A. Thomas, J.F. Kay, M. Jarcho. Hydroxyapatite-coated porous titanium for use as an orthopedic biologic attachment system. Clin. Orthop. 230 (1988) 303-312.

56. M. Jatsy, H.E. Rubash, G.D. Paiement, C.R. Bragdon, J. Parr, W.H. Harris. Porous-coated uncemented components in experimental total hip arthroplasty in dogs. Clin. Orthop. 280 (1992) 300-309.

57. M. Tanzer, J. Gollish, R. Leighton, K. Orrell, A. Giacchino, P. Welsh, B. Shea, G. Wells. The effect of adjuvant calcium phosphate coating on a porous coated femoral stem. Clin. Orthop. 424 (2004) 153-160.

58. S.A. Hacking, M. Tanzer, E.J Harvey, J.J. Krygier, J.D. Bobyn. Relative contributions of chemistry and topography to the osseointegration of hydroxyapatite coatings. Clin. Orthop. Relat. Res. 405 (2002) 24-38.

59. G.L. Darimont, R. Cloots, E. Heinen, L. Seidel, R. Legrand. In vivo behavior of hydroxyapatite coatings on titanium implants: a quantitative study in the rabbit leads to loosening. Biomaterials. 23 (2002) 2569-2575.

60. A. Ezra, G. Golomb, Administration routes and delivery systems of bisphosphonates for the treatment of bone resorption. Adv. Drug Deliv. Rev. 42 (2000) 175-195.

61. T.J. Martin, V. Grill, Bisphosphonates – mechanisms of action. Austr. Prescr. 23 (2000) 130-132.

62. J.P. Walsh, L.C. Ward, G.O. Stewart, R.K. Will, R.A. Criddle, R.L. Prince, B.G. Stuckey, S.S. Dhaliwal, C.I. Bhagat, R.W. Retallack, G.N. Kent, P.J. Drury, S. Vasikaran, D.H. Gutteridge. A randomized clinical trial comparing oral alendronate and intravenous pamidronate for the treatment of Paget's disease of bone. Bone. 34 (2004) 747-754.

63. B. Ramaswamy, C.L. Shapiro. Bisphosphonates in the prevention and treatment of bone metastases. Oncology. 17 (2003) 1261-1270.

64. A.R. Belch, D.E. Bergsagel, K. Wilson, S. O'Reilly, J. Wilson, D. Sutton, J. Pater, D. Johnston, B. Zee. Effect of daily etidronate on the osteolysis of multiple myeloma. J. Clin. Oncol. 9 (1991) 1397-1402.

65. P. Roschger, S. Rinnerthaler, J. Yates, G.A. Rodan, P. Fratzl, K. Klaushofer. Alendronate increases degree and uniformity of mineralization in cancellous bone and decreases the porosity in cortical bone of osteoporotic women. Bone. 29 (2001) 185-191.

66. J. Iwamoto, T. Takeda, Y. Sato. Prevention and treatment of corticosteroid-induced osteoporosis. Yonsei Med. J. 46 (2005) 456-463.

67. S.R. Frenkel, W.L. Jaffe, C.D. Valle, L. Jazrawi, S. Maurer, A. Baitner, K. Wright, D. Sala, M. Hawkins, P.E. Di Cesare, The effect of alendronate (Fosamax™) and implant surface on bone integration and remodeling in a canine model. Biomed. Mater. Res. (Appl. Biomater.) 58 (2001) 645-650.

68. D.G. Little, M. McDonald, I.T. Sharpe, R. Peat, P. Williams, T. McEvoy. Zoledronic acid improves femoral head sphericity in a rat model of perthes disease. J. Orthop. Res. 23 (2005) 862-868.

69. M. von Knoch, C. Wedemeyer, A. Pingsmann, F. von Knoch, G. Hilken, C. Sprecher, F. Henschke, B. Barden, F. Loer. The decrease of particle-induced osteolysis after a single dose of bisphosphonate. Biomaterials. 26 (2005) 1803-1808.

70. J. Astrand, P. Aspenberg. Topical, single dose bisphosphonate treatment reduced bone resorption in a rat model for prosthetic loosening. J. Orthop. Res. 22 (2004) 244-249.

71. T. A. Soininvaara, J. S. Jurvelin, H. J. A. Miettinen, O. T. Suomalainen, E. M. Alhava, P. J. Kroger. Effect of alendronate on periprosthetic bone loss after total knee arthroplasty: a one-year, randomized, controlled trial of 19 patients. Calcif Tissue Int. 71 (2002) 472-477.

72. J.M. Wilkinson, A.C. Eagleton, I. Stockley, N.F. Peel, A.J. Hamer, R. Eastell. Effect of pamidronate on bone turnover and implant migration after total hip arthroplasty: a randomized trial. J. Orthop. Res. 23 (2005) 1-8.

73. J.D. Bobyn, S.A Hacking, J.J. Krygier, E.J. Harvey, D.G. Little, M. Tanzer. Zoledronic acid causes enhancement of bone growth into porous implants. J. Bone Joint Surg. Br. 87 (2005) 416-420.

74. H. Denissen, E. van Beek, C. Lowik, S. Papapoulos, A. van den Hooff. Ceramic hydroxyapatite implants for the release of bisphosphonate. Bone Min. 25 (1994) 123-134.

75. M. Yoshinari, Y. Oda, T. Inoue, K. Matsuzaka, M. Shimono, Bone response to calcium phosphate-coated and bisphosphonate-immobilized titanium implants. Biomater. 23 (2002) 2879-2885.

76. M. Yoshinari, Y. Oda, H. Ueki, S. Yokose, Immobilization of bisphosphonates on surface modified titanium. Biomater. 22 (2001) 709-715.

77. S.J. Meraw, C.M. Reeve, Qualitative analysis of peripheral peri-implant bone and influence of alendronate sodium on early bone regeneration. J. Periodontol. 70 (1999) 1228-1233.

78. S.J. Meraw, C.M. Reeve, P.C. Wollan, Use of alendronate in peri-implant defect regeneration. J. Periodontol. 70 (1999) 151-158.

79. H. Kajiwara, T. Yamaza, M. Yoshinari, T. Goto, S. Iyama, I. Atsuta, M.A. Kido, T. Tanaka. The bisphosphonate pamidronate on the surface of

titanium stimulates bone formation around tibial implants in rats. Biomaterials. 26 (2005) 581-587.

80. B. Peter, D.P Pioletti, S. Laib, B. Bujoli, P. Pilet, P. Janvier, J. Guicheux, P.Y. Zambelli, J.M. Bouler, O. Gauthier. Calcium phosphate drug delivery system: influence of local zoledronate release on bone implant osteointegration. Bone. 36 (2005) 52-60.

81. P. Tengvall, B. Skoglund, A. Askendal, P. Aspenberg. Surface Immobilized bisphosphonate improves stainless-steel screw fixation in rats. Biomaterials. 25 (2004) 2133-2138.

82. R. Chang. Chemistry. 5th ed. McGraw-Hill, Inc. New York. 1994.

83. G.L. Burke. The corrosion of metals in tissues; and an introduction to tantalum. Canad. Med. Assoc. J. 43 (1940) 125-128.

84. J.D. Bobyn, G.J. Stackpool, S.A. Hacking, M. Tan zer, J.J. Krygier. Characteristics of bone ingrowth and interface mechanics of a new porous tantalum biomaterial. J. Bone Joint Surg. (Br.) 81B (1999) 907-914.

85. L.D. Zardiackas, D.E. Parsell, L.D. Dillon, D.W. Mitchell, L.A. Nunnery, R. Poggie. Structure, metallurgy and mechanical properties of a porous tantalum foam. J. Biomed. Mater. Res. (Appl. Biomater.) 58 (2001) 180-187.

86. J.D. Bobyn, S.A. Hacking, S.P. Chan, K.K. Toh, J.J. Krygier, M. Tanzer. Characterization of a new porous tantalum biomaterial for reconstructive orthopaedics. Anaheim, CA: A scientific exhibit at the annual AAOS; 1999.

87. J.D. Bobyn, K.K. Toh, A. Hacking, M. Tanzer, J.J. Krygier. Tissue response to porous tantalum acetabular cups: a canine model. J. Arthroplasty. 14 (1999) 347-354.

88. S.A. Hacking, J.D. Bobyn, K.K. Toh, M. Tanzer, J.J. Krygier. Fibrous tissue ingrowth and attachment to porous tantalum. J. Biomed. Mater. Res. 52 (2000) 631-638.

89. J.D. Bobyn, M. Tanzer, J.J. Krygier, D.G. Lewallen, A.D. Hassen, R.J. Lewis, A.S. Unger, T.J. O'Keefe, M.J. Christie, S. Nasser, J.E. Wood, D. Stulberg, R.A. Poggie. Clinical validation of a structural porous tantalum biomaterial for adult reconstruction. San Francisco, CA: A Scientific exhibit at the annual AAOS; 2004.

90. D.A. Skoog, F.J. Holler, T.A. Nieman. Principles of Instrumental Analysis. 5th ed. Saunders College Publishing. Philadelphia, 1998.

91. N. Nardelli, G. Pelizzi. A structural study on metal binding of gem-diphosphonates, bone growth regulators. Inorg. Chim. Acta. 80 (1983) 259-271.

92. R.W. Sparidans, J. den Hartigh, P. Vermeij. High-performance ion-exchange chromatography with in-line complexation of bisphosphonates and their quality control in pharmaceutical preparations. J. Pharm Biomed. Anal. 13 (1995) 1545-1550.

93. E.W. Tsai, S.D. Chamberlain, R.J. Forsyth, C. Bell, D.P. Ip, M.A. Brooks. Determination of bisphosphonate drugs in pharmaceutical dosage formulation by ion chromatography with indirect UV dectection. J. Pharm. Biomed. Anal. 8 (1994) 983-991.

94. P. Perjesi, T. Kim, A.D. Zharikova, X. Li, T. Ramesn, J. Ramasubbu, L. Prokai. Determination of clodronate content in liposomal formulation by capillary zone electrophoresis. J. Pharm. Biomed. Anal. 31 (2003) 929-935.

95. V. Virtanen, J. Pursiainen, L.H. Lajunen. Complexometric determination of clodronate in aqueous solution and urine. Acta Chem Scand. 47 (1993) 1071-1077.

96. X.Z. Qin, E.W. Tsai, T. Sakuma, D.P. Ip. Pharmaceutical application of liquid chromatography-mass spectrometry : II. Ion chromatography-ion spray mass spectrometric characterization of alendronate. J. Chromatogr. A. 686 (1994) 205-212.

97. D. Ostovic, C. Stelmach, B. Hulshizer. Formation of a chromaphoric complex between alendronate and copper (II) ions. Pharm. Res. 10 (1993) 470-472.

98. P. Perugini, I. Genta, B. Conti, T. Modena, F. Pavanetto. Long-term release of clodronate from biodegradable microspheres. AAPS PharmSciTech. 2 (2001) article 10. www.pharmscitech.com.

99. J. Kuljanin, I. Jankovic, J. Nedeljkovic, D. Prstojevic, V. Marinkovic. Spectrophotometric determination of alendronate in pharmaceutical formulations via complex formation with Fe (III) ions. Pharm. Biomed. Anal. 28 (2002) 1215-1220.